Universidade de Aveiro
2018

Departamento de Ambiente e Ordenamento

Ana Patrícia da Silva Fernandes

Estudo de aerossóis atmosféricos naturais em Portugal: análise integrada usando modelação da qualidade do ar e dados de satélite

Study of natural atmospheric aerosols in Portugal: integrated analysis using air quality modelling and satellite data

Universidade de Aveiro
2018

Departamento de Ambiente e Ordenamento

Ana Patrícia da Silva Fernandes

Estudo de aerossóis atmosféricos naturais em Portugal: análise integrada usando modelação da qualidade do ar e dados de satélite

Study of natural atmospheric aerosols in Portugal: integrated analysis using air quality modelling and satellite data

Tese apresentada à Universidade de Aveiro para cumprimento dos requisitos necessários à obtenção do grau de Doutor em Ciências e Engenharia do Ambiente, realizada sob a orientação científica da Doutora Oxana Tchepel, Professora Auxiliar da Faculdade de Ciências e Tecnologia da Universidade de Coimbra e sob coorientação científica do Doutor Carlos Borrego, Professor Catedrático do Departamento de Ambiente e Ordenamento da Universidade de Aveiro e do Doutor Stefan Wunderle, Professor Associado do Departamento de Geografia da Universidade de Berna.

Apoio financeiro da Fundação para a Ciência e Tecnologia (FCT) através do POPH-QREN, comparticipado pelo Fundo Social Europeu (FSE) e por fundos nacionais do MCTES pela Bolsa de Doutoramento com a referência SFRH/BD/86307/2012.

Apoio Financeiro do FEDER através do Programa Operacional Fatores de Competitividade (COMPETE) e por Fundos Nacionais através da FCT do PTDC no âmbito dos Projetos EMOSAT (PTDC/CTE-ATM/103253/2008, FCOMP-01-0124-FEDER-009305), CLICURB (EXCL/AAG-MAA/0383/2012) e FUTURAR (PTDC/AAG-MAA/2569/2014 - POCI-01-0145-FEDER-016752).

Para a minha filha LARA e restante FAMÍLIA.

Para TODOS os que me apoiaram na realização deste trabalho.

o júri

presidente

Professor Doutor Jorge Ribeiro Frade
Professor Catedrático, Universidade de Aveiro

Professora Doutora Ana Isabel Couto Neto da Silva Miranda
Professora Catedrática, Universidade de Aveiro

Doutor Nelson Augusto Cruz De Azevedo Barros
Professor Associado, Faculdade de Ciências e Tecnologia da Universidade Fernando Pessoa

Doutora Oxana Anatolievna Tchepel
Professora Auxiliar, Universidade de Coimbra

Doutora Isabel Alexandra Martinho Franco Trigo
Investigadora, Instituto Português do Mar e da Atmosfera

agradecimentos

Mais uma etapa chega ao fim e faz todo o sentido agradecer a algumas pessoas, sem as quais, a realização desta Tese não seria possível.

Em primeiro lugar, à minha orientadora Doutora Oxana Tchepel, obrigada pelos conhecimentos que me transmitiu, pelas sugestões e críticas ao longo da orientação deste trabalho e pela paciência nos momentos mais difíceis.

Ao meu co-orientador, Professor Carlos Borrego, pelos comentários e sugestões no decorrer deste trabalho e ao longo destes anos no GEMAC.

Ao meu co-orientado, Doutor Stefan Wunderle, pelo acolhimento prestado na Universidade de Berna e por toda a orientação. À Família Burkhalter que me acolheu durante a minha estadia na Suíça.

A todos Gemaquianos com quem tive o prazer de partilhar experiências pessoais e profissionais durante estes últimos 7 anos. Sem dúvida uma "Família" que me ajudou a crescer. Elisa, Daniela, Cristina, Carla, Vera, Joana F. e Sandra R. muito obrigada pelo apoio constante e por me ajudarem a vencer alguns dos momentos mais difíceis. Aos meus mais recentes colegas, Sara e Bruno, pelas palavras amigas. Ao Daniel por toda a ajuda nesta fase final.

À Cátia Gonçalves, Ana Vicente, Ana Calvo, Paula Quinteiro, Diana Patoilo, Professora Teresa Nunes e Doutora Célia Alves pela amizade e por todo o apoio ao longo destes anos.

À Joana Cavadas e Susana Freiria pela partilha de gabinete, companhia e pelo apoio nesta fase final.

Ao Gabriel e à sua Família por todo o apoio e carinho.

Por fim, mas não menos importante, ao meu Pai, à minha Mãe, ao meu irmão Rodolfo e restantes familiares, OBRIGADA por tudo!

palavras-chave

Aerossóis atmosféricos, poeiras minerais, modelação de qualidade do ar, dados de satélite, fusão de dados.

resumo

Ao longo dos últimos anos, a degradação da qualidade do ar tornou-se um grande problema em Portugal. A concentração elevada de partículas (PM), que excedem os valores limite diários legislados, é uma das principais preocupações no que se refere à gestão da qualidade do ar.

O objetivo principal deste trabalho é desenvolver uma metodologia consistente para melhorar a caracterização de aerossóis e avaliar a contribuição dos episódios de poeira mineral na poluição atmosférica em Portugal. Para atingir o objetivo, primeiro estudou-se a influência dos episódios de poeira mineral em Portugal. Posteriormente foi realizada a análise e a comparação dos resultados da modelação da qualidade do ar e das observações de satélite. Finalmente, implementou-se uma técnica de fusão de dados utilizando dados de modelação e de satélite com o objetivo de melhorar a quantificação dos aerossóis.

A caracterização da distribuição espacial da poeira mineral sobre Portugal Continental foi realizada para o ano de 2011. É notória a influência dos episódios de poeira mineral em Portugal durante a primavera, nomeadamente nos meses de abril e maio. Assim, o período de estudo selecionado para realizar a comparação e integração dos resultados da modelação da qualidade do ar e das observações de satélite foi maio de 2011. Foram explorados dados de satélite obtidos pelo instrumento Spinning Enhanced Visible and Infrared Imager (SEVIRI) com elevada resolução temporal e resultados da modelação da qualidade do ar do Comprehensive Air Quality Model (CAMx). Os dados foram avaliados em termos de espessura ótica dos aerossóis (AOD) a 550 nm e concentração de PM. A validação dos dados de modelação e de satélite em termos de AOD foi realizada com base nas observações de quatro estações AERONET (Aerossol Robotic Network) localizadas dentro do domínio de estudo. As concentrações de PM obtidas com o modelo foram validadas utilizando valores medidos nas estações de qualidade do ar.

A metodologia desenvolvida neste estudo revela que a intercomparação e a integração das observações de satélite com os resultados da modelação da qualidade do ar contribui para uma melhor compreensão das discrepâncias apresentadas no padrão espacial de AOD e podem fornecer informação adicional à validação in-situ. A metodologia de fusão de dados proporcionou uma melhoria dos resultados da modelação de qualidade do ar no que diz respeito aos valores de AOD e aos valores de concentração de PM junto à superfície.

Este estudo constitui um contributo científico inovador que pode ser relevante para uma futura e cuidada gestão da qualidade do ar, uma vez que promove uma melhoraria na quantificação dos aerossóis relevante para aplicações no âmbito da Diretiva da qualidade do ar.

keywords Atmospheric aerosol, mineral dust, air quality modelling, satellite data, data fusion

abstract

Over the last years, air quality degradation has become an important issue in Portugal. The high concentrations of particulate matter (PM), exceeding the daily limit values, are one of the main concerns for air quality management.

The main objective of this work is to develop a consistent methodology to improve the characterization of aerosol concentrations and to evaluate the contribution of mineral dust for air pollution episodes in Portugal. In order to achieve the objective, firstly the influence of the African dust outbreaks over Portugal were studied. Subsequently, the study and comparison of the air quality modelling results and satellite observation were performed. Finally, we developed and applied a data fusion methodology using modelling and satellite data to improve the quantification of the atmospheric aerosol loading.

The characterization of the spatial distribution of mineral dust over mainland Portugal was performed for the entire year of 2011. The influence of the African dust outbreaks over Portugal that is notorious during the spring period, namely in April and May. For this reason, May 2011 was selected as the study period to perform the comparison and integration of the air quality modelling results and satellite observation. Satellite data obtained by the Spinning Enhanced Visible and Infra-Red Imager (SEVIRI) instrument with high temporal resolution and air quality modelling results from the Comprehensive Air Quality Model (CAMx) were explored. The data were assessed in terms of aerosol optical depth (AOD) at 550 nm and PM concentrations. The validation of the AOD values obtained from air quality modelling and satellite observations was performed using observations from four Aerosol Robotic Network (AERONET) stations located within the study area. The PM concentrations were validated using measurements from air quality monitoring stations.

The methodology developed in this study revealed that the intercomparison and the integration of satellite observations with air quality modelling contributes to a better understanding of the discrepancies presented in the spatial pattern of AOD and may provide valuable information to in-situ validation with ground-based observations. The data fusion methodology provides an improvement of the modelling results in terms of AOD data and PM concentrations near the surface. This study constitutes an innovative scientific support for forthcoming air quality management in order to improve the quantification of aerosols, relevant for policy applications in the framework of Air Quality Directives.

Table of contents

CHAPTER 1 1

1 INTRODUCTION 3
1.1 Motivation 3
1.2 Research Questions and Objectives 6
1.3 Thesis structure 8

CHAPTER 2 11

2 MINERAL DUST 13
2.1 Introduction 13
2.2 Methodologies for the identification of mineral dust events 16
2.3 Mineral dust over Portugal 17
2.3.1 BSC-DREAM8b model description 18
2.3.2 Model application and validation 19
2.3.3 Long-term assessment of mineral dust over Portugal 25
2.3.4 Analysis of mineral dust episodes 29
2.4 Summary and conclusions 35

CHAPTER 3 37

3 REMOTE SENSING OF AEROSOLS 39
3.1 Introduction 39
3.2 Aerosol optical properties 43
3.3 Remote sensing techniques 49
3.3.1 AErosol RObotic NETwork (AERONET) 50
3.3.2 Spinning Enhanced Visible and Infrared Imager (SEVIRI) 52
3.4 Methodology for SEVIRI and AERONET data processing 55
3.5 Results and discussion 57
3.5.1 AERONET observations 57
3.5.2 Evaluation of SEVIRI observations 59
3.6 Summary and conclusions 63

CHAPTER 4 65

4 AIR QUALITY MODELLING OF AEROSOLS 67
4.1 Introduction 67
4.2 Methodology for the air quality modelling system WRF-CAMx application 71
4.3 Modelling results and discussion 76
4.3.1 Assessment of air quality modelling system 76
4.3.2 Aerosols vertical distribution analysis 79
4.3.3 Spatial distribution of the AOD modelling results 80
4.3.4 Evaluation of AOD modelling results 82
4.4 Summary and conclusions 83

CHAPTER 5 85

5 COMPARISON OF SATELLITE OBSERVATIONS AND AIR QUALITY MODELLING RESULTS ... 87
5.1 Introduction 87
5.2 Methodology 89
5.3 Results and discussions 94
5.3.1 Comparison of satellite observations and modelling results 94
5.3.2 Validation with AERONET data 96
5.4 Summary and conclusions 100

CHAPTER 6 103

6 INTEGRATION OF AIR QUALITY MODELLING AND SATELLITE OBSERVATION 105
6.1 Introduction 106
6.2 Data fusion 109
6.2.1 Data fusion of AOD from modelling and satellite observations 110
6.2.2 Comparison between the modelling results before and after data fusion .. 113
6.2.3 AOD data validation with AERONET observations 115
6.3 Quantification of PM concentrations using data fusion 118
6.3.1 Methodology to obtain new PM concentrations after data fusion 118
6.3.2 Validation of PM concentrations before and after data fusion 119
6.4 Summary and conclusions 121

CHAPTER 7 123

7 CONCLUSIONS 125
7.1 Research question 1 125
7.2 Research question 2 126
7.3 Research question 3 128
7.4 Future developments 129

REFERENCES 131

List of figures

Figure 1.1. Map of annual mean concentrations of PM10 in 2011 (EEA, 2013)..... 4
Figure 1.2. Map of annual mean concentrations of PM10 in 2011 ($\mu g \cdot m^{-3}$) (Borrego et al., 2012a)..... 5
Figure 1.3. Thesis structure. 8
Figure 2.1. Illustration of natural sources of aerosols (Andreae, 2007)..... 14
Figure 2.2. African mineral dust event occurred over the Iberian Peninsula in February 2016. This Figure shows: a) The Moderate Resolution Imaging Spectroradiometer (MODIS) on NASA's Aqua satellite acquired a natural-colour image (lower). b) Spatial distribution of mineral dust load ($g \cdot m^{-2}$) from BSC-DREAM8b model, c) HYSPLIT backward trajectories for 500, 1500 and 2000 m above sea level for the centre of Portugal and d) Measured PM10 concentrations from Air Quality Stations. 17
Figure 2.3. BSC-DREAM8b v1.0 model simulation domain, with the domain over Portugal highlited [correspondig to 396 grid cells (18x22)]. 20
Figure 2.4. Location of PM_{10} monitoring sites over Portugal. 21
Figure 2.5. Time series of daily mean observed PM10 (solid gray line) and simulated MD10 (dashed black line) for four sites: Lamos D'Olo, Fundão, Ervedeira and Chamusca for 2011. 22
Figure 2.6. Time series of daily mean observed PM10 (solid gray line) and simulated MD10 (dashed black line) for three sites: Terena, Monte Velho and Joaquim Magalhães for 2011. 23
Figure 2.7. Monthly mean of modeled mineral dust surface concentration ($\mu g \cdot m^{-3}$) for 2011. 26
Figure 2.8. Annual mean of modelled mineral dust surface concentration ($\mu g \cdot m^{-3}$) for 2011. 27
Figure 2.9. Spatial representation of 25^{th} (P25), 50^{th} (P50), 75^{th} (P75) and 95^{th} (P95) percentiles of the modelled mineral dust concentrations for 2011. 28
Figure 2.10. Cluster mean trajectories identified for each study site (see Figure 2.4) during the selected episodes days, and modelled mineral dust concentration statistics associated to each of the identified trajectories (same color representation). 32
Figure 2.11. Cluster mean trajetories obtained for the entire year of 2011, for diferent sites (JMG, MVE, TER, CHA, ERV, FUN and OLO)..... 34

Figure 3.1. Mass extinction efficiencies for hygroscopic aerosols at wavelength 500 nm as a function of RH. The r_{eff} values are indicated at the top of each graph (Chin et al., 2002). 46
Figure 3.2. Example of Aerosol size distribution for urban environment (Seinfeld and Pandis, 2006). 48
Figure 3.3. An example of AERONET instrument located at Évora station [URL3] 51
Figure 3.4. RGB image of the full SEVIRI disk from 17 October 2016 acquired from Meteosat-8 at 12:00 UTC. Copyright by EUMETSAT. 53
Figure 3.5. AERONET sites in Portugal and adjacent regions. 56
Figure 3.6. Daily average of Aerosol Optical Depth from AERONET observations during May 2011. 58
Figure 3.7. Daily average of Ångström coefficient from AERONET observations during May 2011. 59
Figure 3.8. Example of the SEVIRI data for 14 May 2011: a) Hourly data (between 6h-17h) with original pixel size (3x3 km^2), b) Daily mean data with original cell size (3x3 km^2) and c) Daily mean data with the grid cell size and projection compatible with the modelling outputs (9x9 km^2). 60
Figure 3.9. Number of days with AOD data from SEVIRI observations considered for the analysis. 60
Figure 3.10. Spatial representation of percentile 25^{th} (P25), 50^{th} (P50), 75^{th} (P75) and 90^{th} (P90) of the AOD obtained from SEVIRI for May 2011. 61
Figure 3.11. Scatterplot of daily mean AOD values from AERONET versus SEVIRI observations. 62
Figure 4.1. Modelling domains for WRF and CAMx modelling applications and location of the emissions point sources (circles) considered in the study. 72
Figure 4.2. Structure of the air quality modelling system WRF-CAMx. 73
Figure 4.3. Location of the mainland Portuguese air quality monitoring stations (a); part of Northern region (b) and Lisbon region (c). Note the differentiation of urban (square), suburban (triangle) and rural (circle) background stations. 75
Figure 4.4. Average of measured and modelled PM10 daily concentrations for all a) Rural b) Suburban and c) Urban background stations. The modelled PM10 data were represented in terms of aerosol compound (OC, BC, SO_4 and Dust) contribution. 77

Figure 4.5. Vertical distribution of aerosol compounds concentrations in Huelva on May 14, 2011. 79
Figure 4.6. Monthly mean of AOD for May 2011 for: a) SO_4, b) OC and c) BC. (Notice the colour scales' ranges are different) 80
Figure 4.7. Spatial distribution of monthly mean AOD for May 2011 from: a) OC+BC+SO_4 and b) mineral dust obtained from modelling. 81
Figure 4.8. Spatial pattern of the monthly mean AOD for May 2011 obtained with modelling approach. 82
Figure 4.9. Scatterplot of daily mean AOD values from AERONET versus modelling results. 83
Figure 5.1. Study domain (9 x 9 km^2) and location of AERONET stations. 90
Figure 5.2. Hourly SEVIRI AOD data for 14 May 2011 (between 6h-17h) with original pixel size (3x3 km^2). 91
Figure 5.3. Daily mean AOD SEVIRI data (14 May 2011) with original cell size (3x3 km^2). 92
Figure 5.4. Daily mean SEVIRI data (14 May 2011) with the grid cell size and projection compatible with the modelling grid (9x9 km^2). 93
Figure 5.5. Spatial distribution of monthly mean AOD for May 2011 obtained with: a) Modelling approach and b) SEVIRI observations. 94
Figure 5.6. Relative differences between the monthly mean AOD obtained from the modelling system and SEVIRI: a) Spatial distribution and b) Frequency histogram. 95
Figure 5.7. Correlation between modelling results and SEVIRI observations during May 2011 a) Spatial distribution, b) Frequency histogram (in percentage, %). 96
Figure 5.8. Time series of daily mean AOD and AC values from AERONET stations and daily mean AOD values from modelling and SEVIRI data. a) Caceres, b) Huelva, c) Évora and d) Cabo da Roca. 97
Figure 5.9. Scatter diagram of AC versus AOD provided by AERONET stations. 98
Figure 5.10. Scatterplot of daily mean AOD values from: a) AERONET versus SEVIRI, b) AERONET versus modelling approach. The daily AOD values are also represented in function of the AC values as defined from AERONET measurements: Cluster 1 (AOD>0.2 and AC<1.0, triangles), Cluster 2 (AOD <0.2 and AC>1.0, squares) and Cluster 3 (AOD<0.2 and AC<1.0, circles). 99

Figure 6.1. Scheme of the data fusion methodology applied to AOD data. 111
Figure 6.2. Illustrations of the focal statistics tool used for a neighborhood operation. . 112
Figure 6.3. Scheme of the satellite data processing. 113
Figure 6.4. Spatial pattern of monthly average AOD for May 2011: a) Modelling results before data fusion and b) Modelling results after data fusion. 114
Figure 6.5. Differences between the monthly AOD values before data fusion minus AOD values after data fusion. 115
Figure 6.6. Scatter plot of daily average AOD values from modelling results versus AERONET observations. a) Before data fusion and b) After data fusion. .. 116
Figure 6.7. Taylor diagram with AOD values from: modelling data before data fusion, modelling data after data fusion. All values are normalized with AERONET observations. 117
Figure 6.8. Schematic representation of methodology used to obtain new PM mass concentrations at near-surface level. 119
Figure 6.9. Delta tool plots for modelling system for PM10 data before (above) and after (below) satellite data fusion (target plot (left) and Taylor diagram (right)). The red marks represent the air quality stations available and considered in this study (see Figure 4.3). 120

List of tables

Table 2.1. Dust size bins distribution parameters. From left to right: bin number, minimum and maximum radius of each size bin (r_{min}-r_{max}), effective radius of each bin (r_{eff}), extinction efficiency (Q_e) at 532 nm and 1064 nm (Pérez et al. 2006b). 19
Table 2.2. Statistical indicators used for model validation (RMSE and BIAS). 24
Table 2.3. Identification and characterisation of the selected episode days for 2011..... 29
Table 3.1. Hygroscopic growth factors of $r_{eff}/r_{eff,dry}$ at different RH (Adapted from Chin et al., 2002). 45
Table 3.2. Spectral channel characteristics of SEVIRI in terms of central, minimum and maximum wavelength of the channels and the main application areas for each channel. Adapted from Schmetz et al. (2002). 54
Table 4.1. Quality indicators applied in the WRF-CAMx system validation. 74
Table 4.2. Statistical parameters computed for PM10 daily concentrations. 78

List of abbreviations and symbols

AEMET	Spanish Meteorological Agency
AERONET	AErosol RObotic NETwork
AOD	Aerosol Optical Depth
AVHRR	Advanced Very High Resolution Radiometer
BC	Black Carbon
BIAS	Systematic error
BSC-CNS	Barcelona Supercomputing Center – Centro Nacional de Supercomputación
CAMx	Comprehensive Air Quality Model
CTM	Chemical Transport Model
EEA	European Environment Agency
EMEP	European Monitoring and Evaluation Programme
ESA	European Space Agency
EUMETSAT	European Organisation for the Exploitation of Meteorological Satellites
GIS	Geographic information system
GOES	Geostationary Operational Environmental Satellites
IPCC	International Panel on Climate Change
MGS	Meteosat Second Generation
MODIS	Moderate Resolution Imaging Spectroradiometer
MQI	Model Quality Indicator
NASA	National Aeronautics and Space Administration
NCEP	National Centers for Environmental Prediction
NO_2	Nitrogen dioxide
O_3	Ozone
OC	Organic Carbon
PM	Particulate matter
PM10	Particulate matter with an equivalent aerodynamic diameter of less than 10 μm
PM2.5	Particulate matter with an equivalent aerodynamic diameter of less than 2.5 μm
r	Correlation Coefficient
RH	Relative Humidity
SDS-WAS	Sand and Dust Storms Warning Advisory and Assessment System
SEVIRI	Spinning Enhanced Visible and Infrared Imager
SO_4	Sulphate
SSA	Single Scattering Albedo
TOMS	Total Ozone Mapping Spectrometer
WHO	World Health Organization
WMO	World Meteorological Organization
WRF	Weather Research & Forecasting

Chapter 1

Introduction

Chapter Index:

1.1 Motivation……3

1.2 Research Questions and Objectives……6

1.3 Thesis structure……....7

1 Introduction

"*Poor air quality from natural sources is by definition outside of our control*."

Jacqueline McGlade, European Environment Agency (EEA) Executive Director

This Chapter is divided in three sections. Section 1.1 makes an overview of this PhD work. The objectives and the main research questions are given in Section 1.2. Finally, the thesis structure is described in Section 1.3.

1.1 Motivation

Atmospheric aerosols are associated with various environmental impacts from local to global scales. Aerosols cause detrimental health effects (e.g. Pope and Dockery, 2006; WHO 2006a, WHO 2006b) and have direct and indirect effects on the climate system (IPCC, 2001; IPCC, 2007; IPCC, 2013). In Europe, air quality problems are evident in several countries since the concentration of air pollutants are surpassing the legislated values, namely the particulate matter with an equivalent aerodynamic diameter lesser than 10 µm (PM10) (Figure 1.1). As shown on Figure 1.1, the red and purple colours refer to values above the PM10 annual limit value (40 $\mu g \cdot m^{-3}$) in 2011 in several air quality stations located

at the Po Valley in Italy, and urban centres in some of the Balkan countries, Turkey, Poland, Slovakia, Spain and Portugal.

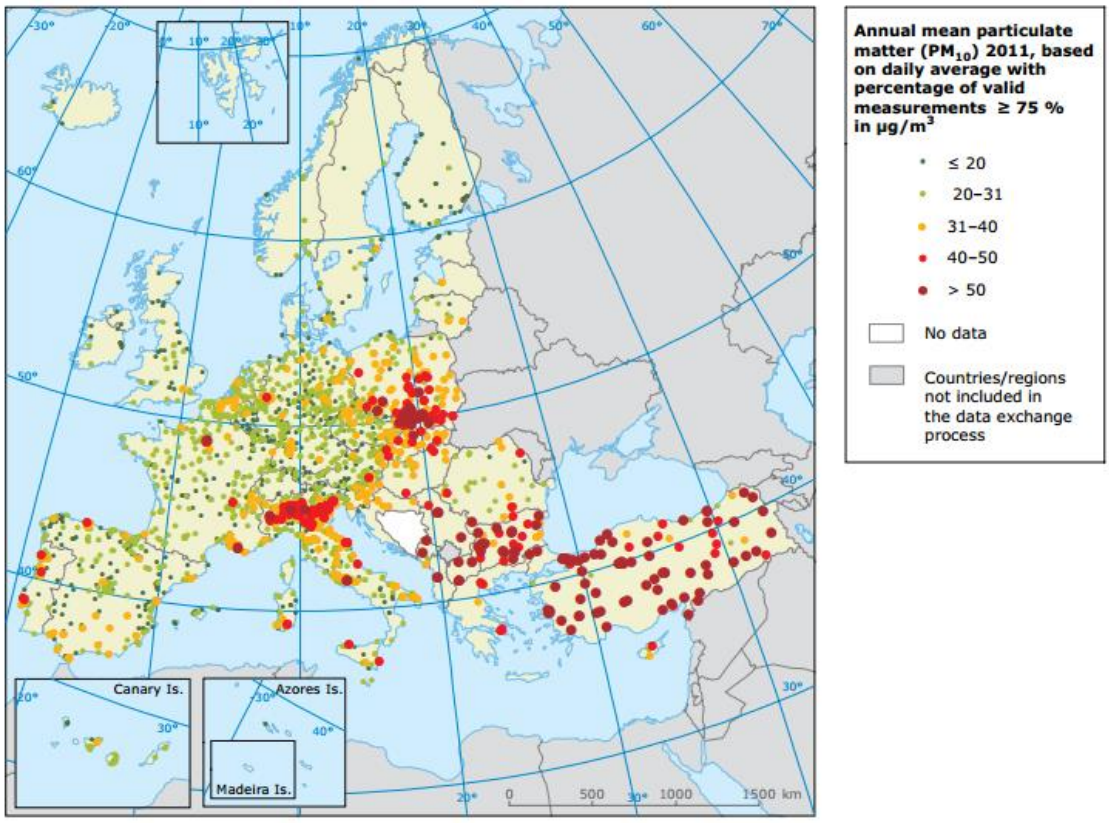

Figure 1.1. Map of annual mean concentrations of PM10 in 2011 (EEA, 2013).

Looking in more detail, it is evident that there are air quality problems over Portugal (Figure 1.2), mainly due to the surpassing of the legislated annual limit values of PM10 at several air quality monitoring stations, specially over two main regions: Lisboa and Vale do Tejo region and the Northern Region (Borrego et al., 2012a).

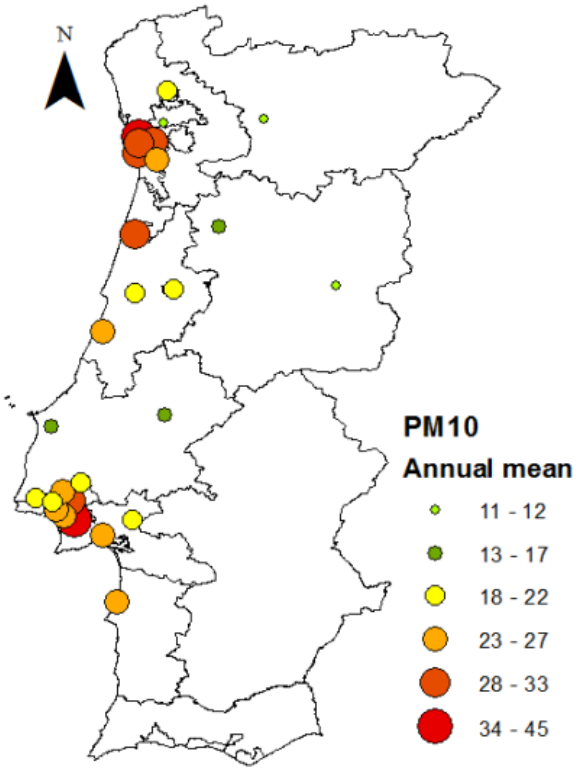

Figure 1.2. Map of annual mean concentrations of PM10 in 2011 ($\mu g \cdot m^{-3}$) (Borrego et al., 2012a).

Atmospheric aerosols, such as PM10, can come from natural or anthropogenic sources. In recent years, there has been a substantial increase in interest on the influence of anthropogenic aerosols. However, there are far fewer studies on natural aerosols than on anthropogenic aerosols, despite their importance (Satheesh and Krishnamoorthy, 2005; Allen and Sherwood, 2010). Natural sources are identified as sea salt, naturally suspended mineral dust, pollen and volcanic ash (EEA, 2012).

An abundant type of natural atmospheric aerosol is related to the suspension and long-range transport of mineral dust. Formed mainly in desert and semi-arid zones, these aerosols may play an important role in the occurrence of pollution episodes over Europe (Niemi et al., 2006, Pérez et al., 2006b). Wind-blown desert dust from Africa is the largest PM10 component in rural background southern sites of the Mediterranean, where it makes up between 35 % and 50 % of PM10 (Pey et al., 2013, EEA, 2013). Also, several studies highlight the importance of mineral dust long-range transport in Portugal (Fialho et al., 2006, Marell, 2007, Tchepel et al., 2013, Monteiro et al., 2015, Fernandes et al., 2015).

The EU Air Quality Directive 2008/50/EC allows Member States to subtract the contribution of natural sources before comparing the ambient concentrations to the relevant limit values since the PM10 contributions from natural sources cannot be controlled. Thus, the natural contributions to PM10 pollutants in ambient air have to be determined with sufficient certainty before subtracted. Therefore, definition of a harmonized methodology for assessing the contribution of the natural sources to the atmospheric aerosols is an important issue.

Air quality models are powerful tools to predict the fate of aerosols after their release into the atmosphere (Pérez et al., 2006, Kishcha et al., 2011, Tchepel et al., 2013, Monteiro et al., 2015). They provide quantitative information on spatial and temporal variations of the pollutant concentrations as well as vertical profiles. Emission data are used as an input to air pollution models and their quality is a strong determinant for the model performance. Currently, several modelling tools are available to characterize emission sources and the atmospheric life cycle of the natural aerosols (Pérez et al., 2006, Kishcha et al., 2011, Monteiro et al., 2015).

Moreover, the use of satellite data in combination with air pollution modelling opens the challenging perspective to analyse the contribution of different pollution sources and transport processes. An increasing interest in the use of satellite observations in air pollution modelling is mainly related with two important properties of the data, when compared with surface measurements: more complete spatial coverage and characterization of atmospheric components for vertical column (Engel-Cox et al., 2004a; Vijayaraghavan et al., 2008). The satellite data may be used to evaluate, initialize, constrain, and improve the performance of air pollution models (Vijayaraghavan et al., 2008). Aerosol optical depth (AOD) is one of the satellite products that has been shown to be a good proxy for pollution monitoring, especially when long-range transport is involved.

1.2 Research Questions and Objectives

The main goal of this research work is the development of a consistent approach, based on air quality modelling system and satellite observations, for assessing the contribution of natural sources to the atmospheric pollution and improving the quantification of particulate matter (PM) in Portugal. It will be focused on mineral dust. To reach this goal, three main questions should be answered:

1. How is air quality in Portugal is affected by mineral dust?

2. What are the advantages and the limitations of Air Quality Modelling and Satellite Observations to perform the aerosols characterization?

3. What is the best strategy to combine modelling and observation data in order to improve aerosols quantification?

To answer the questions, five specific objectives were established to be accomplished during this work:

- ✓ Characterization of the spatial and temporal distribution of mineral dust over Portugal;
- ✓ Implementation of a modelling system able to account for the natural emission sources and to provide aerosol mass concentration, size distribution, chemical composition and optical depth;
- ✓ Selection, processing and analysis of satellite data to characterize spatial aerosol loading with high temporal and spatial resolution;
- ✓ Analysis of the benefits combining the AOD data provided by satellite observations and air quality modelling;
- ✓ Development of a methodology to improve the quantification of the atmospheric aerosols using data fusing technique.

This research work contributes to a better understanding of natural events such as the atmospheric transport of mineral dust from dry regions to Portugal. The methodology developed and implemented in this work intends to improve the modelling system for the identification and quantification of natural processes on particulate matter (PM) near the surface and, in this way, provide an important contribution to the implementation of the Directive 2008/50/EC on ambient air quality objectives.

1.3 Thesis structure

In order to address the questions previously described, this thesis is organized in seven distinct chapters. The structure of this thesis is schematically represented in Figure 1.3.

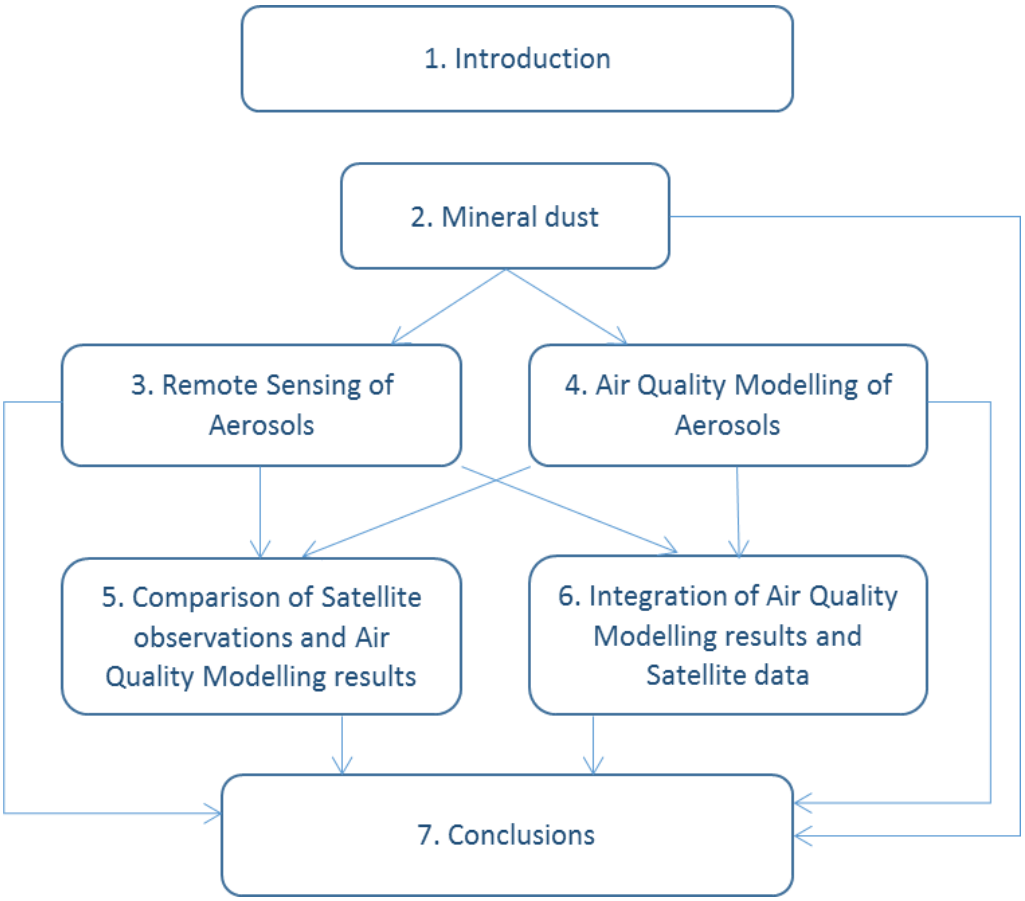

Figure 1.3. Thesis structure.

Chapter 2 presents the characterization of the spatial distribution of mineral dust over Portugal, for the entire year of 2011. The contribution of mineral dust to the particulate matter (PM) concentrations is relevant for air quality management. Thus, mineral dust is assessed in this chapter, in what concerns both, long-term and high peak episodes. Results from this chapter were important to select the study period as presented in the next chapters of the thesis. The results of this chapter were published in Monteiro et al. (2015).

In Chapter 3, the AOD data from two different remote sensing techniques are analysed. The evaluation of satellite data is performed using measurements from ground based observation networks. The aerosol optical depth (AOD) data presented in this chapter will be important to compare and integrate with modelling outputs as presented in the upcoming chapters.

In order to explore the spatial, vertical and temporal distribution of the aerosols concentration, the air quality modelling system WRF-CAMx is described and applied in Chapter 4. In this chapter, PM concentrations near the surface and on all vertical column are calculated and evaluated. The results from this chapter will be used in the upcoming chapters.

Before proceeding to an integration approach, it is firstly necessary to analyse the benefits of combining the AOD data provided by satellite observations with high temporal resolution and air quality modelling. In Chapter 5, satellite data obtained by Spinning Enhanced Visible and Infra-Red Imager (SEVIRI) instrument and air quality modelling results from the Comprehensive Air Quality Model (CAMx) over Portugal were explored.

In Chapter 6, the methodology developed to improve the quantification of the atmospheric aerosols is presented. In order to achieve the main objectives, a statistical approach was applied to combine the air quality modelling outputs with satellite observations. The development and application of the data fusion technique is described. Furthermore, new PM concentrations near the surface are calculated using the results of AOD after data fusion.

Finally, Chapter 7 presents a brief summary of the main achievements and discusses them in the context of the main research questions. The innovative character of the study is highlighted, as well as its limitations and future research.

Chapter 2

Mineral Dust

Chapter Index:

2.1 Introduction……..13

2.2 Methodologies for the identification of mineral dust events……..16

2.3 Mineral dust over Portugal……...17

2.3.1 – BSC-DREAM8b model description……...18

2.3.2 – Model application and validation……..20

2.3.3 – Long-term assessment of mineral dust over Portugal……...25

2.3.4 – Analysis of mineral dust episodes……29

2.4 Summary and conclusions……...35

2 Mineral Dust

The results of this chapter were published in:

*Monteiro, A., **Fernandes, A.P.**, Gama, C., Borrego, C., Tchepel, O., 2015. Assessing the mineral dust from North Africa over Portugal region using BSC-DREAM8b model. Atmospheric Pollution Research, 6, 1, 70-81. doi: 10.5094/APR.2015.009.*

An abundant type of natural atmospheric aerosol is related with the suspension and long-range transport of mineral dust from North Africa deserts. For this reason, quantitative analysis of the contribution of mineral dust to the concentrations of particulate matter (PM) is relevant for air quality management.

In this chapter, mineral dust over Portugal is assessed, in what concerns both long-term and high peak episodes. To this end, the BSC-DREAM8b v1.0 model (Pérez et al., 2006a; Pérez et al., 2006b; Basart et al., 2012b) was applied to a domain which includes North Africa and Middle East regions, for the entire year of 2011, allowing the characterisation of the spatial distribution of mineral dust over Portugal.

This chapter is divided in four sections. Section 2.1 gives an introduction to aerosols focusing on mineral dust. A brief description of the methodologies of mineral dust characterisation is given in section 2.2. Section 2.3 concerns the study of mineral dust over Portugal. The last section (Section 2.4) presents a summary and some conclusions.

2.1 Introduction

Aerosols play a crucial role in all processes involved the atmosphere of the Earth. An aerosol is defined as liquid or solid particles, such as mineral dust, fume, smoke, mist, fog,

haze and smog suspended in a gas (Seinfeld and Pandis, 2006). Atmospheric aerosols are associated with environmental impacts at local and global scales. They have detrimental effects on the health of living organisms (e.g. Pope and Dockery, 2006; WHO 2006a, WHO 2006b) and have direct and indirect effects on the climate system (IPCC, 2001; IPCC, 2007). Atmospheric aerosols are emitted by anthropogenic and natural sources. According to the definition in the Directive 2008/50/EC (EC, 2007), the natural sources are the emission of pollutants not caused directly or indirectly by human activities, including natural events (Figure 2.1) such as volcanic eruptions, seismic activities, geothermal activities, wild-land fires, high wind events, sea sprays or the atmospheric re-suspension or transport of natural particles from dry regions.

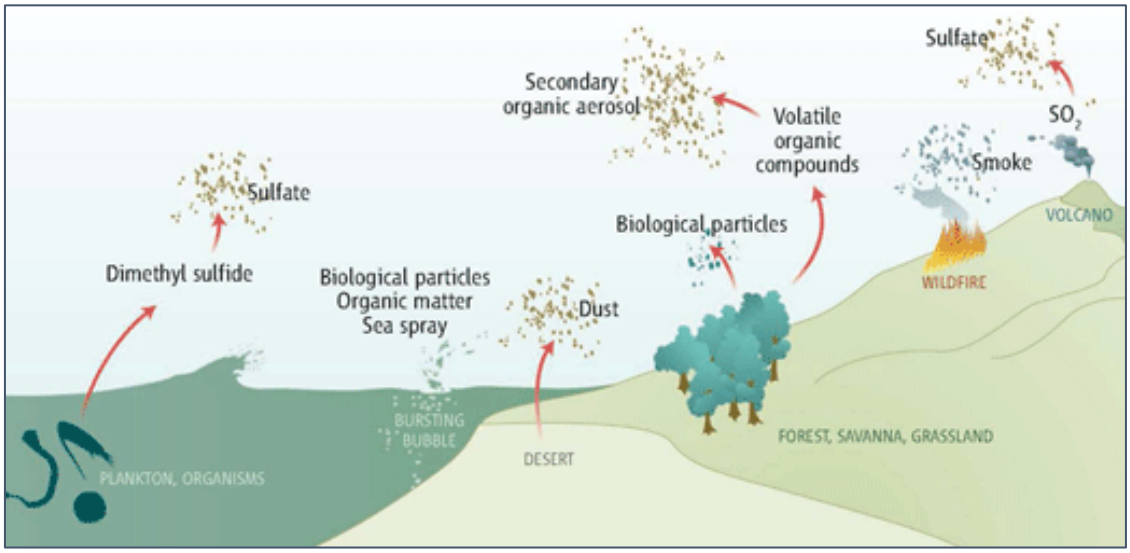

Figure 2.1. Illustration of natural sources of aerosols (Andreae, 2007).

In recent years, there has been an increasing interest to research the influence of natural aerosols in air quality. Natural sources of atmospheric aerosols may play an important role in the occurrence of pollution episodes (Pérez et al., 2006a; Niemi et al., 2009; Allen and Sherwood, 2010).

On a global scale, most atmospheric particles are emitted by natural sources. Thus, mineral dust being the second most abundant component after sea spray-derived aerosols (IPCC, 2007). In addition, in Europe, mineral dust and sea salt are the most important natural sources contributing to the total aerosol loading. According to the EU Report (IES-JRC,

2007), the contribution of the natural sources to the PM levels in Europe may range from 5% to 50%. Contributions from natural sources to atmospheric aerosols vary widely with time and as a function of the distance to the source. Mineral dust outbreaks are one of the main causes of high PM10 particle mass concentrations in Southern Europe (Rodríguez et al., 2001; Borge et al., 2007; Wagner et al., 2009, Pey et al., 2013) and several studies stress the importance of mineral dust long-range transport from North Africa deserts to specific Mediterranean Southern European countries like Portugal (Reis et al., 2002; Fialho et al., 2006; Freitas et al., 2007; Wagner et al., 2009; Preißler et al., 2011; Tchepel el at., 2013).

Mineral dust aerosols are soil particles suspended in the atmosphere emitted from soils in arid and semi-arid regions under favourable weather conditions. These are mainly composed of oxides (e.g. SiO_2, Al_2O_3, FeO, Fe_2O_3, CaO) and carbonates ($CaCO_3$, $MgCO_3$). For a long time, the Sahara Desert was considered the main source of mineral dust on the Earth, with 60-200 millions of mineral dust tons emitted every year (Junge, 1979; Morales, 1986).

During strong dust events caused by surface winds due to intense low pressure systems, mineral dust has a significant impact on human health, weather, climate and biogeochemistry. There is substantial evidence of its association with mortality, morbidity and incidence of meningitis during episodes of high concentrations such as Saharan dust storms that affect Europe (Perez et al. 2008; Mallone et al. 2011; Pérez García-Pando et al, 2014). Mineral aerosols represent one of the most important aerosols in mass and aerosol optical depth (Tegen et al., 1997), and can significantly impact the radiation balance during strong events or even in the annual mean (Li et al., 2004). Desert dust can interact with liquid or ice clouds, and thereby modify the optical properties and lifetimes of clouds (Smoydzin et al., 2012), as well as affect precipitation processes (Creamean et al., 2013). Once dust particles are deposited on the surface, they provide micro nutrients to the ocean (e.g. Jickells et al., 2005) or to land ecosystems (e.g. Okin et al., 2008), and can modify the snow albedo (Painter et al., 2007).

For mineral dust aerosols, both composition and size vary greatly over space and time. The lifetime of particles on the atmosphere depends on their size, as larger particles fall much faster than smaller particles, due to friction. (Seinfeld and Pandis, 2006; Mahowald et al., 2014). Smaller particles (with a diameter <20 μm) can be lifted into the atmosphere and travel long distances. The size distribution of the mineral dust particles strongly depends of the distance between the location of the receptor area and the emission source. Thus,

during episodes of transport of particles towards the American continent the size mode is within the fine fraction (<2.5 μm), while during episodes over the Mediterranean the main size mode is in the coarse fraction (>2.5 μm). In Southern Europe, natural episodes are more frequent in spring/summer, when synoptic conditions are favourable for the transport of dust from North Africa (IES-JRC, 2007).

In this chapter, the main objective is to study the influence of African dust outbreaks over Portugal in 2011. Results from this chapter are important to justify the study period that was selected for the work presented in this thesis.

2.2 Methodologies for the identification of mineral dust events

Natural events such as mineral dust episodes may drastically increase the particulate matter (PM) levels over the usual background concentrations, in many cases exceeding the daily limit value of PM10 (particulate matter with diameter <10 μm) of 50 $\mu g \cdot m^{-3}$ established in the European Directive for air quality (2008/50/EC). The contributions from natural sources can be assessed but cannot be controlled. Therefore, the European Directive for air quality (2008/50/EC) provides the possibility to subtract the contribution of natural sources before comparing the ambient air pollutant concentrations to the limit values, which may therefore reduce the number of exceedances in the reporting system due to non-anthropogenic origin of the pollution (EC, 2011). The identification of such episodes and the quantification of daily and annual contributions of desert dust to PM are currently necessary. In the absence of a single, recognised standard procedure, various studies have been conducted to assess the impact of Saharan dust on PM10 concentrations in Europe, especially in the Iberian Peninsula (e.g. Escudero et al., 2007a; Escudero et al., 2007b).

The occurrence of natural events is detected using different methodologies in the different European regions (Viana et al., 2014). In terms of mineral dust events, the most widely used methods are based on the methodology described by Escudero et al (2007b). This methodology is based on the interpretation of aerosol maps simulated by atmospheric models (e.g., DREAM8b-BSC, NMMB/BSC-Dust model and SKIRON), back trajectories and satellite imagery (e.g. SeaWIFS, TOMS, MODIS, SEVIRI and OMI), and the assessment of PM time series at regional background stations by means of the calculation of the 40^{th} percentile. Figure 2.2 illustrates the type of data used to identify the mineral dust

events. These methods allow to quantify the mass African dust load without chemical speciation.

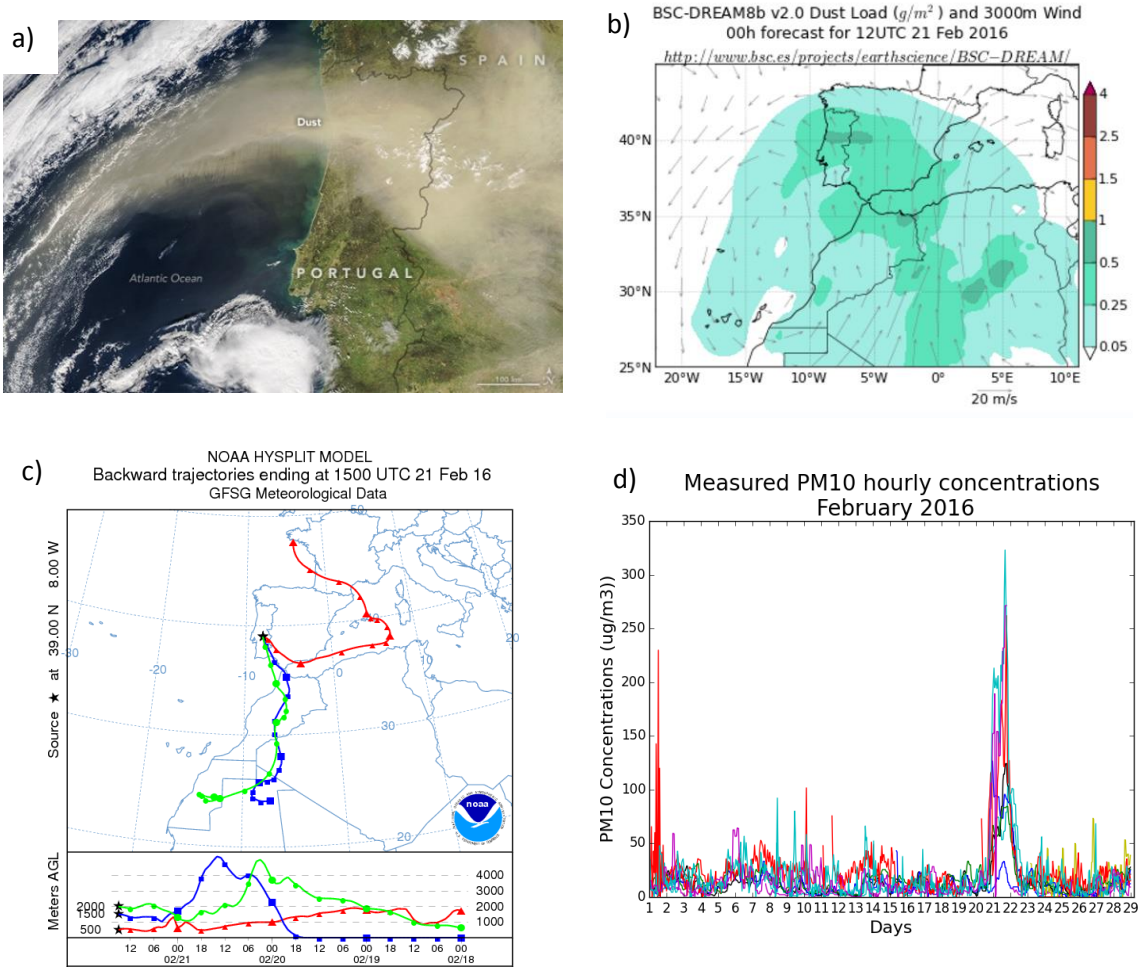

Figure 2.2. African mineral dust event occurred over the Iberian Peninsula in February 2016. This Figure shows: a) The Moderate Resolution Imaging Spectroradiometer (MODIS) on NASA's Aqua satellite acquired a natural-colour image (lower). b) Spatial distribution of mineral dust load ($g \cdot m^{-2}$) from BSC-DREAM8b model, c) HYSPLIT backward trajectories for 500, 1500 and 2000 m above sea level for the centre of Portugal and d) Measured PM10 concentrations from Air Quality Stations.

2.3 Mineral dust over Portugal

Air quality models are powerful tools to predict the fate of aerosols after their release into the atmosphere. Several models have been designed to describe the atmospheric life cycle

of the eroded desert dust, which take into account all major processes of the life cycle of dust, such as production, horizontal and vertical diffusion and advection, and wet and dry deposition. The World Meteorological Organization (WMO) recently established the Sand and Dust Storms Warning Advisory and Assessment System (SDS-WAS) to enhance the ability of countries to deliver timely and high-quality sand and dust forecasts, observations, information, and knowledge to users. Within this program, the North Africa, Middle East and Europe Regional Center SDS-WAS, hosted by the Spanish Meteorological Agency (AEMET) and the Barcelona Supercomputing Center – Centro Nacional de Supercomputación (BSC-CNS), aims to lead the development and implementation of a system for dust observation and forecast. Currently, this Regional Center distributes forecasts over North Africa and Europe from eight models, including the regional BSC-DREAM8b model (Pérez et al., 2006a; Pérez et al., 2006b; Basart et al., 2012b), which are near-real-time evaluated.

In this section, the influence of mineral dust outbreaks over Portugal is studied using mineral dust surface concentrations simulated by the BSC-DREAM8b v1.0 model (Pérez et al., 2006a; Pérez et al., 2006b; Basart et al., 2012b) over the whole year of 2011. The BSC-DREAM8b v1.0 model was selected due to its large past application. The spatial and temporal patterns of mineral dust over Portugal are analysed, in terms of concentration in the long term and during high peak episodes. The synoptic patterns associated with the high peak episodes are also analysed using a back trajectories clustering approach and their relevance is discussed.

2.3.1 BSC-DREAM8b model description

The BSC-DREAM8b v1.0 model (Pérez et al., 2006a; Pérez et al., 2006b; Basart et al., 2012b), developed at the BSC-CNS, was used in this work to characterise the long-range transport of mineral dust from North African deserts to Portugal. The model solves the Euler-type partial differential non-linear equation for dust mass continuity, and it is fully embedded as one of the governing prognostic equations in the Eta/NCEP (National Centers for Environmental Prediction) atmospheric model (Black, 1994). Thus, the model is able to simulate and predict the three-dimensional field of dust concentration in the troposphere taking into account all major processes of the dust life cycle. During the modelling process the calculation of the dust injection is processed over the model points classified as deserts. Once injected into the air, the mineral dust is driven by atmospheric variables. First, the

mineral dust is integrated by turbulent parameters in the early stage of the process when dust is lifted from the ground to the upper levels. After, the mineral dust is influenced by winds fields provided by meteorological models. Finally, by thermodynamic processes and rainfall it was obtained wet and dry deposition results of the mineral dust over the Earth surface.

The main features of BSC-DREAM8b, described in detail by Pérez et al. (2006b) and Gama et al. (2015), include a source function based on the aridity categories of the 1 km USGS land use data set, a dust size distribution profile described by 8 size bins within the 0.1-10 μm radius range according to Tegen and Lacis (1996) (see Table 2.1), a source distribution derived from D'Almeida (1987), and dust radiative feedbacks (Pérez et al., 2006b). The emission scheme implemented in BSC-DREAM8b, described in detail in Basart et al. (2012b), directly entrains dust-sized particles into the atmosphere and includes the influence of soil structure and particle size distribution, as well as of the atmospheric conditions – the near-surface wind speed must exceed the local threshold velocity to force dust mobilization.

Table 2.1. Dust size bins distribution parameters. From left to right: bin number, minimum and maximum radius of each size bin (r_{min}-r_{max}), effective radius of each bin (r_{eff}), extinction efficiency (Q_e) at 532 nm and 1064 nm (Pérez et al. 2006b).

Bin	r_{min} - r_{max} (μm)	r_{eff} (μm)	Q_e 532 nm	Q_e 1064 nm
1	0.1 – 0.18	0.15	1.373	0.217
2	0.18 – 0.3	0.25	3.303	1.043
3	0.3 – 0.6	0.45	3.245	3.300
4	0.6 – 1.0	0.78	2.413	3.509
5	1.0 – 1.8	1.3	2.262	2.293
6	1.8 – 3.0	2.2	2.260	2.282
7	3.0 – 6.0	3.8	2.162	2.217
8	6.0 – 10.0	7.1	2.108	2.164

2.3.2 Model application and validation

In this work, the simulation domain covers a large area, including North Africa, Middle East and Europe, with Portugal highlighted in dark blue in Figure 2.3. The initial state of the dust

concentration is defined by the 24-h forecast of the previous-day model run. Meteorological fields are initialized every 24 h, at previous-day 12 UTC, and boundary conditions updated every 6 h with the Global Forecast System (GFS) of NCEP. The resolution is set to a third of a degree in the horizontal direction and to 24 layers extending up to approximately 15 km in the vertical direction, where the near surface corresponds to approximately 86 meters AGL. Model outputs are processed in a 3-hour basis.

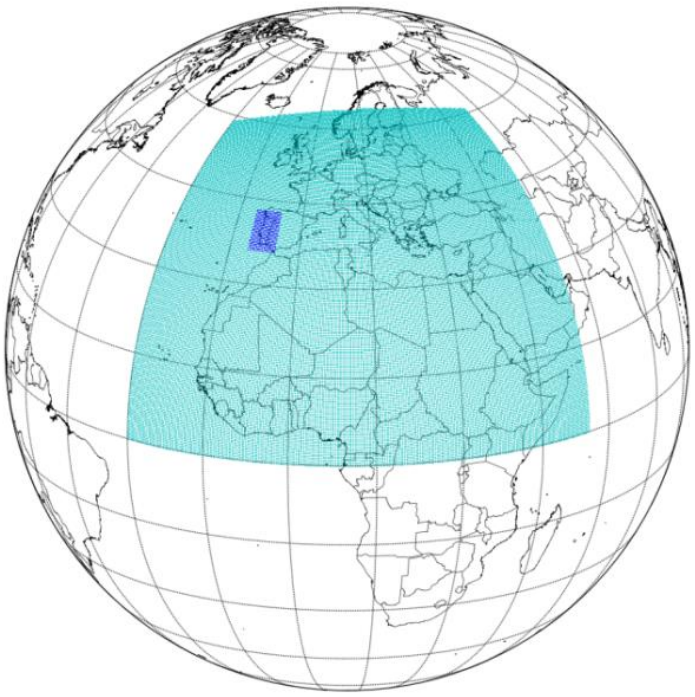

Figure 2.3. BSC-DREAM8b v1.0 model simulation domain, with the domain over Portugal highlited [correspondig to 396 grid cells (18x22)].

Several case studies have outlined the accuracy of BSC-DREAM8b. In the last years, this model has been used for dust forecasting and as a dust research tool in North Africa and Southern Europe (Jiménez-Guerrero et al., 2008; Amiridis et al., 2009; Klein et al., 2010; Pay et al., 2010; Alonso-Perez et al., 2011; Basart et al., 2012b; Kokkalis et al., 2012) and in the Cape Verde region (Gama et al., 2015). The model has also been tested over longer time periods in Europe (Basart et al., 2012a; Pay et al., 2012; Tchepel et al., 2013) and against measurements at source regions (Haustein et al., 2009; Todd et al., 2008).

Furthermore, daily evaluation of BSC-DREAM8b with near-real-time observations is conducted at BSC-CNS [URL1]. Currently, the daily operational model evaluation includes observations from satellites (MODIS and MSG) and AErosol RObotic NETwork (AERONET)

sun photometers. The work presented here uses the BSC-DREAM8b surface concentration data estimated for Portugal to assess and characterise the mineral dust concentrations over a one-year period (2011), after a model validation exercise regarding this particular application over Portugal.

In order to support the use of model results for the assessment of mineral dust over Portugal, a validation exercise was performed using the comparison between the modeled mineral dust concentration with diameter below 10 µm (MD10) and the observed particulate matter with aerodynamic diameter below 10 µm (PM10). This was done for seven different locations, spatially distributed along mainland Portugal, and corresponding to background air quality monitoring sites where PM10 is measured continuously (Figure 2.4). The daily mean time series comparison is shown in Figure 2.5.

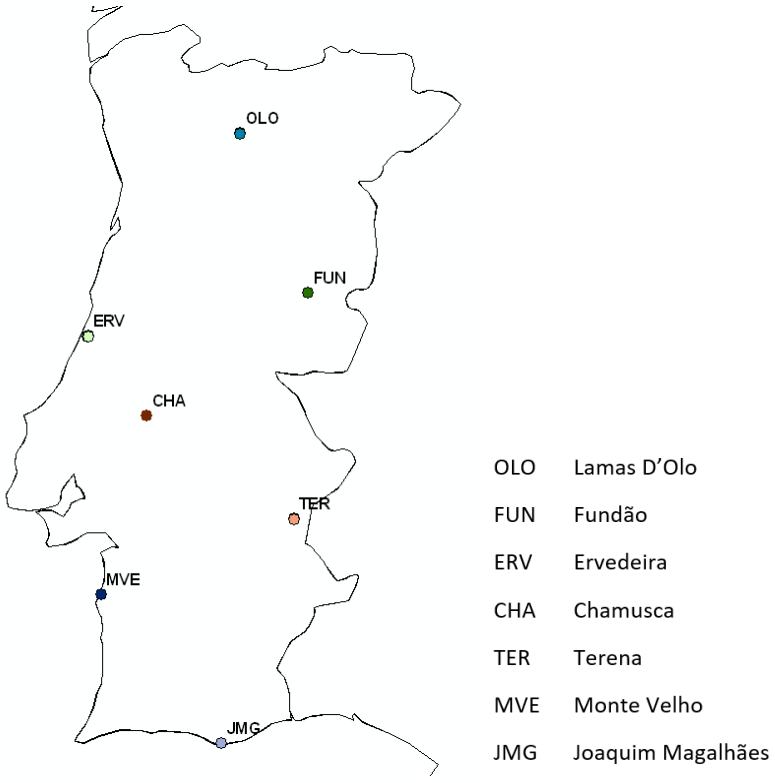

Figure 2.4. Location of PM_{10} monitoring sites over Portugal.

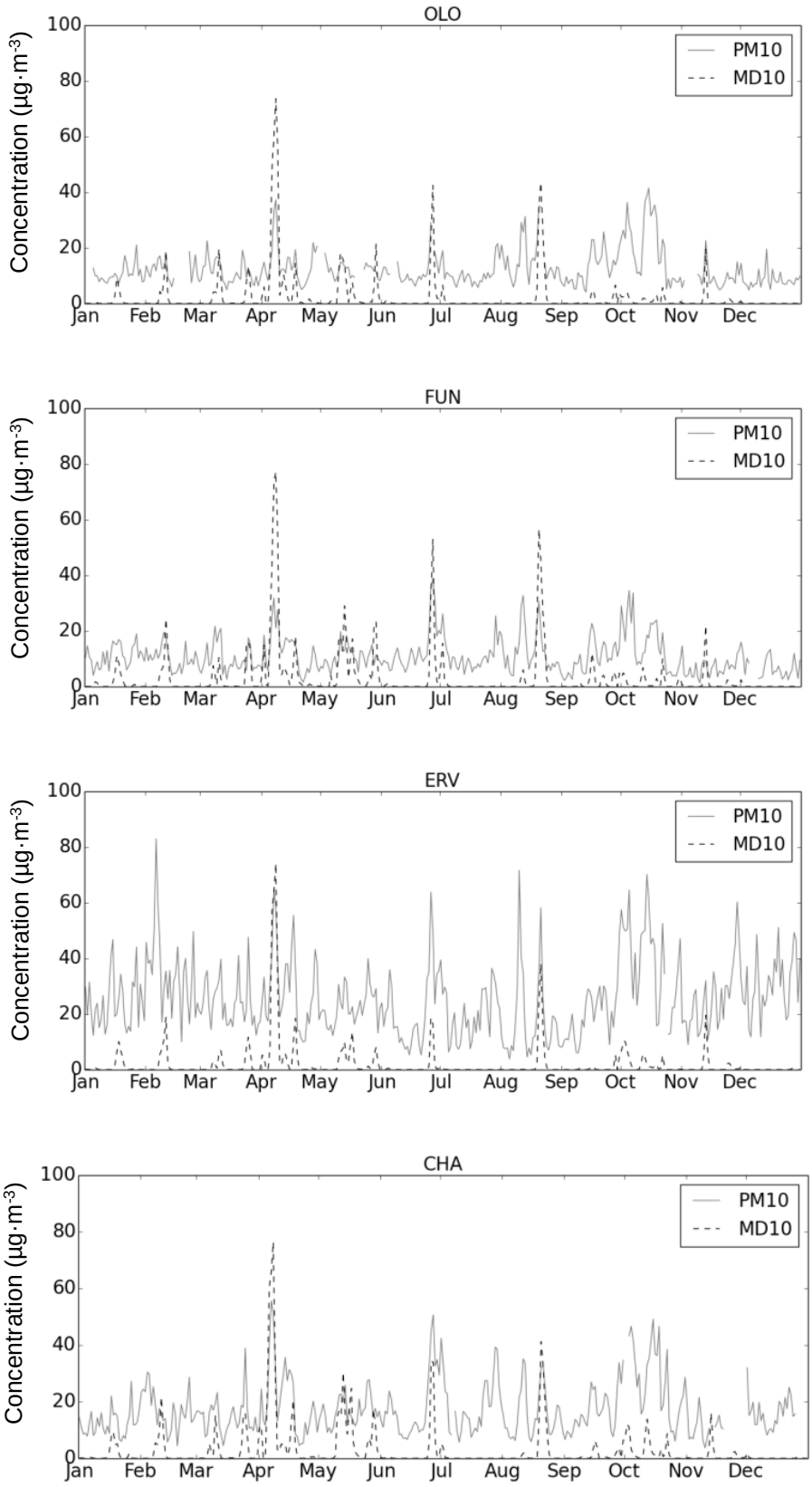

Figure 2.5. Time series of daily mean observed PM10 (solid gray line) and simulated MD10 (dashed black line) for four sites: Lamos D'Olo, Fundão, Ervedeira and Chamusca for 2011.

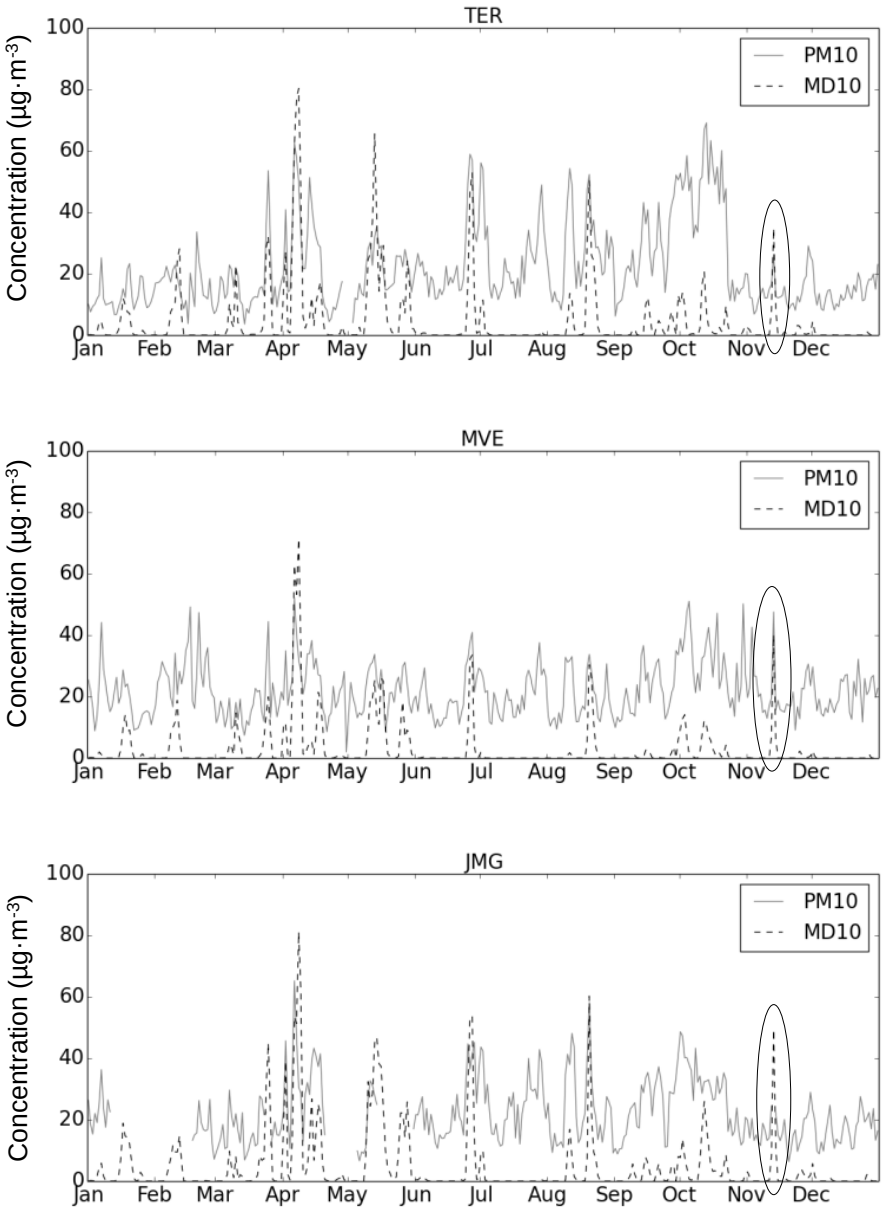

Figure 2.6. Time series of daily mean observed PM10 (solid gray line) and simulated MD10 (dashed black line) for three sites: Terena, Monte Velho and Joaquim Magalhães for 2011.

As expected, Figure 2.5 and Figure 2.6 show that the PM10 observed concentrations are, in general, higher than the MD10 modelled concentrations. In general, the peaks of dust concentration coincide with PM10 peaks, which suggests a good performance of the BSC-DREAM8b model. Nevertheless, the model overestimates the dust concentrations in some cases, namely in April (e.g. in OLO, FUN, CHA). This overestimation in the spring period had already been identified. According to Basart et al (2012b), the model shows an overestimation of the dust activity in Northern Algeria when compared to satellite estimates, thus affecting the dust transported towards the Western and Central Mediterranean mainly in spring.

A quantitative analysis was performed using statistical indicators, namely the Root Mean Square Error (RMSE) and the Mean Systematic Error (BIAS) which are measures of the unsystematic (random) and systematic errors obtained within the observed-predicted pairs of results, respectively (Borrego et al., 2008). The statistical results are shown in Table 2.2, taking into account only the episodes period (simulated ground dust concentration > 5 $\mu g \cdot m^{-3}$), since in the other periods the dust concentration is approximately zero.

Table 2.2. Statistical indicators used for model validation (RMSE and BIAS).

Monitoring stations	**Observed mean (PM10)($\mu g \cdot m^{-3}$)**	**Simulated mean (MD10)($\mu g \cdot m^{-3}$)**	**RMSE** (Eq. 2.1) **($\mu g \cdot m^{-3}$)**	**BIAS** (Eq. 2.2) **($\mu g \cdot m^{-3}$)**
OLO	16.9	11.9	14.9	-4.8
CHA	25.7	14.8	16.5	-10.9
ERV	34.0	13.3	24.4	-23.7
FUN	17.1	16.0	14.4	-1.0
JMG	34.5	22.2	23.2	-12.4
MVE	28.3	14.8	18.4	-13.5
TER	35.3	22.8	22.1	-13.5
Average	**27.45**	**16.02**	**19.1**	**-11.3**

$$RMSE = \frac{1}{N}\sqrt{\sum_{i=1}^{N}(Model_i - Obs_i)^2} \qquad \text{Equation 2.1}$$

$$BIAS = \frac{1}{N}\sum_{i=1}^{N}(Model_i - Obs_i) \qquad \text{Equation 2.2}$$

On average the deviation of the BSC-DREAM8b model results is below 20 $\mu g \cdot m^{-3}$, and the negative values of the BIAS indicate that, in general, model results (MD10) are below PM10 observations. Since we are comparing just one fraction of the total PM10, the magnitude of this error is low. During the dust episodes the values of PM10 can contain large fractions of other particulate matter content besides the mineral dust portion (MD10).

2.3.3 Long-term assessment of mineral dust over Portugal

The mineral dust surface concentrations simulated with the BSC-DREAM8b v1.0 model over mainland Portugal during an entire year (2011) were analysed in terms of monthly averages and percentiles, in order to assess their spatial and temporal distribution. In this chapter, we analyse not only the mineral dust fraction with diameter below 10 µm (MD10, but also the total mineral dust simulated by the model (MD), which includes particles with diameter up to 20 µm, as presented in Section 2.1. Figure 2.7 shows the BSC-DREAM8b v1.0 model results for the mineral dust monthly average over 2011.

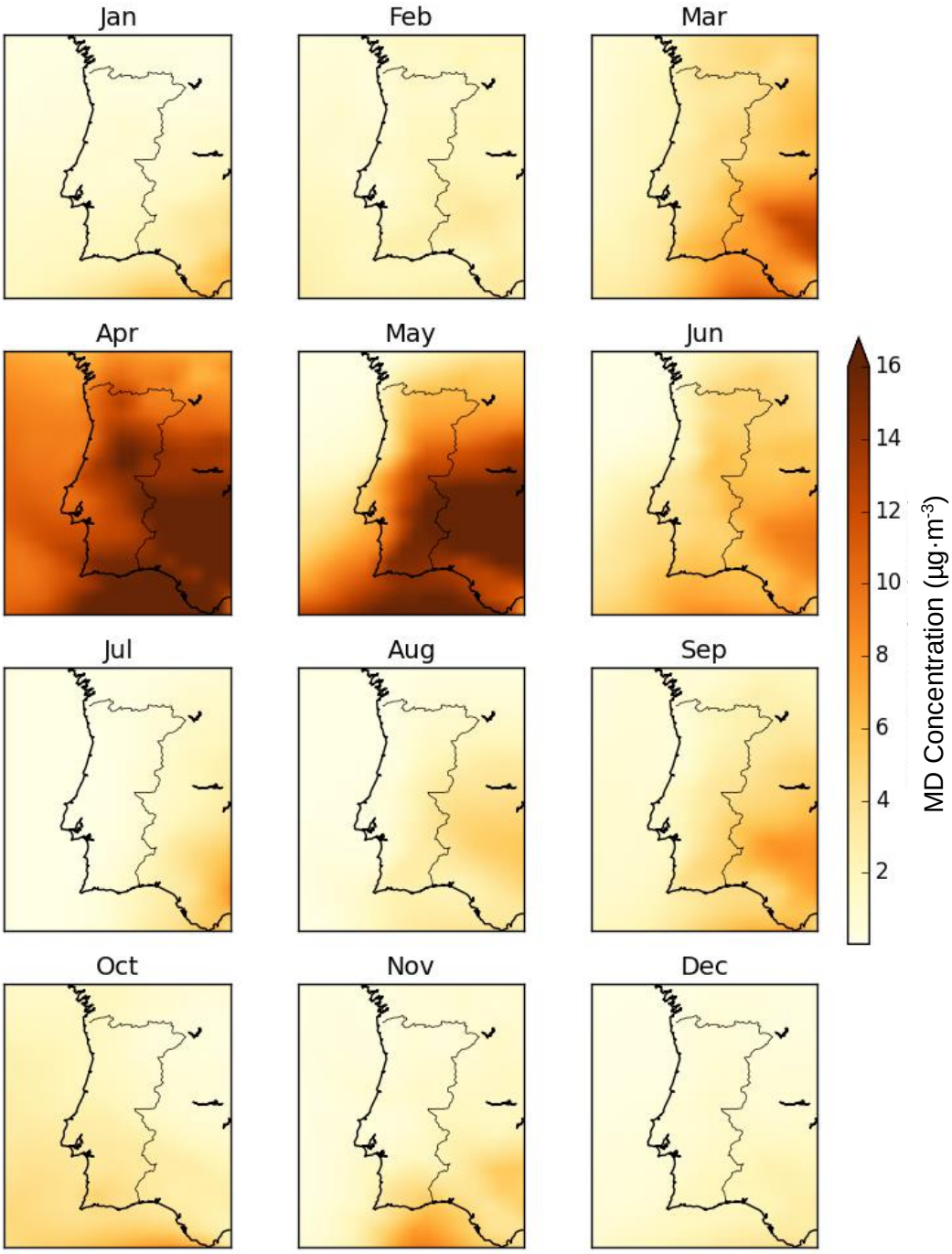

Figure 2.7. Monthly mean of modeled mineral dust surface concentration (µg·m^{-3}) for 2011.

Figure 2.7 highlights that the average values for mineral dust concentrations are significantly higher in April and May than in the rest of the year. During these spring months, mineral dust over Portugal has average contributions over 10 µg·m^{-3} (10-18 µg·m^{-3}), while during summer and winter seasons the mean values are below 6 µg·m^{-3} (0-6 µg·m^{-3}). April

is the month when the highest mean values are expected, and December exhibits the lowest contribution. The spring events were already noticed in previous works, over the Iberian Peninsula and Southwestern Europe (Laurent et al., 2008; Basart et al., 2012b; Gkikas et al., 2012; Pey et al., 2013). However, in the annual BSC-DREAM8b model evaluation shown in Basart et al. (2012b), it is highlighted that the model overestimates the Aerosol Optical Depth (AOD) in Morocco and North Algeria during spring, which may indicate that the strength of this source is being overestimated, thus influencing the modelled surface concentrations in the nearby areas such as the Iberian Peninsula.

The annual mean pattern, shown in Figure 2.8, reflects the several months where the influence of the Sahara mineral dust is not frequent. Only the Southwest region of Spain exhibits a high annual average of mineral dust (> 10 $\mu g \cdot m^{-3}$). Throughout the Portuguese territory, the magnitude of the annual average values varies between 2-6 $\mu g \cdot m^{-3}$.

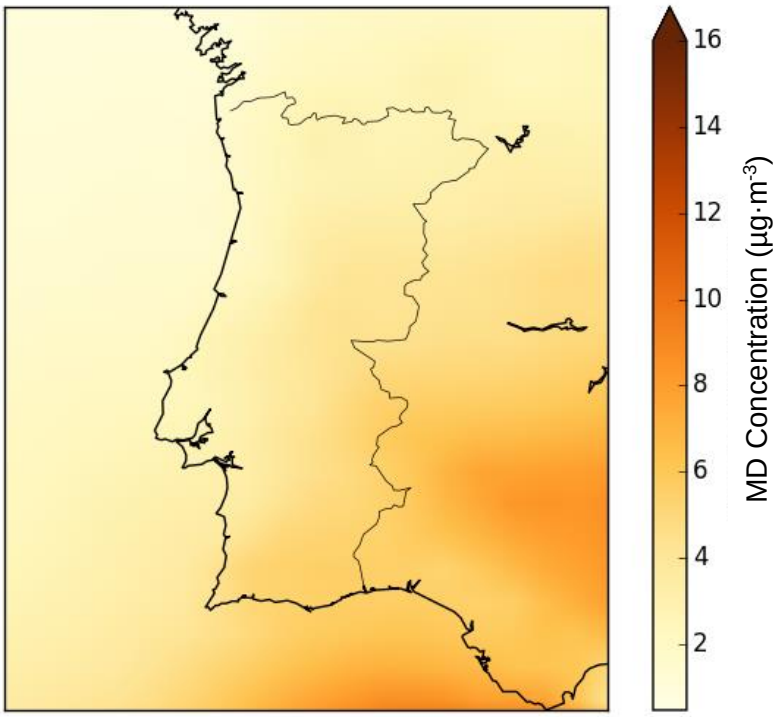

Figure 2.8. Annual mean of modelled mineral dust surface concentration ($\mu g \cdot m^{-3}$) for 2011.

Besides the monthly and annual characterisation, the frequency of low, median and high values of mineral dust was also analysed. Figure 2.9 presents the results obtained with the BSC-DREAM8b v1.0 annual simulation for different percentiles, in order to show the spatial distribution of mineral dust.

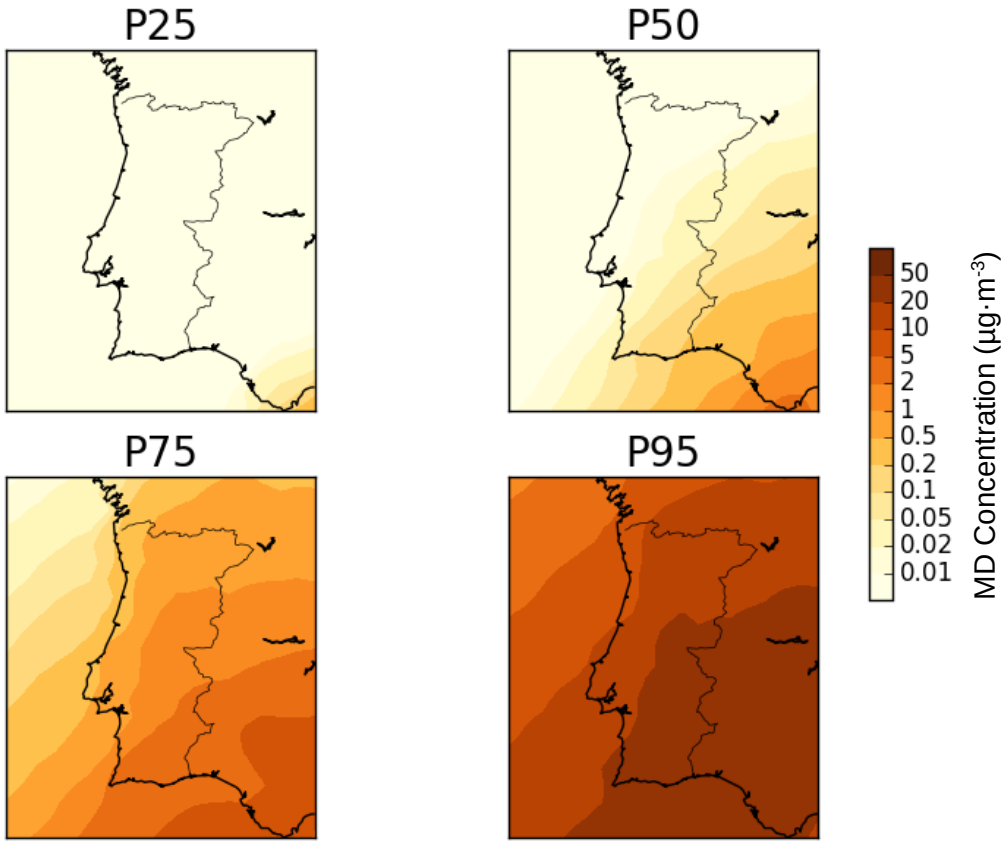

Figure 2.9. Spatial representation of 25th (P25), 50th (P50), 75th (P75) and 95th (P95) percentiles of the modelled mineral dust concentrations for 2011.

Starting with the percentile 25 (P25), and as one would expect, the lowest values of mineral dust over mainland Portugal are close to 0 µg·m^{-3}. The analysis of P50 indicates that the influence of the transport of mineral dust over Portugal is time-scale limited, since during 50% of the time this contribution is below 0.2 µg·m^{-3}. Only when higher percentiles are analysed (e.g. P75) does the concentration of mineral dust over Portugal domain become ≥ 2 µg·m^{-3}. At percentile 95 (P95), one observes the magnitude and location of the episodes of mineral dust which occurred in Portugal over 2011. These episodes are significantly stronger in the Southeastern region of the country, exhibiting P95 values higher than 30 µg·m^{-3}. In the rest of the Portuguese territory, the peak contribution of mineral dust is around 10-25 µg·m^{-3}.

2.3.4 Analysis of mineral dust episodes

Identification and selection of mineral dust episodes

In addition to the long-term assessment of mineral dust over Portugal, this work aims to assign and analyse the days when a significant contribution of mineral dust is transported over Portugal. With this in mind, a threshold above 5 $\mu g \cdot m^{-3}$ (above the magnitude of the simulated annual average; see Figure 4) was considered to select this group of days. Simulated mineral dust data were extracted for the 7 locations of Figure 2.4 (monitoring sites used to analyse the behaviour of the model) taking into account the threshold mentioned above .

Seventeen episodes for 2011 were selected from the time series with mineral dust daily mean concentrations above 5 $\mu g \cdot m^{-3}$ over all the analysed sites. The duration of the chosen episodes ranges from 2 to 9 days. Table 2.3 summarises the selected episodes, the corresponding days, the maximum concentration of mineral dust, and the location where the maximum was registered.

Table 2.3. Identification and characterisation of the selected episode days for 2011.

Episode No.	Months	Days	Duration (No. of Days)	Maximum Concentration of MD10 ($\mu g \cdot m^{-3}$) and Location	
1	January	17 -19	3	18.9	JMG
2	February	08 – 12	5	28.1	TER
3	March	10 – 11	2	22.8	TER
4	March	24 – 26	3	44.9	JMG
5	April	01 – 02	2	39.1	JMG
6	April	05 – 09	5	81.1	JMG
7	April	12 – 19	8	26.8	JMG
8	May	10 – 18	9	65.5	TER
9	May	28 – 29	2	25.8	JMG
10	June	25 – 28	4	53.7	JMG
11	July	01 – 02	2	15.6	FUN
12	August	19 – 23	5	60.2	JMG
13	September	15 – 17	3	12.2	TER
14	September/ October	30 / 01 – 03	4	14.1	MVE
15	October	11 – 13	3	25.9	JMG
16	October	21 – 22	2	9.9	FUN
17	November	12 – 14	3	49.4	JMG

The selected episodes (concentrations of mineral dust higher than 5 $\mu g \cdot m^{-3}$) occurred on the same days in all analysed sites, but with different magnitudes. The episodes are distributed over the entire year, with predominance on the months of April, May and June. The longest episode was registered in May (episode no. 8) and lasted for 9 days (10-18 May 2011). Besides this one, the duration of the majority of the episodes was about 2-6 days, which is consistent with the synoptic patterns lifetime as described by Cahynová and Huth (2009).

The episode with the highest concentrations was simulated in April (5th-9th), when mineral dust surface concentrations reached around 60-80 $\mu g \cdot m^{-3}$ over all the different locations. The Southern sites (JMG, TER and MVE) show the highetintensity on the peak episodes. The last episode identified (12th-14th November) is a good example of the higher magnitude over the Southern sites (emphasized with a black circle in Figure 2.6).

Clustering analysis of the mineral dust episodes

In this section, the origin of the air parcels trajectories that arrive at each monitoring site during the selected episode days was studied. A cluster analysis of the obtained back trajectories was performed to reduce the number of ‘‘origins of air masses’’, appointing every calculated individual back trajectory to the most appropriate cluster, in order to identify and to better interpret mean synoptic situations related to the mineral dust episodes.

The back trajectories technique is a useful tool in tracing source regions of air pollution and determining transport patterns at receptor sites (Jorba et al., 2004). In this study, five-day (120 h) kinematic back trajectories arriving at 12 UTC at 1000 m AGL at each of the study sites were estimated for the whole year 2011. The air parcel trajectories were obtained with version 4.8 of the Hybrid Single-Particle Lagrangian Integrated Trajectory model (HYSPLIT) developed by the National Oceanic and Atmospheric Administration (NOAA) Air Resources Laboratory (ARL) (Draxler and Hess, 1998; Draxler and Hess, 1997). Meteorological data from the NCEP Global Data Assimilation System - GDAS (Kanamitsu, 1989), with a horizontal resolution of one degree and a 3-hour time resolution, was used to compute the trajectories. Even though the meteorological inputs for HYSPLIT and BSC-DREAM8b are different, the predicted synoptic patterns are quite similar, at least for the periods studied in this work.

A hierarchical clustering method was chosen to extract a natural number of clusters for the different individual back trajectories, corresponding to the episodes that occurred during

both the study day and the whole year. The clustering iterations involved the calculation of a statistical measure, the cluster spatial variance (SPVAR, defined as the sum of the squared distances between the endpoints of the component trajectories of the cluster and the mean of the trajectories in that cluster), for every possible combination of trajectory/cluster pairs. In each iteration, a pair of clusters was returned and chosen to be the one associated with the lowest increase in the total spatial variance (TSV, defined as the sum of all the SPVAR). Before the first clustering iteration, each trajectory was defined to be a cluster, e.g. there were N trajectories and N clusters, and TSV was equal to zero. After the first iteration, the number of clusters was N-1. The iterations continued until the last two clusters were combined, resulting in all the individual trajectories combined in the same cluster (Dorling et al., 1992).

In the first few clustering iterations, the TSV increases greatly, then for much of the clustering it typically increases at a small, generally constant rate, but at some point it again increases rapidly, indicating that the clusters being combined are not very similar. This last increase suggests where to stop the clustering method and it is clearly seen in a plot of the percentage of change in TSV vs. the number of clusters (not shown). Using the minimum optimal number of clusters as a selection criterion, different groups of clusters were identified for each specific site and are plotted in Figure 2.10, along with the respective mineral dust modelled statistics associated to each of the designed trajectories.

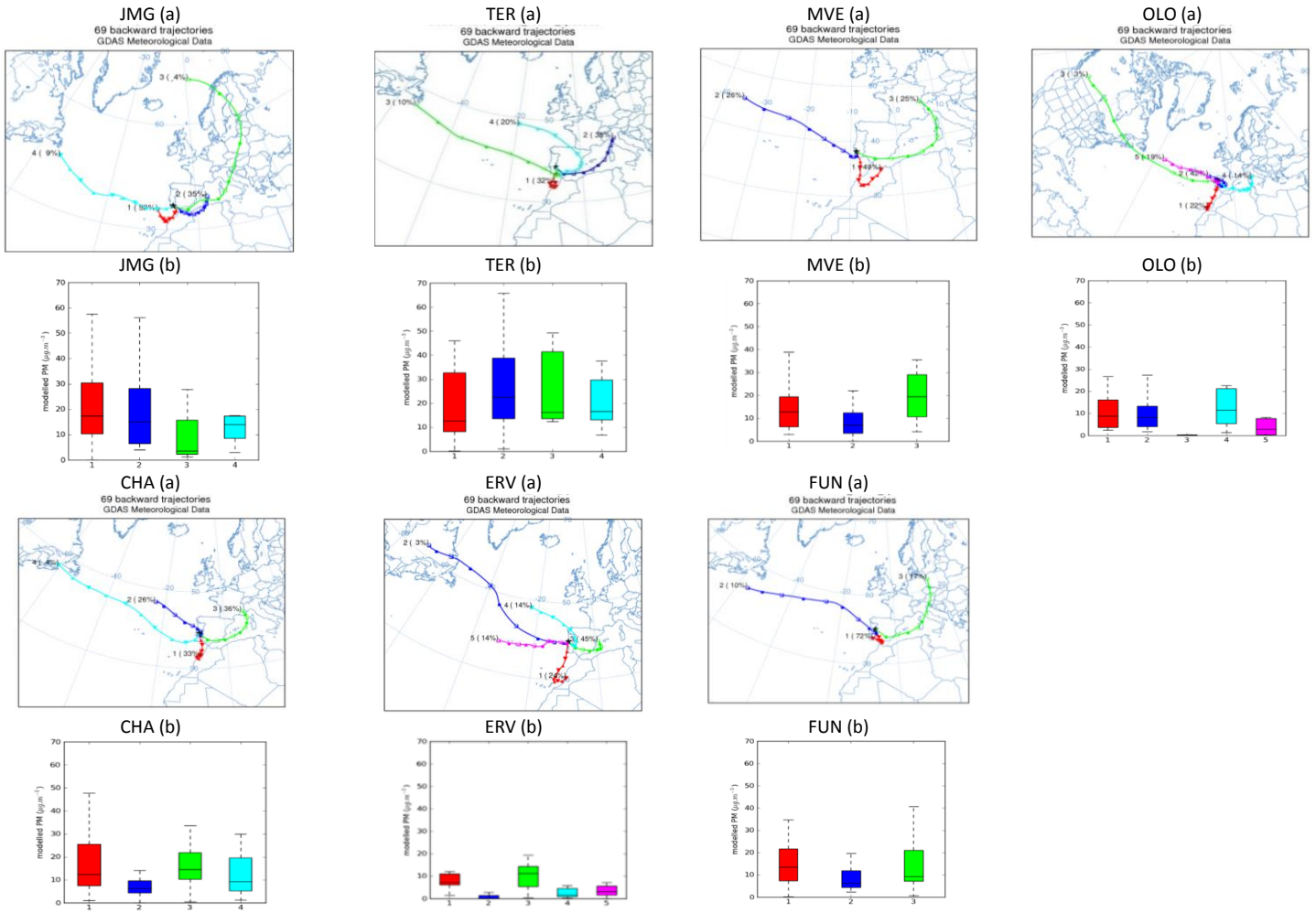

Figure 2.10. Cluster mean trajectories identified for each study site (see Figure 2.4) during the selected episodes days, and modelled mineral dust concentration statistics associated to each of the identified trajectories (same color representation).

Between three and five major types of flow patterns are identified for the study period. These mean flow pathways (clusters) obtained for the different sites can easily be distinguished in terms of spatial, dynamic and temporal patterns.

The site of JMG (in the South coast of Portugal) is the one where the trajectories of air masses coming from the North African coast are more pronounced (cluster 1 with a frequency of occurrence of 52% and cluster 2 with 35%, Figure 2.10a) and are responsible for the highest modelled mineral dust concentrations (box plot, Figure 2.10b). The site of TER, closer to JMG in the North direction, also exhibits a prevalence of the flow regimes coming from the African coast (cluster 1 and cluster 2 with 32% and 38% frequency, respectively) but with a less expressive contribution for modelled concentrations.

The MVE site, located in the South-west coast of Portugal, and FUN, sited in the interior central domain, also present a high predominance of the flow regimes coming from North Africa during the selected episode days (MVE - cluster 1: 49% and cluster 3: 25%; FUN - cluster 1: 72% and cluster 3: 17%), associated with higher modelled concentrations.

The last three sites – CHA, ERV and OLO – located in the central and Northern regions of Portugal, present a lower influence of the air flow trajectories coming from North Africa (cluster 1 with 33%, 24% and 22% of frequency; respectively) associated with lower mineral dust concentration values (Figure 2.10). The lowest influence of the North Africa flow regimes and thus lower associated PM concentrations were found at the OLO site, which can be justified mainly by its remote location in the North of Portugal. Nevertheless, even in this distant place, during the selected episode days, a contribution of 22% of the air masses regime (cluster 1) was estimated and concentrations of 5-25 $\mu g \cdot m^{-3}$ of mineral dust (associated to these air masses trajectories) were predicted by the model.

In order to analyse the representativeness and relevance of the selected episode days regarding the entire year of 2011, Figure 2.11 presents the cluster annual mean trajectories for the whole 2011, for the different study sites.

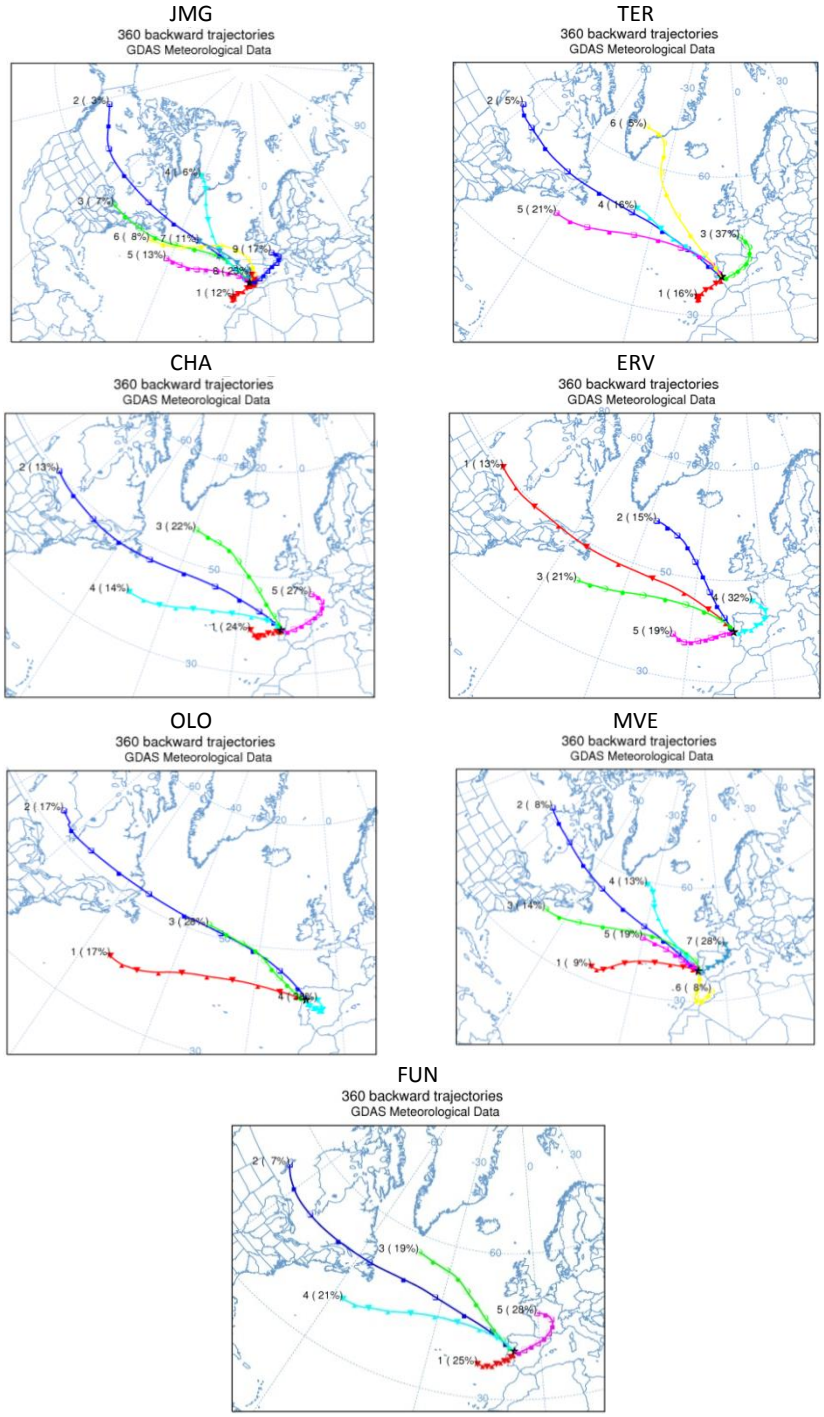

Figure 2.11. Cluster mean trajetories obtained for the entire year of 2011, for diferent sites (JMG, MVE, TER, CHA, ERV, FUN and OLO).

There are two distinct groups of sites regarding the relevance of the air flow patterns coming with influence from North Africa. The first group includes the sites of JMG, TER and MVE, located in the South and Southwestern coasts of Portugal, where the frequency of occurrence of these Southern patterns is about 8-16% of the total air masses trajectories

occurred during the entire year. This percentage is, however, not significantly high, when compared to the dominant flow patterns from the Atlantic Northwest corridor.

All the other study sites – FUN, CHA, ERV and OLO – located in the central and Northern part of Portugal show a cluster pattern with lower Southern influence, which is more evident for OLO site. This indicates that in these particular sites the prevailing air flow patterns have other origins, predominantly from the Atlantic Northwestern direction, but also from the Northeastern inner part of the Peninsula. This Atlantic Northwest dominant pattern is even more evident for the OLO site, where the entire mean clusters have this direction.

2.4 Summary and conclusions

This chapter focused on the study of the mineral dust transported to Portugal, in terms of long-term assessment and also high episode peaks. The application of the BSC-DREAM8b v1.0 model (already validated in previous studies) to a domain which includes North Africa and Middle East source regions, for the entire year of 2011, allows the characterisation of the magnitude and spatial distribution of mineral dust over Portugal. The annual mean pattern of the simulated dust has a magnitude of 2-6 $\mu g \cdot m^{-3}$, where the monthly average highlights the largest mineral dust values in April and May (on average 4 $\mu g \cdot m^{-3}$ higher than during the other months). The influence of the transport of mineral dust to Portugal is limited on time scale, since in 50% of the time (percentile 50) this contribution is below 0.2 $\mu g \cdot m^{-3}$. Only when high percentiles are analysed does the concentration of mineral dust over Portugal become relevant (> 3 $\mu g \cdot m^{-3}$; with peak contribution around 10-25 $\mu g \cdot m^{-3}$).

In order to characterise the highest episodes of dust occurred in Portugal, a group of episode days with dust daily concentration above 5 $\mu g \cdot m^{-3}$ was selected, and data were extracted for 7 different locations, spatially distributed along the country (and coincident with monitoring sites). A cluster analysis of the air parcels back trajectories that arrive at each site was performed in order to identify the mean flow patterns associated to each mineral dust episode. At the Southern study sites, during the episode days, the trajectories of air masses coming from the North African coast are predominant (with frequency above 70%). The prevalence of the flow regimes coming from Northern Africa during the episode days decreases for the upper latitude sites: the two central region sites still exhibit a frequency above 50%, but this frequency decreases to below 33% for the two sites located in the Northern region.

Chapter 3

Remote Sensing of Aerosols

Chapter Index:

3.1 Introduction……...39

3.2 Aerosol optical properties……43

3.3 Remote sensing techniques……49

3.3.1 - AErosol RObotic NETwork (AERONET)……..50

3.3.2 - Spinning Enhanced Visible and Infrared Imager (SEVIRI)……52

3.4 Methodology for SEVIRI and AERONET data processing……55

3.5 Results and discussion……..57

3.4.1 - AERONET observations……..57

3.4.2 - Evaluation of SEVIRI observations……59

3.6 Summary and conclusions……63

3 Remote Sensing of Aerosols

This chapter comprises a discussion of the main measurement techniques to characterize aerosols through remote sensing. Remote sensing techniques use the interaction between electromagnetic radiation and the atmosphere to obtain aerosol properties, based on principles of light scattering and radiative transfer theories.

This chapter is divided in five sections. Section 3.1 gives an introduction of aerosol remote sensing and an overview of the most common sensors. A brief description about the optical properties of aerosols is given in section 3.2. Section 3.3 presents a description of the main remote sensing techniques used in this thesis. The methodology applied is presented in Section 3.4. Data from the remote sensing techniques are analysed in Section 3.5. A summary and some conclusions are presented on the last section (Section 3.6).

3.1 Introduction

The amount of aerosols present in the atmosphere is highly variable in space and in time. Aerosols play an important role in many physical and chemical processes that change the composition of the atmosphere and thereby affect cloud formation, visibility and air quality. They interact both directly and indirectly with radiation and thus affect the amount of radiative energy reaching the surface and reflected to space (Laszlo et al., 2008). Nowadays, the use of remote sensing techniques to improve the characterisation of aerosols is increasing. Their use for air quality assessment is a current topic of research. Over the last decades, remote sensing observation has been used to obtain information on aerosol properties taking advantage of technical and scientific developments. The

difficulties of aerosols retrieval lie in the fact that, for the characterisation of aerosols, it is not enough to specify their concentration (as it happens for gases) – information on particle size, along with concentration, chemical composition and particle shape as function of size are needed. Currently, aerosol retrievals from passive sensors are available only for the cloud-free sky.

Remote sensing of aerosols from space is a comparatively new emerging technique with the development of satellite technology in the second half of the last century (Lee et al., 2009; Kokhanovsky, 2013). Remote sensing of aerosols over land is particularly important because the sources of most aerosols (mainly anthropogenic aerosols) are located in land. It is very useful to identify aerosol sources and understand aerosol transformations in the atmosphere. A major problem in aerosol retrieval over land is the surface reflectance because it varies spatially and temporally (Lee and Kim, 2010). Another problem is the assumed radiative properties of aerosols because in most of the time does not exist detailed information about size, shape and composition. This information is included in single scattering albedo (SSA) describing the relation between absorption and reflectance behaviour. Depending on the origin of the aerosol, this is changing. Furthermore, precise knowledge of surface reflectance is essential. Small error in this value results in large errors of AOD retrieval. Other problem in aerosol retrieval is the difficulty to distinguish atmospheric aerosols from clouds (Koren et al., 2007, 2008). In particular, it is difficult to tell a cloud from a wet aerosol (Kokhanovsky, 2013).

In the past few decades, satellite measurements have become a valuable and indispensable means to quantify and monitor the concentrations, properties, and atmospheric dispersion of aerosols. Satellite sensors are the only means to provide spatially homogeneous observations about airborne particles. A lot of studies are using Earth observations from satellites because the information provided is both timely and global in coverage and it is better than using local station observations (e.g. Popp et al., 2007).

Nowadays, there are different several types of earth observation satellite systems, distinguished by the type of their orbits, such as sun synchronous (or polar) and geostationary orbits. Geostationary satellites have geosynchronous orbits characterised by their circularity, an altitude of about 36000 km directly above the Earth’s equator (0º latitude). At this altitude, a satellite needs almost 24 hours to orbit around the earth, the same time the earth takes to perform a complete revolution around its axis. For an observer on the Earth's surface, geostationary satellites seem to be stationary in the sky. Hence, these satellites always observe the same section of the earth surface and atmosphere.

Several studies used data from geostationary satellites to obtain the properties of aerosols. For example, Popp et al. (2007) obtained the aerosol optical depth (AOD) estimation from Spinning Enhanced Visible and InfraRed Imager (SEVIRI) data for Central Europe. They show that the spatial distribution of SEVIRI AOD maps for August 2004 represent expectable features like higher concentrations in industrialized regions or lower loading in higher altitudes. They concluded that the method applied in their study is able to provide an estimate of AOD from MSG-SEVIRI data. Furthermore, their aerosol maps of high temporal frequency could be of interest to atmospheric related sciences with track aerosol particle transport. Fraser et al. (1984) estimated AOD from the Geostationary Operational Environmental Satellites (GOES) imager over the eastern US. This study show that principal advantage of the observations from a geostationary satellite is that the columnar mass density of aerosol constituents that are strongly correlated with the aerosol scattering coefficient can be estimated when the sky is cloudless. On the other hand, the disadvantages of satellite observations for measuring aerosol properties are that they can not be used below clouds, and that vertical profiles of mass density, relative humidity, and winds can not be derived routinely from satellite observations. Knapp (2002) and Knapp et al. (2002) estimated the surface albedo from GOES-8 images and retrieved the AOD from the US and South America. Their results suggest that the GOES satellite can be used to monitor aerosols over land. Furthermore, some exceptions are located where the surface reflectance is large. Zhang et al. (2001) and Christopher et al. (2002) used a similar method to estimate the surface albedo and retrieved the AOD from high temporal resolution GOES-8 imager radiances and detailed radiative transfer calculations. They concluded that the retrieved optical thicknesses results are sensitive to single scattering albedo and surface reflectance. Furthermore, the aerosol properties are adequate to characterize biomass burning aerosols and can be used in studies that model the role of biomass burning on regional climate. Pinty et al. (2000a, b) exploited the frequent (every 30 min) Meteosat observations to estimate the surface albedo and the AOD simultaneously. The results of their study, suggest that anthropogenic fire activities induce significant perturbations of the surface albedo values in the intertropical zones at the continental scale.

Another type of earth observation satellites is sun synchronous (or polar) orbit. As satellites pass both Polar Regions with an inclination near 90° (angle between orbit and equatorial plane), their orbits are called polar orbits. The term sun synchronous means that the section monitored by the satellites is always radiated by the sun in the same way. Satellites in this orbit provide medium to high resolution images of the whole earth which are mostly used for environmental monitoring. They orbit at altitudes of 300 to 2000 km above earth. These

orbits are elliptical or circular with an orbit period of about 90 min. Polar satellites observe different sections of the earth in narrow bands always at the same local time. Days or weeks later, the satellite observes the same section again. Hence, the temporal resolution of these satellites is limited compared to geostationary satellites. Furthermore, geostationary observations provide lower spatial resolution when compared to that from most polar orbiters.

In the past few decades, important scientific findings about atmospheric aerosols have been achieved based on measurements from polar orbiting instruments, such as the Total Ozone Mapping Spectrometer (TOMS), the Advanced Very High Resolution Radiometer (AVHRR), or the Moderate Resolution Imaging Spectroradiometer (MODIS). For example, Ichoku et al. (2002) and Chu et al. (2002) performed an extensive validation of AOD data from MODIS with AOD data provided from a ground-based sun photometer. The AOD information and the Aerosol Index (AI) data from the TOMS and the OMI has been collected (Torres et al., 2007; Torres et al., 2002; Hsu et al., 1999), but there are no daily AOD data with the global coverage needed for more accurate albedo information. In addition, Jääskeläinen et al. (2016) estimates AOD from the AI data obtained by TOMS and the OMI in order to perform an AOD time series, which can be used for atmospheric correction. By definition, AI is the difference between the measured data and calculated data from the radiative transfer theory from an aerosols on atmosphere with the same surface reflectivity and measurement conditions. It is approximately linearly proportional to the AOD if the index of refraction, particle size distribution and the aerosol layer height are known from the other measurements, with the residence height being a key assumption.

Satellite sensors on a polar orbit are not capable of considering the high temporal variability of aerosol concentrations due to their restricted overpass frequency. Aerosol information gained from geostationary instruments is therefore an important complement to the results from polar orbiting sensors. Their high temporal resolution significantly broadens the diurnal coverage and allows to better account for the high spatial and temporal variabilities of aerosols. Frequent observations of the same area available only from geostationary orbits are also important for air quality monitoring since they allow tracking of the rapid movement of pollution (Laszlo et al., 2008).

This chapter has two main objectives. The first is assessing and evaluating the AOD data from two different remote sensing techniques. The second is to validate satellite data using measurements from ground-based observation networks. The AOD data presented in this

chapter will be important in the upcoming chapters to compare and integrate with modelling outputs.

3.2 Aerosol optical properties

Aerosols have an impact on climate and radiation balance because of their optical properties. Particles most strongly affect the radiation balance when their size is similar to the wavelength of the radiation. Aerosols in the fine mode (0.1 to 1.0 µm) are similar in size to the wavelengths of solar radiation within the atmosphere. The important properties of aerosol particles are their size, shape, structure (homogeneous or inhomogeneous particles), and chemical composition (Kokhanovsky, 2007). Optical properties of aerosols are determined by their microphysical properties and spectral refractive index. It is a common practice in satellite aerosol remote sensing to consider atmospheric aerosol as a mixture of a set of components composed of spherical particles (Kokhanovsky et al., 2007).

The task of retrieving aerosol properties using passive optical satellite techniques has long been known for its complexity (Kokhanovsky et al., 2007). This is true for both measurements performed over land and ocean. The difficulty lies in the need to separate the contribution of the surface reflectance from that caused by aerosols in the atmosphere (Kokhanovsky et al., 2007).

The aerosol parameters, such as Aerosol Optical Depth (AOD), Ångström wavelength exponent, aerosol size distribution, single scattering albedo and refractive index are briefly defined and explained below.

Aerosol Optical Depth (AOD)

Aerosol optical depth (AOD) is a measure of the extinction of the solar beam by particles in the atmosphere such as dust and smoke. In other words, these aerosol particles can block sunlight by absorbing or by scattering light. AOD represents how much direct sunlight is blocked from reaching the ground by these aerosol particles. Extinction is the process where photons get removed from the direct propagation of incident radiation, including scattering and absorption. Thus, the extinction (σ_{ext}) is calculated as the sum of the contribution of all absorbing (σ_{abs}) and scattering (σ_{sca}) components (gases and aerosol) for the cross-sections (Equation 3.1).

$$\sigma_{\text{ext}}(\lambda) = \sigma_{\text{sca}}(\lambda) + \sigma_{\text{abs}}(\lambda) \quad \text{Equation 3.1}$$

The aerosol optical depth (τ) is the integral of the aerosol mass extinction coefficient (β_{ext}) over a vertical path from the surface to the top of the atmosphere (TOA) and hence a measure of the atmospheric aerosol load (Equation 3.2). This parameter is a dimensionless number that is related to the amount of aerosol in the vertical column of atmosphere.

$$\tau(\lambda) = \int_{Z=0}^{\text{TOA}} \beta_{ext,p}(\lambda, z)\, dz \quad \text{Equation 3.2}$$

where *p* represents the contribution from the particles (to be separated from molecular or Rayleigh optical depth). AOD is the main variable describing the effect of aerosols on radiative transfer in the atmosphere of the Earth and the most common aerosol parameter derived from remote sensing data. AOD are derived from many Earth observation satellites such as the Advanced Very High Resolution Radiometer (AVHRR) (Rao et al., 1989; Stowe, 1991, Riffler et al. 2010), the Moderate Resolution Imaging Spectro-radiometer (MODIS) (Kaufman et al., 1997), the Multi-angle Imaging SpectroRadiometer (MISR) (Diner et al., 1998), and the Sea-viewing Wide Field-of-view Sensor (SeaWiFS) (Gordon and Wang, 1994; von Hoyningen-Huene et al., 2003). Typically, AOD values measured at λ=0.55 μm range from 0.05 over the remote ocean to 1.0, 2.0 or even 5.0, during episodes of smoke, dust or heavy pollution. This is verified for sky without clouds. On the other hand, if the sky present clouds, very often an AOD > 1.0 is “classified” as cloud. Cloud masking algorithms mask these areas before an AOD retrieval will be started.

The mass specific extinction coefficient, β_{ext}, represents the aerosol specific extinction in $m^2 \cdot g^{-1}$, which is (Chin et al., 2002):

$$\beta_{ext} = \frac{3Q_{ext}}{4\rho r_{eff}} \quad \text{Equation 3.3}$$

where ρ is the average particle density, Q_{ext} is the mass extinction coefficient (a function of particle size distribution and refractive index) and r_{eff} is the effective radius (or area-weighted mean radius) of the aerosol particle. From here, the mass concentration coefficient (*Mc*) is defined as follows:

$$M_c = \frac{1}{\beta_{ext}} \quad \text{Equation 3.4}$$

Equation 3.4 represents the aerosol mass dry for unit AOD, per unit surface area. To calculate the dry aerosol mass, one should take into account the relative humidity (RH) and

the aerosol hygroscopicity (Chin et al., 2002). The aerosol particles are assumed spherical and homogeneous thus allowing us to study their optical properties, such as the complex refractive index and the size distribution, based on the Mie theory (Mie, 1908). This assumption is justified because most atmospheric particles have hygroscopic properties and contain water vapour. With the exception of dust, aerosols are considered to have different degrees of hygroscopic growth rate with ambient moisture. Table 3.1 shows the growth factors of particle radius $r_{eff}/r_{eff,dry}$ for different aerosol types at ambient RH.

Table 3.1. Hygroscopic growth factors of $r_{eff}/r_{eff,dry}$ at different RH (Adapted from Chin et al., 2002).

RH (%)	0	50	70	80	90	95	99
Sulphate	1	1.4	1.5	1.6	1.8	1.9	2.2
OC	1	1.2	1.4	1.5	1.6	1.8	2.2
BC	1	1.0	1.0	1.2	1.4	1.5	1.9

Figure 3.1 demonstrates the relative humidity and wavelength dependence of β for hygroscopic aerosols.

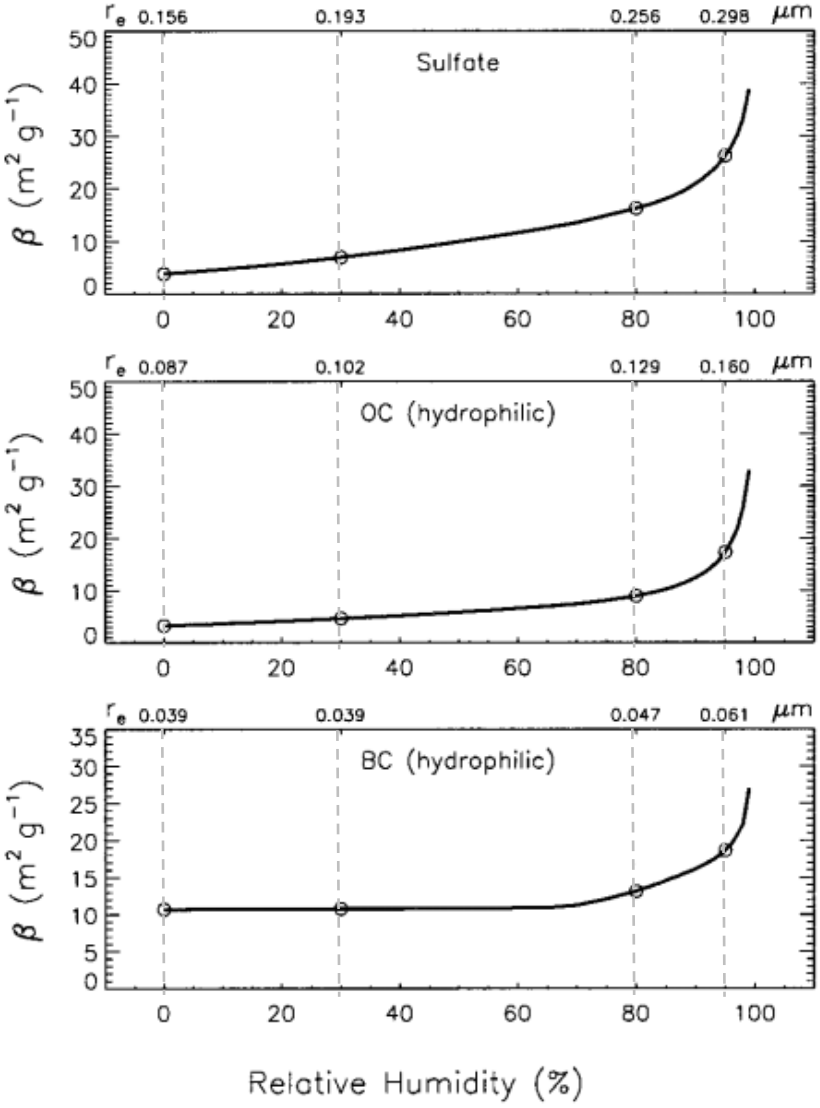

Figure 3.1. Mass extinction efficiencies for hygroscopic aerosols at wavelength 500 nm as a function of RH. The r_{eff} values are indicated at the top of each graph (Chin et al., 2002).

Ångström Wavelength Exponent

One of the parameter widely used in atmospheric sciences dealing with optical properties of aerosol particles is the Ångström wavelength exponent. The Ångström wavelength exponent or Ångström coefficient (α) is a dimensionless measure of the aerosol size and can be calculated from different aerosol optical depths ($\tau_{\lambda 1}$,$\tau_{\lambda 2}$) at different wavelength, λ1 and λ2 (Equation 3.5) (Ångström, 1929).

$$\alpha = \frac{\ln(\tau_{\lambda 2}/\tau_{\lambda 1})}{\ln(\lambda 1/\lambda 2)} \qquad \text{Equation 3.5}$$

The Ångström exponent is inversely related to the average size of the particles in the aerosol. Larger aerosol size is related to smaller values of α, such that aerosol distributions dominated by fine aerosols have α ≥ 1.0**,** whereas those dominated by coarse aerosols have α ≤ 0.6 but might also become negative for very large particles. Thus, the Ångström exponent is a useful parameter to assess the particle size of atmospheric aerosols or clouds. For example, aerosols with large sizes and therefore a very small Ångström exponent (nearly zero) are spectrally neutral, which means that the optical depth does not change with wavelength.

Aerosol Size Distribution

The size distribution of atmospheric aerosols is one of the key elements in understanding and managing aerosol effects on visibility, climate and health. Different aerosol types naturally consist of particles with different sizes, from a few nanometers to around 100 μm. Aerosol size distributions can be mathematically described as the sum of n lognormal distributions (Equation 3.6).

$$\frac{dN}{dlnr} = \sum_{i=0}^{n} \frac{N_i}{\sqrt{2\pi} ln\sigma_i} \exp\left(-\frac{(ln\, r_i - ln\, \bar{r}_{gi})^2}{2ln^2\sigma_i}\right) \qquad \text{Equation 3.6}$$

where N_i is the particle number concentration, r_i are the particle radii, $\bar{r}_{gi}$ is the geometric mean radius, and i is the geometric standard deviation of the ith lognormal mode (Kokhanovsky and De Leeuw, 2009).

Figure 3.2 shows an example of the distributions of the number, area, and volume concentration as a function of the particle diameter for urban conditions. The number size distribution as a function of radius is related to the area size and volume size distribution (Kokhanovsky and De Leeuw, 2009). As seen from Figure 3.2, the size distributions follow lognormal distributions with single or multiple modes.

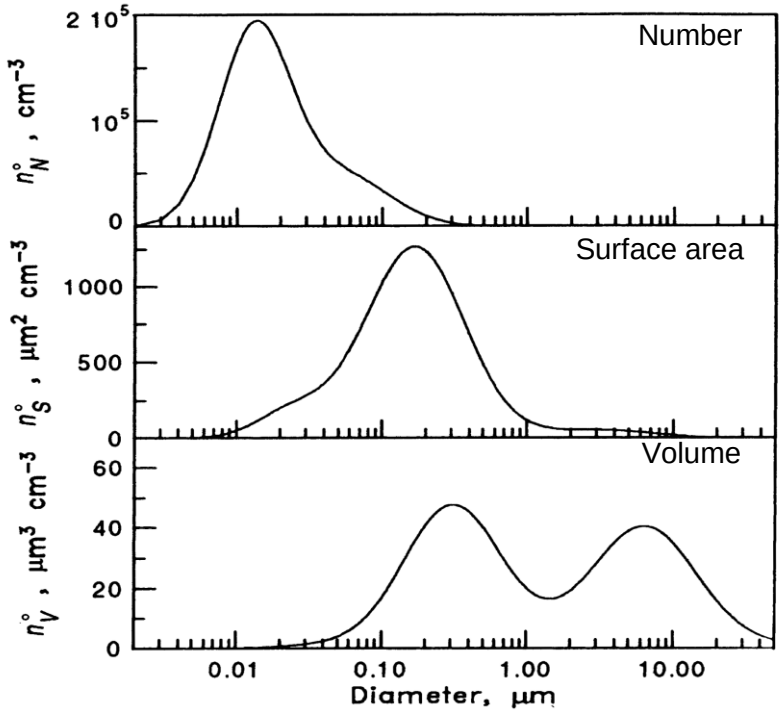

Figure 3.2. Example of Aerosol size distribution for urban environment (Seinfeld and Pandis, 2006).

In an urban environment with particles mainly from primary particulate emissions of combustion processes, natural sources, and secondary particles from gas-to-particle conversion mechanisms (Seinfeld and Pandis, 2006), two distinct modes of fine and coarse particles are obvious.

Single Scattering Albedo (SSA)

The Single Scattering Albedo (SSA) is an aerosol parameter that provide information about the absorbing properties of the aerosols and used to quantify the impact of aerosols on climate. It was considered one of the critical parameters in determining the impact of absorbing aerosol on the Earth's radiative balance (Pokhrel et al., 2016). The aerosol SSA (ω_0) describes the ratio of scattering to total extinction at a small layer of aerosols and is based on the chemical composition of the particles. It is calculated as follows:

$$\omega_0 = \frac{\sigma_{\mathrm{sca}}}{\sigma_{\mathrm{sca}} + \sigma_{\mathrm{abs}}} \qquad \text{Equation 3.7}$$

where σ_{sca} and σ_{abs} are the scattering and absorption coefficients, respectively. Highly absorbing aerosol types have a low ω_0 and vice versa. For example, ω_0 becomes lower when a large amount of black carbon is emitted into the atmosphere as a result of biomass burning, leading to increased absorption.

Refractive Index

Other important parameter is the complex refractive index of aerosols affecting calculation of radiative budget and aerosol climate effect. This parameter describing scattering and absorption properties of atmospheric particulate matters. When optical and radiative characteristics of atmospheric aerosols are modelled, data are needed for the components of the complex refractive index. One of the problems occurring during their simulation is that the chemical composition and, consequently, the refractive index of the particles are inhomogeneous in space and time. Thus, improving the knowledge on aerosol complex refractive index is of great interests to decrease the uncertainties associated to aerosols in for example the climate change assessment (Boucher et al., 2013).

The complex refractive index (m) of an aerosol particle is a function of its chemical composition

$$m = n + iK \qquad \text{Equation 3.8}$$

where the real part n represents the nonabsorbing and the imaginary part K the absorbing components. The refractive index plays a role as input to Mie calculations which allow us to compute the angle-dependent scattering and absorption of small particles.

3.3 Remote sensing techniques

The simplest remote sensing techniques is sunphotometry (Kokhanovsky and de Leeuw, 2009.), where the solar disk is observed through a collimator. The sunphotometer measures the extinction of direct radiation in distinct wavelength bands, and derives the aerosol contribution to the total extinction. The measurement assumes that the radiation has had little or no interaction with the surface or clouds, and there is minimal (or known) gas absorption in the chosen wavelength, λ. In other words, sunphotometry is a basic application of the Beer-Bouguer-Lambert law (Levy, 2009).

The satellite measurements of AOD are usually tested and calibrated against the measurements of ground-based observation networks, since the ground based instruments are more stable, well calibrated and well-characterised. For ground-based remote sensing, uplooking sunphotometry measurements that provide AOD observation are available globally at many large ground-based networks: AERONET (Aerosol Robotic Network) (Holben et al., 1998), MFRSR (Multifilter Rotating Shadowband and Radiometer) (Alexandrov, et al., 2002) and WMO/GAW/PMOD (World Meteorological Organization Global Atmosphere Watch Physikalisch-Meteorologisches Observatorium Da-vos) (Wehrli, 2000).

In this thesis, the ground-based network data from AERONET were processed and analysed to validate the AOD data obtained by different sources such as satellite observations from SEVIRI and modelling outputs. Thus, it is described below the AERONET and SEVIRI instruments.

3.3.1 AErosol RObotic NETwork (AERONET)

The AErosol RObotic NETwork (AERONET) (Holben et al., 1998) is a global network of ground-based sun photometer measurements of aerosol optical properties, such as aerosol optical depth, Ångström exponent, single scattering albedo and particle size distribution. AERONET was established by the National Aeronautics and Space Administration (NASA) and the Laboratoire d'Optique Atmosphérique (LOA)-Photons with many collaborating institutions all over the world. Operating at hundreds of sites globally, the AERONET sunphotometers have been reporting at some websites (e.g.,URL3).

The AERONET stations are equipped with CIMEL multiband photometers (Figure 3.3) that perform measurements of spectral sun irradiance and sky radiances with 1.2 º full field of view at eight spectral bands (340, 380, 440, 500, 670, 870, 940, 1020 nm) (Holben et al., 1998). The aerosol optical depth (AOD) is recorded every 15 minutes based on the transmission of direct sunlight inferred from the radiance measurement in the sun direction. The collection of radiance data from the different directions is used in combination with the aerosol optical depth to derive aerosol properties such as size distribution, complex refraction index, partition of spherical/non spherical particles. The aerosol optical depth derived from these measurements is available on a free-access database. AERONET database also provides other inversion products (Dubovik and King, 2000) characterising

aerosol optical, microphysical and radiative properties which are of great interest for aerosol research studies and satellite validation.

Figure 3.3. An example of AERONET instrument located at Évora station [URL3]

AERONET data can be freely accessed on the web and are available for three quality levels: Level 1.0 (unscreened), Level 1.5 (cloud-screened), and Level 2.0 (cloud-screened and quality assured). With the exception of Level 2.0 data, which have post-field yearly calibration applied, all products are provided on a near real-time basis. Level 1.0 and 1.5 data are retrieved instantaneously in near real-time; whereas for Level 2.0 data the instrument needs to be calibrated and checked once a year according to the quality control checklist. The quality control checklist accounts for seven important points: 1) Evaluation of the performance of the instrument to determine instrument failure and possible causes, such as water on the window, poor tracking and spider weed in the collimators; 2) Identification of anomalies on the temperature sensor which may influence the temperature correction of the 1020 nm channel; 3) Evaluation of the pre- and post-field calibration to determine if filter degradation or non-linear changes of the calibration constants occurred over time; 4) Inspect AOD data for any spectral dependence abnormalities, such as rapid increase of transparency in the UV in the early morning or late afternoon due to filter leakage or degradation; or sudden increases and decreases of the AOD in the UV channels due to electronic problems; 5) Assessment of the AOD data for any possible cloud contaminated outliers; 6) Evaluation of the consistency data through visual inspection of the data for

abnormal data points and identification of unusual optical events using additional available information such as MODIS imagery, lidar data and back trajectories; 7) Evaluation of the impact of the new data on existing aerosol climatology. Data from AERONET stations with quality assured Level 2.0 were analysed in Section 3.5 and used for validation in the next chapters. These products are considered more stable and realistic.

3.3.2 Spinning Enhanced Visible and Infrared Imager (SEVIRI)

The Meteosat Second Generation (MSG) system has been established through cooperation between the European Space Agency (ESA) and the European Organisation for the Exploitation of Meteorological Satellites (EUMETSAT, Schmetz et al., 2002). The MSG is operating in geostationary orbit centred on the equator and Greenwich meridian. The Spinning Enhanced Visible and Infrared Imager (SEVIRI) is the main instrument aboard the geostationary MSG satellites.

The total field of view of the SEVIRI instrument is approximately 70° providing coverage of the earth from about 70°S to 70°N and 70°W to 70°E (Hanson and Muller, 2005) as shown in Figure 3.4. There are 3712×3712 pixels covering the full disc. SEVIRI is a line-by-line radiometer that provides a complete scan with a repeat cycle of 15 minutes.

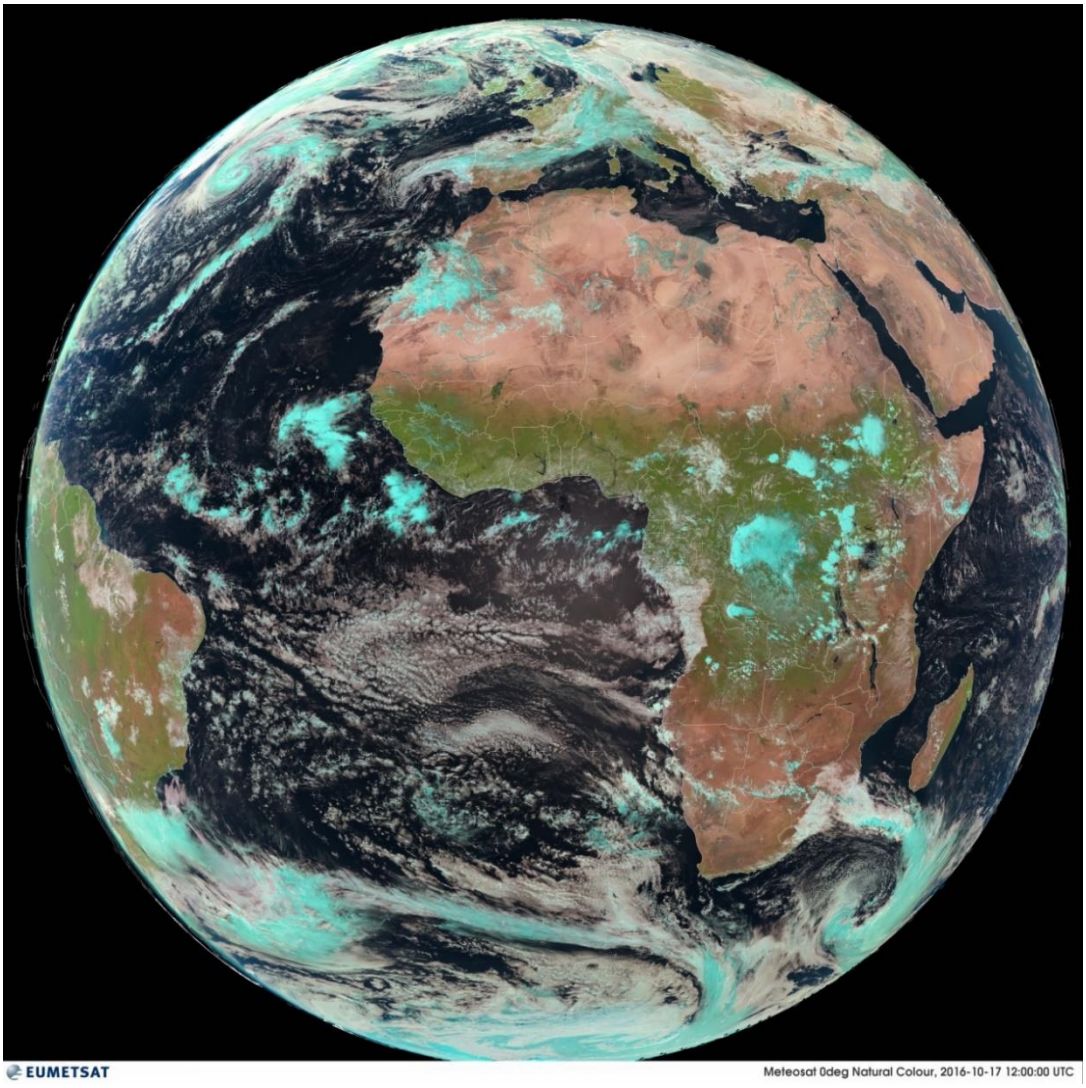

Figure 3.4. RGB image of the full SEVIRI disk from 17 October 2016 acquired from Meteosat-8 at 12:00 UTC. Copyright by EUMETSAT.

The SEVIRI sensor measures the emitted and reflected electromagnetic radiation of the surface and the atmosphere of the Earth using 11 spectral channels and one broad band. The spectral channels, which include 3 solar channels suitable for the determination of atmospheric aerosol parameters (0.6 μm, 0.8 μm and 1.6 μm) and 8 infrared wavelengths (3.9 μm, 6.2 μm, 7.3 μm, 8.7 μm, 9.7 μm, 10.8 μm, 12.0 μm and 13.4 μm), provide data at a spatial resolution of 3x3 km^2 (sampling distance of the sub-satellite point of 3 km). The broad band channel covers the spectral range between 0.4 μm and 1.1μm, and has a higher spatial resolution than the standard channels with 1x1 km^2 at nadir. The spectral features

of the SEVIRI instrument, including the band width, the nominal wavelength of the different channels and their main observational application, are summarised in Table 3.2.

Table 3.2. Spectral channel characteristics of SEVIRI in terms of central, minimum and maximum wavelength of the channels and the main application areas for each channel. Adapted from Schmetz et al. (2002).

Channel No.	Spectral Band (μm)	Characteristics of Spectral Band (μm)			Main observational application
		λ_{cen}	λ_{min}	λ_{max}	
1	VIS0.6	0.635	0.56	0.71	Aerosol, land surface, vegetation, snow, clouds
2	VIS0.8	0.81	0.74	0.88	Aerosol (water), land surface, vegetation, snow, clouds
3	NIR1.6	1.64	1.50	1.78	Discriminates snow and clouds, water and ice clouds
4	IR3.9	3.90	3.48	4.36	Low clouds and fog, surface temperature at night
5	WV6.2	6.25	5.35	7.15	Water vapor, winds, height of semitransparent clouds
6	WV7.3	7.35	6.85	7.85	Water vapor, winds, height of semitransparent clouds
7	IR8.7	8.70	8.30	9.1	Thin cirrus clouds, ice and water clouds
8	IR9.7	9.66	9.38	9.94	Ozone, wind
9	IR10.8	10.80	9.80	11.80	Surface and cloud-top temperature, cirrus clouds
10	IR12.0	12.00	11.00	13.00	Surface and cloud-top temperature, cirrus clouds
11	IR13.4	13.40	12.40	14.40	CO_2 absorption channel, temperature of lower troposphere
12	HRV	Broadband (about 0.4 – 1.1 μm)			Carbon dioxide, Higher resolution, e.g. tracking constraints.

SEVIRI images complement the measurements of polar orbiting sensors, by combining their multi-spectral features and high spatial resolution, with continuous observations at high temporal frequency. The infrared channels of SEVIRI can produce accurate pictures of the temperature of clouds and of land and sea surfaces, at all times of the day and night. Using channels in the absorption band of ozone, water vapour and carbon dioxide, SEVIRI also provides information on the characteristics of atmospheric air masses. The solar channels 'VIS0.6', 'VIS0.8' and 'NIR1.6' of SEVIRI are crucial for cloud detection, and can be used to retrieve both aerosols and surface properties. Thus, the combination of channels supplied by SEVIRI offers a unique opportunity to monitor the weather conditions as they develop, and to study the long-range transport of atmospheric constituents and their impact on the climate system.

SEVIRI solar channels give measurements at similar wavelengths as channels from others instruments like the Advanced Very High Resolution Radiometer (AVHRR), the Moderate Resolution Imaging Spectroradiometer (MODIS) and Geostationary Operatioanl Environmental Satellite (GOES).

3.4 Methodology for SEVIRI and AERONET data processing

In order to study the spatial and temporal variations of Aerosol Optical Depth (AOD) over mainland Portugal, SEVIRI and AERONET [URL3] data were used. May 2011 was chosen as the study period. During this period, Portugal was influenced by African dust outbreaks (Monteiro et al., 2015).

SEVIRI data are available at different processing levels. The level of the data used in this thesis is level 1.5, as it includes geocoded and calibrated data. These data were processed by the Remote Sensing Research Group (RSGB) at the Institute of Geography, University of Bern. RSGB receives SEVIRI images in the HRIT format (High Rate Information Transmission) in almost real time via the dissemination system of EUMETCast (EUMETSAT's Broadcast System for Environmental Data). After processed by RSGB, the AOD data was received in binary format. To convert the format to view and analyse the data, it was necessary develop a set of python programs.

To obtain AOD from SEVIRI data, observations provided by the channel centred at 0.6 μm with a spatial resolution of 3 km were used. The retrieval algorithm was developed at RSGB and its description can be found in Popp et al. (2007). To retrieve AOD values from SEVIRI, it is necessary to separate the measured top-of-atmosphere (TOA) signal into two: the one coming from the surface of the Earth and the atmospheric contribution. In the first step, the surface reflectance for every pixel is estimated selecting the lowest observed reflectance (corrected for ozone, water vapour, and background aerosol concentration) from a temporal window of 15 days. That temporal window was analysed by Knapp et al. (2002, 2005). They found that this period was representative of the length of the time series and the influence of changes in surface reflectance and aerosol loading. The fixed aerosol model (continental aerosol type, single scattering albedo $\omega 0=0.89$ at $\lambda=0.55$ μm) and meteorological data, such as water vapour concentration provided by the European Centre for Medium Range Weather Forecasts (ECMWF) operational analysis, are then fed into a radiative transfer model to invert the AOD data from the (estimated) surface and (measured) TOA reflectance. The Simplified Model for Atmospheric Correction (SMAC) (Rahman and Dedieu, 1994) is applied for the radiative transfer simulations using a parameterized version of 6S (Vermote et al., 1997). In the last step, a spatial averaging filter with a moving 5×5-pixel box was used to compute the retrieved AOD with minimised noise such that, finally, each pixel shows the AOD value of an area with approximately 25×25 km^2.

Additionally, to the satellite data, and for the validation of the AOD provided by satellite and modelling, we used cloud-screened and quality-assured level 2.0 data from May 2011. AERONET level 2.0 AODs were interpolated to the reference wavelength at 550 nm using Equation 3.9 (Cesnulyte et al., 2014),

$$AOD_{550} = AOD_{500} * \left(\frac{550}{500}\right)^{-\alpha} \quad \text{Equation 3.9}$$

where α is the AERONET Ångström exponent of the wavelength range 440-870 nm. It was developed one python program to analyse data and to apply the Equation.

Figure 3.5 displays all AERONET locations with data records available for May 2011 in Portugal and western Spain. Data from these stations were used for validation purposes. The key products accessible to the public are multi-spectral (from ultraviolet UV to near-infrared NIR) aerosol optical depth data retrieved as previously described in this chapter.

Figure 3.5. AERONET sites in Portugal and adjacent regions.

Data from two different passive remote sensing techniques, AERONET and SEVIRI, were obtained and analysed. From AERONET, the AOD data and the Ångström coefficient (AC) were selected. From SEVIRI satellite data, only the AOD was analysed. AOD data from AERONET were used for validation of the AOD from SEVIRI observations. All data were analysed in terms of daily mean values.

The AOD data was processed in terms of temporal and spatial resolution to harmonize the data. For this purpose, a set of python programs was prepared. Concerning the temporal resolution, to computation of daily means was done in two steps. Firstly, the maximum AOD value for each cell was selected in each hour. Secondly, the daily mean values were calculated with at least six hours of data between 6h-17h (sunlight hours). Regarding the spatial resolution, it was necessary to adjust the SEVIRI grid data (3x3 km^2) to the grid of the modelling data (9x9 km^2). Thus, to help this task the spatial analysis tools implemented within geographic information system (GIS) were used.

3.5 Results and discussion

3.5.1 AERONET observations

The Aerosol Robotic Network observations (AERONET, URL3) data available for May 2011, with level 2.0 (cloud-screened and quality-assured) AOD measurements from four stations located within the study domain (Figure 3.3) are investigated and used for validation of the SEVIRI data (sub-section 3.4.2) and modelling results (Chapter 4). AERONET data were treated as daily averages, considering only the days with a minimum of 6 hours of observations in order to obtain reliable results.

Figure 3.6 shows the temporal evolution of the daily mean of AOD values provided by AERONET stations computed using Equation 3.9.

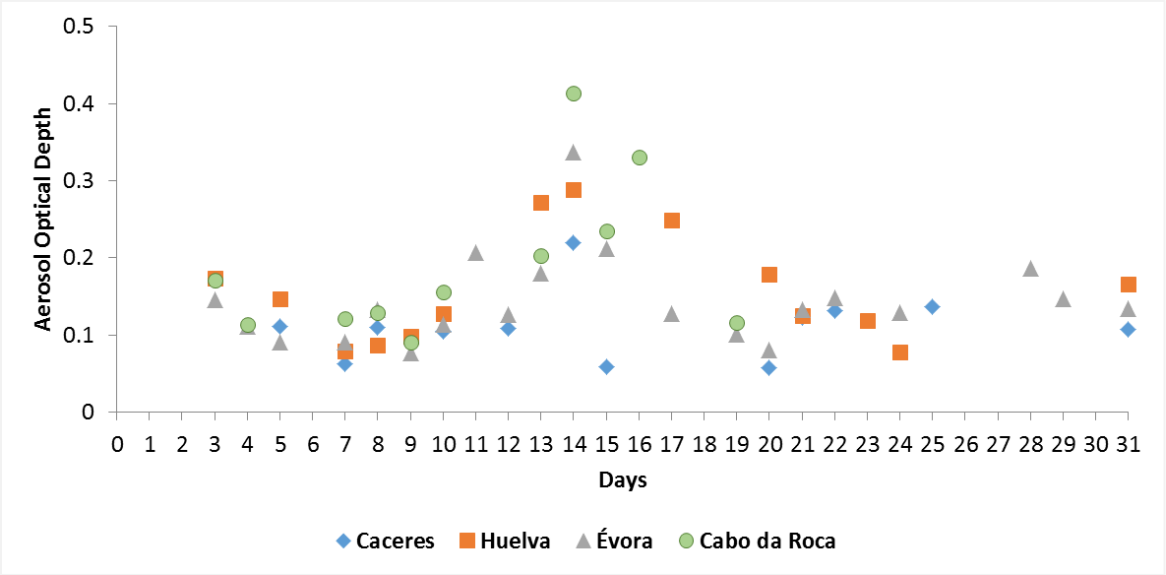

Figure 3.6. Daily average of Aerosol Optical Depth from AERONET observations during May 2011.

The evolution of the daily average of AOD for all stations shows higher values during the period 10th-18th of May 2011. In this period, the influence of the African dust outbreaks over Portugal is notorious (Fernandes et al., 2015, Monteiro et al., 2015). On the 15th of May, at the Caceres station, a low value was observed, approximately 0.05. One possible reason for this is the fact that, in this location, the influence of the aerosols concentrations was not verified.

Figure 3.7 illustrates the temporal evolution of the daily mean Ångström coefficient (α) values provided by AERONET stations computed using the wavelengths at 440 nm and 870 nm.

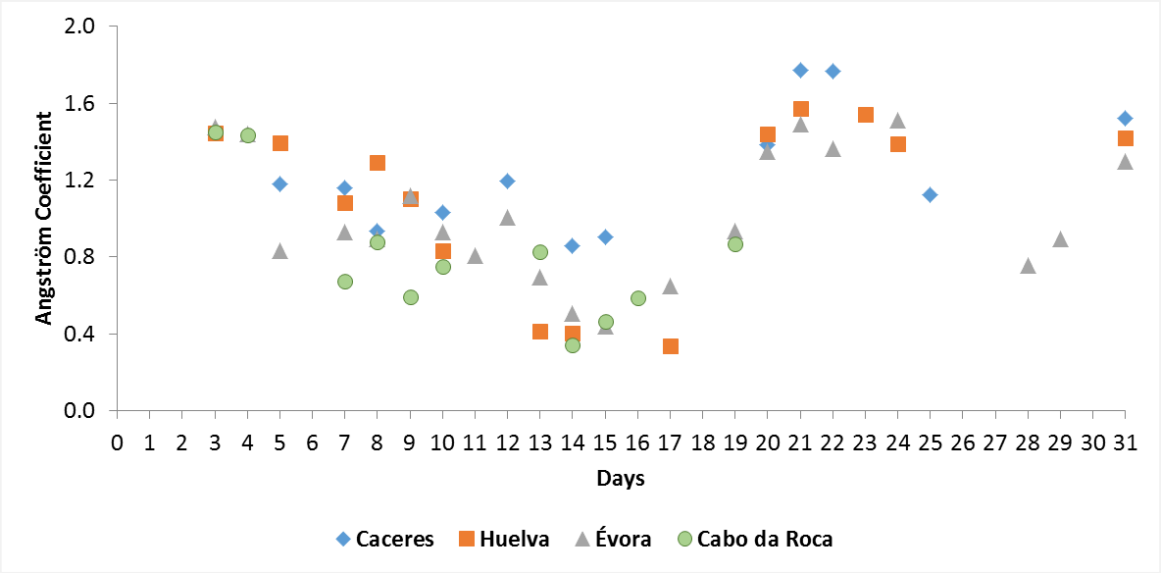

Figure 3.7. Daily average of Ångström coefficient from AERONET observations during May 2011.

As can be seen from Figure 3.7, during the period 10th-18th of May 2011, the Ångström coefficient presents values lower than 1.0. This could be related to the presence of coarse particles of dust. This conclusion is consistent with the conclusion of Figure 3.6 about AOD.

3.5.2 Evaluation of SEVIRI observations

In this thesis, the SEVIRI AOD data were assessed by calculating the daily average over mainland Portugal. Firstly, the maximum value for each cell was selected in each hour (Figure 3.8a). Secondly, the daily mean values were calculated with at least six hours of data (sunlight hours). An example of the daily mean values for 14th May is presented in Figure 3.8b. Finally, spatial analysis tools implemented within geographic information system (GIS) were applied to adjust the SEVIRI grid data to the grid of the modelling data. The result of this method is a grid with a daily mean AOD SEVIRI data adapted to be compared with modelling results (Figure 3.8c).

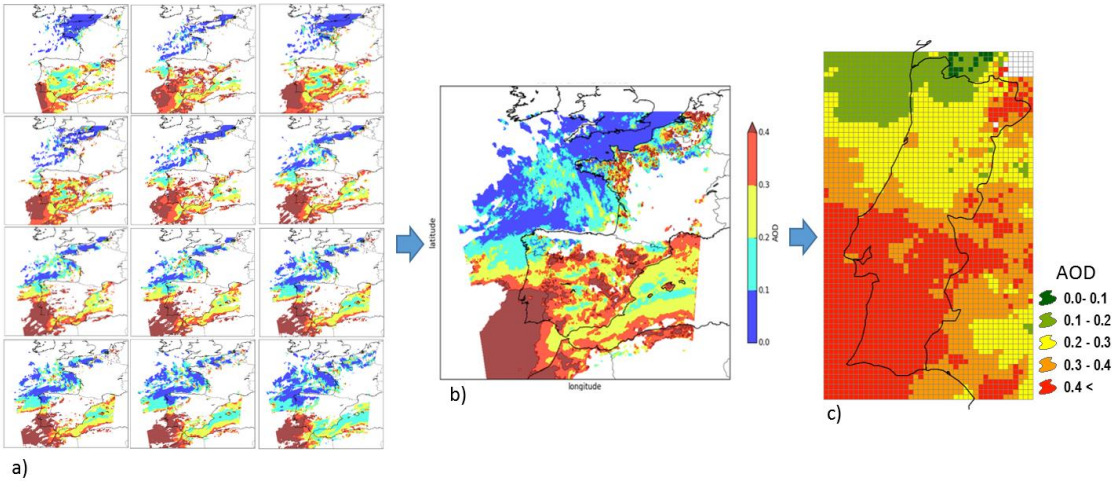

Figure 3.8. Example of the SEVIRI data for 14 May 2011: a) Hourly data (between 6h-17h) with original pixel size (3x3 km^2), b) Daily mean data with original cell size (3x3 km^2) and c) Daily mean data with the grid cell size and projection compatible with the modelling outputs (9x9 km^2).

In order to understand the spatial coverage provided by SEVIRI observation during May 2011, a spatial distribution of the number of the days with AOD data per cell is represented in Figure 3.9.

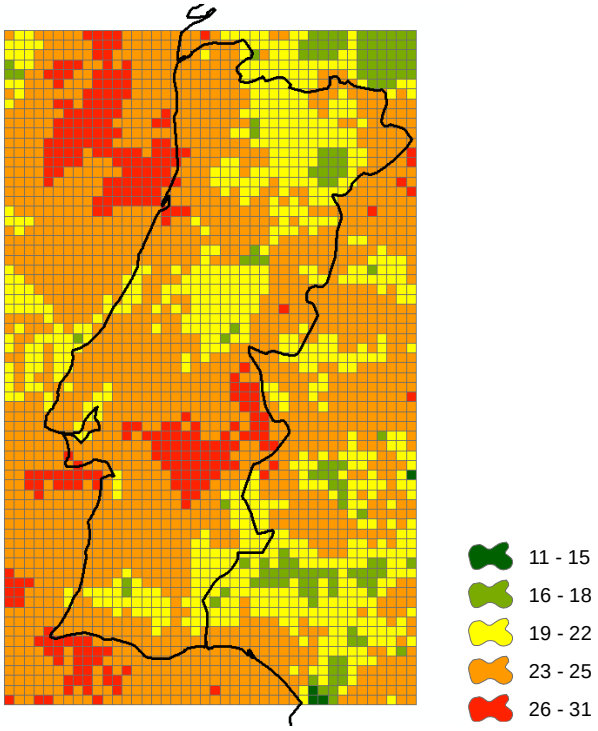

Figure 3.9. Number of days with AOD data from SEVIRI observations considered for the analysis.

Based on the results shown in Figure 3.9, one concludes that SEVIRI data provide a good spatial and temporal coverage with AOD information for the study period. Moreover, this Figure shows a significant number of cells (approximately 82% of the domain (2998 cells)) with AOD values during more than 20 days, corresponding to a data completeness of 65% for the whole period studied.

The frequency of low, median and high AOD values obtained from daily SEVIRI observations was also analysed in order to understand the spatial evolution. Figure 3.10 presents various percentiles for daily values obtained from the SEVIRI data.

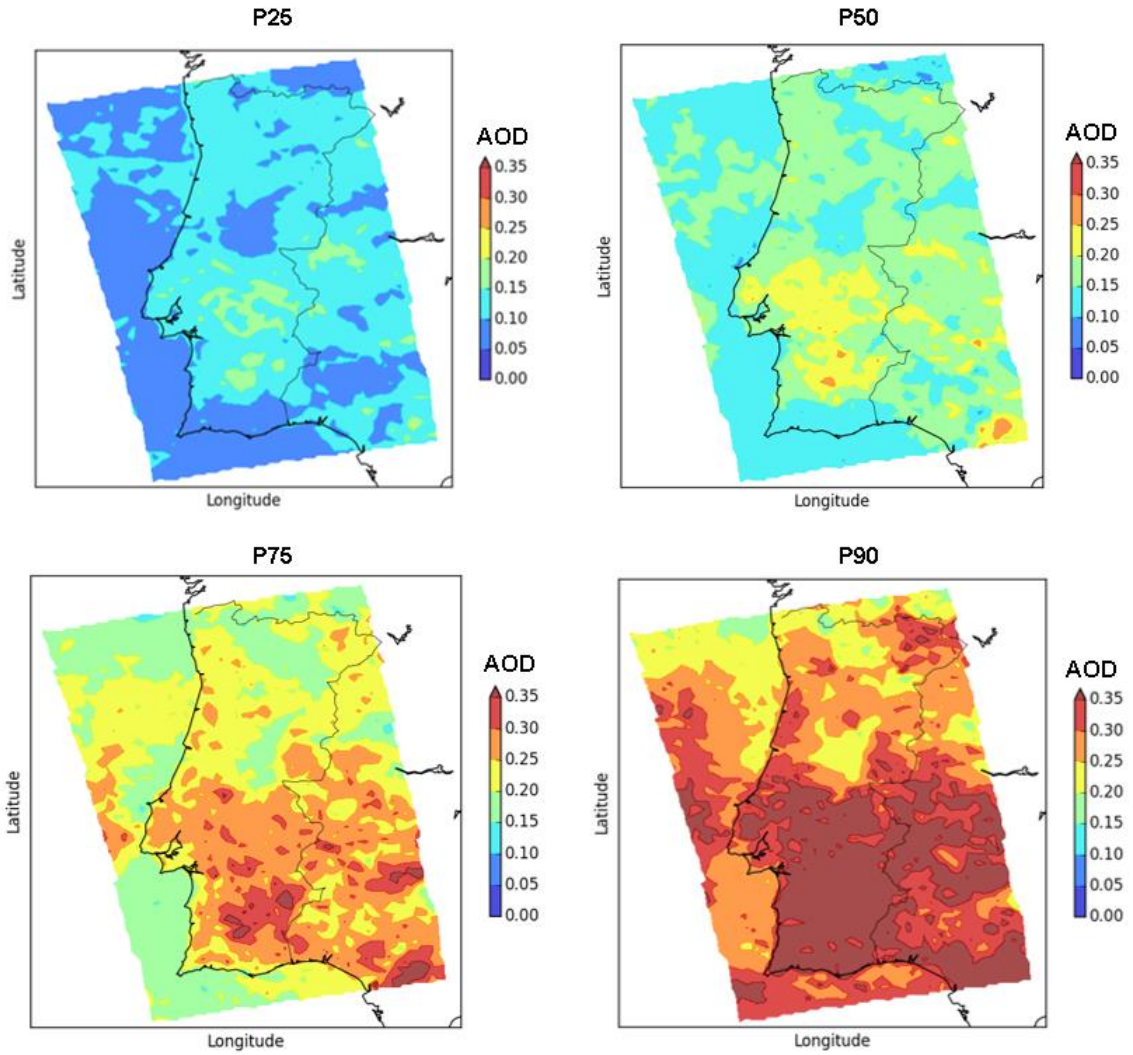

Figure 3.10. Spatial representation of percentile 25th (P25), 50th (P50), 75th (P75) and 90th (P90) of the AOD obtained from SEVIRI for May 2011.

Starting with the Percentile 25 (P25), and as would be expected, the low values of AOD over mainland Portugal are close to 0.1. The analysis of P50 indicates that the presence of the high load aerosols over Portugal is limited on time scale, since during 50% of the time this contribution is below 0.2. Only when high percentiles are analysed (e.g. P75) do the AOD over Portugal achieve values higher than 0.25. P90 values are higher than 0.3 in the Southeast region of the country, showing a clear influence of mineral dust. This behaviour corresponds to a short time period of approximately 3 days during May 2011.

In order to validate de SEVIRI sensor data, the comparison of the AOD obtained by SEVIRI with AERONET observations was performed and presented on Figure 3.11.

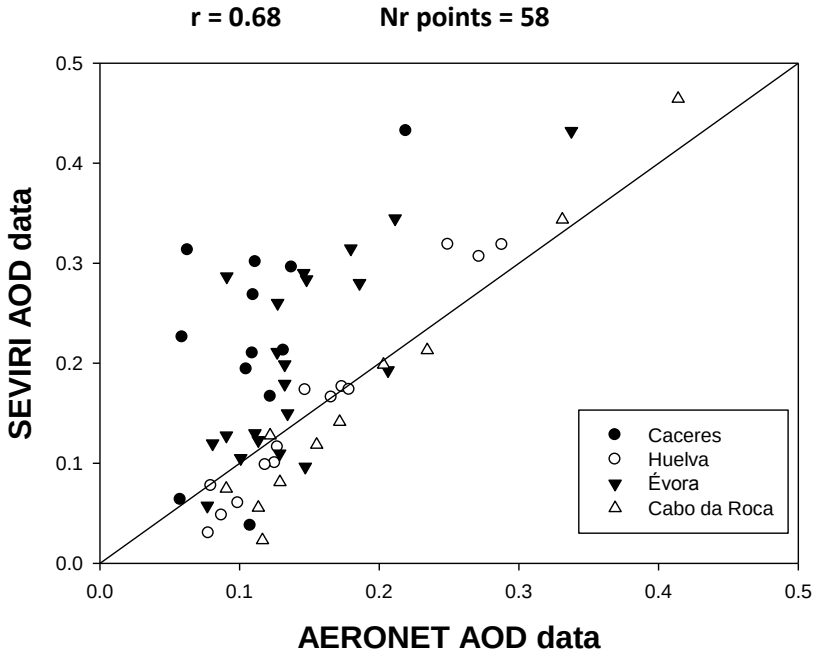

Figure 3.11. Scatterplot of daily mean AOD values from AERONET versus SEVIRI observations.

The satellite data from the SEVIRI sensor provide a good spatial and temporal coverage with AOD information for May 2011. In conclusion, from the comparison of the AOD data provided by satellite observations with AERONET observations, a good agreement was obtained, with a correlation coefficient of 0.68 (Figure 3.11).

3.6 Summary and conclusions

The development of methodologies that contribute to improve the quantification of the atmospheric aerosol loading is an important point to perform air pollution assessment. The use of remote sensing data is one promising approach. In this chapter, data from two different remote sensing techniques, AERONET and SEVIRI, were studied. Both data were treated as daily averages.

The temporal evolution of the daily mean Aerosol Optical Depth (AOD) and Ångström coefficient (AC) values from four AERONET stations was analysed. The evolution of the daily average of AOD for all stations shows higher values during the period 10th-18th of May 2011. In the same period, the Ångström coefficient presents values lower than 1.0. This fact could be due to the presence of mineral dust aerosols.

SEVIRI observations were analysed in terms of temporal and spatial distribution of AOD at 550 nm. From the analysis of the SEVIRI AOD data, one can conclude that the SEVIRI sensor provides a significant number of cells with AOD values, corresponding to a data completeness of 65% for the studied period. The spatial analyses show, on the Southern part of the domain, higher AOD values compared with the other regions of the study domain, influenced mainly by mineral dust.

The results show that the implemented methodology gives agreement between the satellite data and AERONET observations. For the AERONET stations, and during the selected and analysed period (May 2011), a correlation coefficient of 0.68 was found. Caceres and Évora are the only sites for which the AOD values given by SEVIRI are higher than the ones measured by the AERONET stations. The stations where the best agreement between SEVIRI and AERONET was obtained are Cabo da Roca and Huelva.

The analysis performed in this chapter is important to evaluate the spatial and temporal distribution of AOD SEVIRI observations. These data will be used on the upcoming chapters.

Chapter 4

Air Quality Modelling of Aerosols

Chapter Index:

4.1 Introduction……..67

4.2 Methodology for the air quality modelling system WRF-CAMx Application……71

4.3 Modelling results and discussion……76

4.3.1 - Assessment of air quality modelling system……..76

4.3.2 - Aerosols vertical distribution analysis……79

4.3.3 - Spatial distribution of the AOD modelling results……..80

4.3.4 - Evaluation of AOD modelling results……..82

4.4 Summary and conclusions……83

4 Air Quality Modelling of Aerosols

Air quality models are powerful tools to assess the horizontal, vertical and temporal distribution of air pollutants concentrations, and to be used in air quality management.

The main objective of this chapter is to evaluate the air quality modelling system WRF-CAMx over Portugal. For this purpose, PM concentrations at the surface and at all vertical columns were computed and evaluated.

This chapter is divided in four sections. Section 4.1 gives an introduction to Air Quality Modelling focusing on aerosols. A description about the methodology for air quality model applied in this study is given on section 4.2. Section 4.3 presents the analysis of the modelling results and discussion. In the last section (Section 4.4), a summary and some conclusions are presented.

4.1 Introduction

Over the last years, air quality degradation has become an increasingly alarming problem in Portugal. PM10 (Particulate matter with an equivalent aerodynamic diameter of less than 10 μm) annual and daily limit values have been systematically exceeded in Portugal over the last decade (Borrego et al., 2012a, 2012b). The high concentrations of particulate matter (PM), exceeding the daily limit values, are one of the main concerns for air quality management. Depending on their composition and concentration, aerosols affect the climate system (Alizadeh Choobari et al., 2014; IPCC, 2013) and human health, mainly potentiating cardiovascular and respiratory diseases (Lelieveld et al., 2013; WHO, 2006,

2013). Therefore, the first concern on air quality modelling is to better understand the processes in the atmosphere associated to the formation, transport, and deposition of aerosols and to improve the characterisation of emission sources.

To assess the concentration of aerosols and their variability in space and in time, *in situ* observations are widely used. However, due to high operational costs, *in situ* observations are insufficient to capture the high-resolution spatial and temporal variation of PM concentrations (Yap and Hashim, 2013). Therefore, alternative techniques, such as air quality modelling, should be considered to understand these spatial and temporal variations and to characterise the pollution sources and their possible outcomes (e.g. Pozzer et al., 2015; Tchepel et al., 2013; Pay et al., 2010,2012; Basart et al. 2012a, 2012b). Also, the Directives on Ambient Air Quality (Directive 2008/50/EC) and on Cleaner Air for Europe consider air quality models as a powerful tool for the estimation of the concentration of pollutants in the atmosphere. These tools can provide past, present and future estimations of the concentration of pollutants. For that, air quality models simulate the physical and chemical processes that affect air pollutants as they disperse and react in the atmosphere with the use of numerical and mathematical techniques. These models use detailed information on meteorological data and pollution emission rates to characterise primary pollutants that are emitted directly into the atmosphere and secondary pollutants that are formed as a result of complex chemical reactions within the atmosphere. There are three large groups of models: dispersion, photochemical and receptor. The dispersion models are normally used to estimate the concentration of pollutants at specified ground-level receptors surrounding an emissions source. The photochemical models are typically used in regulatory or policy assessments to simulate the impacts from all sources by estimating pollutant concentrations and deposition of both inert and chemically reactive pollutants over large spatial scales. They are applied at several spatial scales: local, regional, national and global. Finally, the receptor models consist in observational techniques which use the chemical and physical characteristics of gases and particles measured at source and receptor to both identify the presence of and to quantify source contributions to receptor concentrations.

Air quality models are the primary tools used by industry, regulators, and other agencies for a diversity of applications (Bonyoung et al., 2015), including development of regulations (EPA, 2011a, 2011b), design of air pollution control strategies and implementation plans (Odman et al., 2009), and short-term operational air quality forecasting (Hu et al., 2010; Menut and Bessagnet, 2010). Recently, their use has been extended to assessing air

quality standards when monitoring data are unavailable (EPA, 2011a) since they produce high spatial resolution data on size distribution, aerosol composition and vertical profiles. In air quality modelling, the meteorological models play an important role, since they provide representations of the weather processes for the air pollution simulations. The importance of meteorological inputs on regional air quality modelling has been clearly identified (e.g. Seaman, 2000) and consequently, the need to have a better insight on the sensitivity and performance of meteorological models.

Nowadays, there are several models that could simulate the chemistry of the atmosphere at long-term and at the regional scale, for example, the American models CAM (Community Atmospheric Model), CMAQ (Community Multi-scale Air Quality) (Tesche et al., 2006), the Australian model TAPM (The Air Pollution Model) (Hurley et al., 2005), the European models CHIMERE (Van Loon, 2004; Vautard et al., 2007) and LOTOS-EUROS (Schaap et al., 2008). In these air quality models, the chemical processes are treated independently of the meteorological model, i.e. “offline”. The offline approach is computationally attractive when the influence of the weather upon the chemistry of the air is not the focus of a study, since it allows to carry sets of chemical transport simulations with a single meteorological dataset.

The complex process of atmospheric dispersion depends not only on meteorology, but also on the emissions (Seinfeld and Pandis, 2006). Nowadays, these data are more detailed, allowing the use of air quality models and an increasingly accurate estimation of atmosphere concentrations (Zhang et al., 2012a; Zhang et al., 2012b). The precision and accuracy of the results of air quality models are typically associated with the emission inventories used as input (Taghavi et al., 2005). Two approaches, top-down and bottom-up, are commonly used to obtain inventories of atmospheric emissions. The bottom-up approach uses quantification of emissions with detailed data from each emission source (Zhao et al., 2011). The top-down approach is based on the disaggregation process of total emissions from a certain area to smaller administrative units or a regular grid with higher resolution using disaggregation factors (Ossés de Eicker et al., 2008). The top-down approach is very useful namely when local detailed information on main emissions generating activities is poor (Palacios et al., 2001). Tuia et al. (2007) verified that for a medium-sized city, the application of a top-down approach presents good results when compared with a bottom-up approach. Nevertheless, the top-down approach has some limitations. This is particularly true for the road traffic sector in urban areas where this sector is responsible for 70% of the emissions of local pollutants (EC, 2007).

Additionally, the ability for the model to reproduce aerosol optical depth (AOD) has been investigated (Pozzer et al., 2015, Li et al., 2013). AOD is one of the most important parameters used in the assessment of the climate impact of aerosols. It represents the fraction of incident light (of any specific wavelength) scattered and absorbed by the total column of aerosol loading (e.g. Remer et al., 2009). The use of the ground-based remote sensing of aerosols such as Aerosol Robotic Network (AERONET) is one of the important source of information to accurately characterise column-integrated aerosol optical and physical properties.

Modelling tools have been applied to identify and analyse the factors that affect aerosol formation and spatial and vertical distribution. According to Pozzer et al. (2015), and based on modelling results without any mineral dust emissions calculation, the obtained increases in AOD values in the modelling simulations were due to meteorological effects. Moreover, the authors suggest that the increase of the AOD data could be enhanced or dampened if interactive mineral dust emissions were calculated instead of using fixed monthly emissions. Also, some studies identified the secondary inorganic aerosols as the main contributors to AOD values and confirmed that those compounds are relevant in AOD estimations over Europe (Balzarini et al., 2015; Basart et al. 2012a). Similar results were obtained by Roy et al. (2007) over the United States, showing for sulphate compounds a relative contribution that can reach up to 60%, for the total AOD, while the sum of OC and EC contributes only 15%.

The main aim of this chapter is to evaluate the air quality modelling system WRF-CAMx to provide 3D aerosols concentrations in order to estimate the Aerosol Optical Depth. The results from this chapter are used in the next two chapters.

4.2 Methodology for the air quality modelling system WRF-CAMx application

The air quality modelling system WRF-CAMx includes the Weather Research & Forecasting (WRF) model (Skamarock et al., 2008) and the Comprehensive Air Quality Model (CAMx) (ENVIRON, 2013). The reason for selecting this air quality modelling system (WRF-CAMx) was the fact that both models are freely available, and have been extensively used and validated worldwide, being subjected to constant improvement and update. The WRF model is considered the "state of the art" in meteorology and allows the application of different combinations of physics parameterizations. Several studies (Borge, et al. 2008, Mercader, et al. 2010, García-Díez, et al., 2011) performed a comprehensive sensitivity analysis to the WRF model for different regions and for different parameterizations, such as planetary boundary layer, microphysics, land surface model and radiation. Moreover, WRF is a community model that has been increasingly used to study atmospheric dynamics and land-atmosphere interaction at various scales (Zhang et al. 2009, Rotunno et al. 2009, Catalano and Moeng 2010). The CAMx is a Chemical Transport Model (CTM) that has been largely applied to assess the air pollution over Portugal (Monteiro et al., 2017; Sá et al., 2016, Fernandes et al., 2015; Tchepel et al., 2013; Ferreira et al., 2012), and, thus, was chosen as a relevant tool for this study.

The WRF-CAMx air quality modelling system was applied to May 2011 to simulate the 3D pollutant concentration fields. Two domains were designed to be used for application of the modelling approach. The main domain (D1) covers Europe with a horizontal resolution of 27 km and the second domain (D2) covers Portugal with a horizontal resolution of 9 km (Figure 4.1), both with about 12 km vertical column subdivided in 23 levels non-regularly (considering higher detail near the ground). Figure 4.1 also shows the location of the emissions point sources. The distribution of the emissions point sources considered in the WRF-CAMx modelling system is useful to interpret some results.

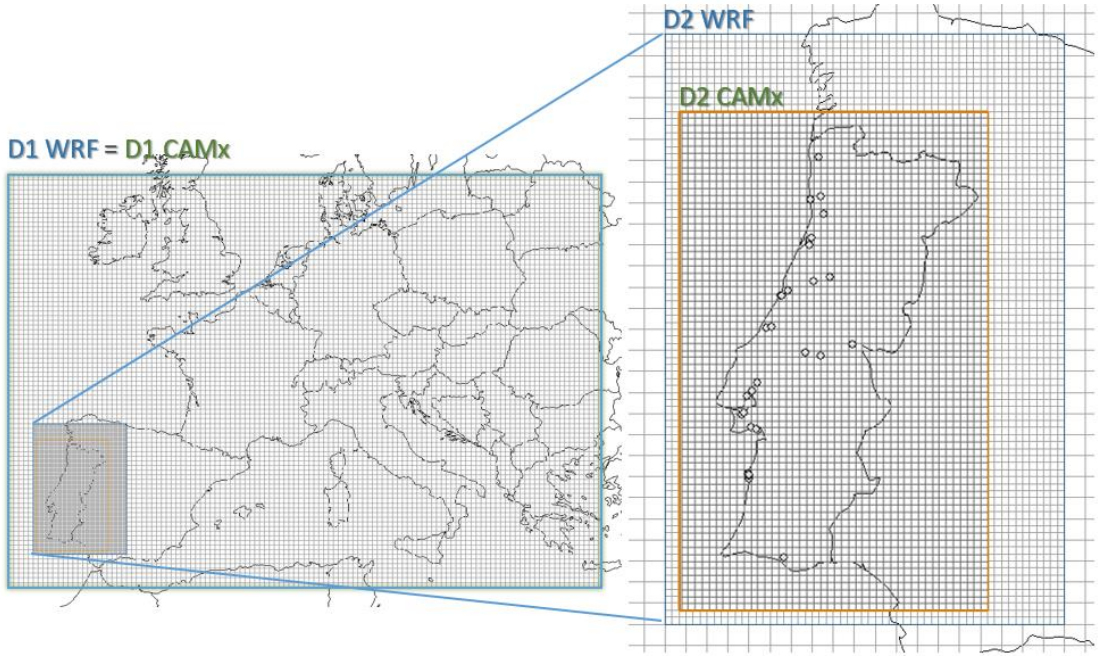

Figure 4.1. Modelling domains for WRF and CAMx modelling applications and location of the emissions point sources (circles) considered in the study.

The meteorological inputs were given by the application of the WRF meteorological model, which was initialized with one-degree resolution ERA-Interim Reanalysis data. The CAMx boundary and initial conditions for Europe (EU) were taken from MOZART, an offline global chemical transport model (Emmons et al., 2010a, b). MOZART outputs were downloaded for May 2011 every 6 hours, at 56 vertical levels and with 1.9ºx2.5º horizontal resolution. The conversion of MOZART aerosol and gaseous species into CAMx species was performed according to the chemical mechanism selected. The chemical mechanism considered includes the gas-phase photochemistry and was resolved through the Carbon Bond (CB5) (Yarwood et al., 2005). The model also contains detailed algorithms for the relevant processes, including aqueous chemistry (RADM-AQ), inorganic aerosol thermodynamics/partitioning (ISORROPIA), and secondary organic aerosol formation/partitioning (SOAP). Mineral dust data were not taken from the initial and boundary conditions from MOZART outputs, since Fernandes et al. (2015) obtained high magnitude values for this aerosol compound compared with measured data. In the present study, the mineral dust was only considered in the post-processing task.

The input data for emissions were prepared for the two domains described on Figure 4.1. The European Monitoring and Evaluation Programme (EMEP) emissions by SNAP sector,

available for gaseous and aerosol species, were disaggregated to the EU grid (D1). The national emission inventory (INERPA) (PEA, 2011) established for regulatory purposes was used for the Portugal domain (D2) (Fernandes et al., 2015, Sá et al., 2016, Tchepel et al., 2013). Emissions of gaseous and aerosol species such as CO, NMVOC, NOx, NH_3, SO_2, PM2.5 and PM10 from anthropogenic sources, by municipality, for Portugal, were disaggregated to the grid cell domain resolution (9x9 km^2) using a top-down methodology. The input/output scheme of the WRF-CAMx system is shown in Figure 4.2.

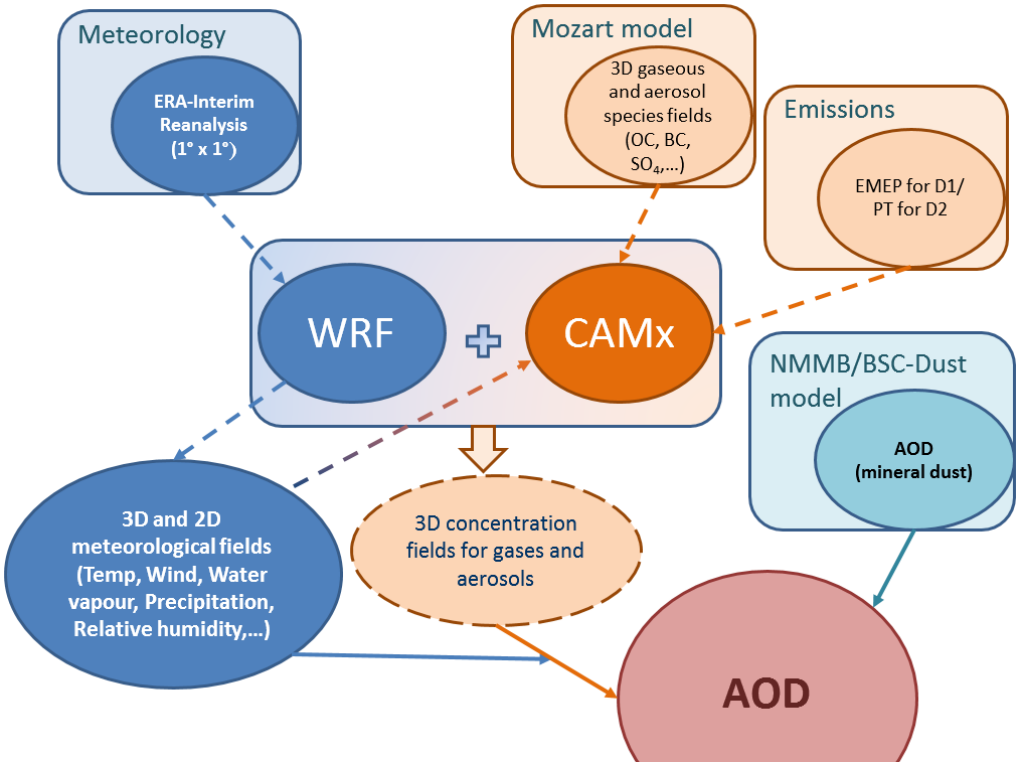

Figure 4.2. Structure of the air quality modelling system WRF-CAMx.

The WRF-CAMx output aerosol compounds considered in this study were total particulate sulphate (PSO4), total primary elemental carbon (PEC), and total primary and secondary organic aerosols (POA + SOA). The mineral dust data used in this work are obtained from the NMMB/BSC-Dust model (downloaded from URL2).

The NMMB/BSC-Dust model (Perez et al., 2011, Haustein et al., 2012) predicts the atmospheric life cycle of the eroded desert dust for a regional and global domain. The resolution is defined to a quarter of a degree (~28 km) in the horizontal direction and to 40

vertical layers stretching up to approximately 15 km in the vertical direction. The available model outputs are processed on a 3–hour basis.

To add the mineral dust AOD from the NMMB/BSC-Dust model to the other compounds provided by the WRF-CAMx system (Figure 4.2), the spatial join tool available in a geographic information system was applied to make both grids compatible. Then, the AOD daily average was computed for each grid cell (9x9 km^2).

To evaluate the performance of the air quality modelling system in terms of surface concentration of PM10, a comparison with measured data from the selected air quality stations (Figure 4.3) was performed. The statistical analysis was applied, using quality indicators such as Correlation Coefficient (r), systematic error (BIAS) and Root Mean Square Error (RMSE) (Table 4.1). BIAS indicates if the model follows the same behaviour of the observed values: if positive, the model results overestimate observations, and if negative, the model results underestimates observations. The RMSE gives information about the absolute errors obtained within the observed-predicted pairs of results. The Pearson Correlation Coefficient (r) value shows the correlation between two data sets in this case between model results and measurements.

Table 4.1. Quality indicators applied in the WRF-CAMx system validation.

Indicator	Equation	Ideal value
BIAS	$BIAS = \frac{\sum_{i=1}^{N}(P_i - O_i)}{N}$	**0**
RMSE	$RMSE = \sqrt{\frac{\sum_{i=1}^{N}(P_i - O_i)^2}{N}}$	**0**
Pearson Correlation Coefficient (r)	$r = \frac{N\left(\sum_{i=1}^{N} O_i P_i\right) - \left(\sum_{i=1}^{N} O_i\right)\left(\sum_{i=1}^{N} P_i\right)}{\sqrt{\left[N\left(\sum_{i=1}^{N} O_i^2\right) - \left(\sum_{i=1}^{N} O_i\right)^2\right]\left[N\left(\sum_{i=1}^{N} P_i^2\right) - \left(\sum_{i=1}^{N} P_i\right)^2\right]}}$	**1**

O_i – observed values, P_i – predicted values; N – Number of values

Measurements data are obtained from air quality stations and currently used to evaluate the performance of the air quality modelling system in terms of surface concentrations. In

Portugal the air quality stations are classified by its type of influence: traffic, industrial and background, and by the surrounding environment: urban, suburban and rural. Figure 4.3 shows the location of the selected background station in terms of data collection efficiency, as is required in the Directive 2008/50/EC. The efficiency required for AQ data is above 85%.

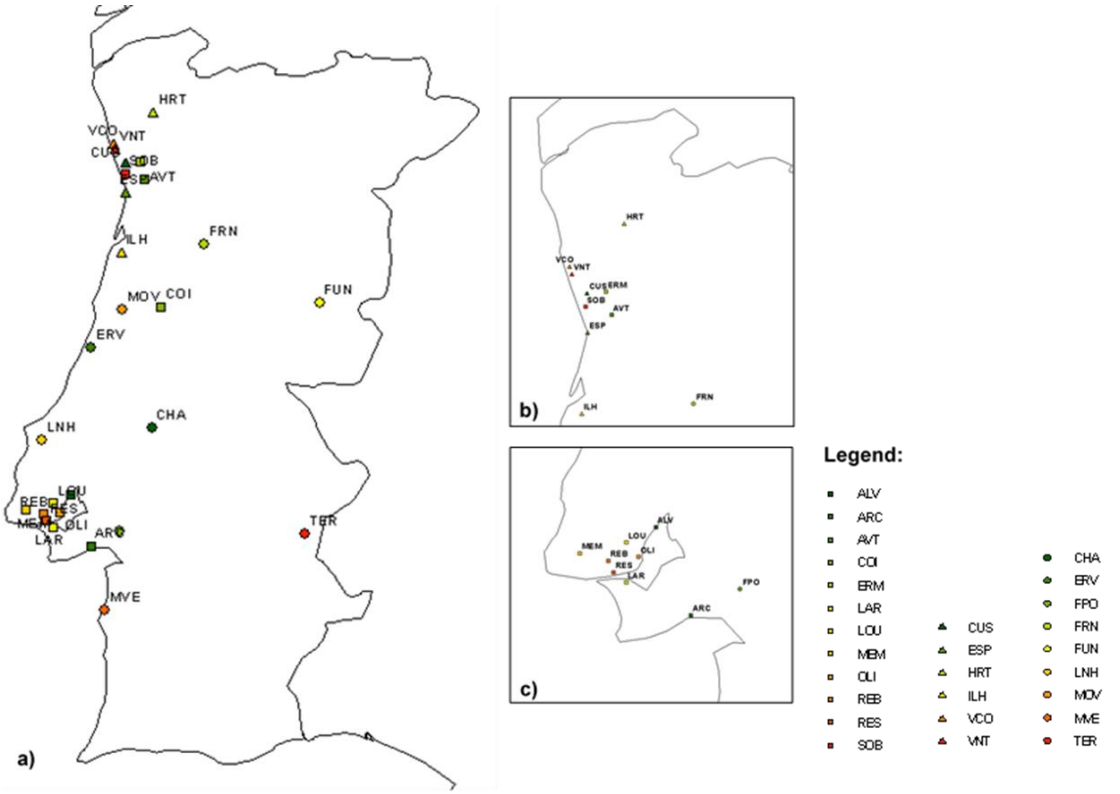

Figure 4.3. Location of the mainland Portuguese air quality monitoring stations (a); part of Northern region (b) and Lisbon region (c). Note the differentiation of urban (square), suburban (triangle) and rural (circle) background stations.

The inter-comparison of modelled aerosol load over the vertical column with measured data is performed in terms of Aerosol Optical Depth (AOD). The aerosol column mass loading and the relative humidity provided by the modelling system are used to compute the AOD at 550 nm. An exhaustive description of the AOD calculation can be found in section 3.2 (Chapter 3). In order to evaluate the AOD values from the air quality modelling system, AERONET observations were used. Figure 3.2 (Chapter 3) presents the location of the AERONET stations.

4.3 Modelling results and discussion

In this section, results from the air quality modelling system are explored. In sub-section 4.3.1, the PM10 concentrations obtained from the model are compared with the measured data from the national air quality monitoring network. The vertical analysis of different particulate matter (PM) components is presented in sub-section 4.3.2. In sub-section 4.3.3, the results from the spatial analysis of aerosol optical depth (AOD) provided by the modelling approach are presented. The AOD data from the modelling approach applied in this work were analysed on a daily average basis and compared with AERONET data observations in order to assess the performance of the model (sub-section 4.3.4). The results were processed and represented using python tools.

4.3.1 Assessment of air quality modelling system

In order to evaluate the performance of the air quality modelling system, the PM10 concentrations were compared with measured data for May 2011. All background air quality stations over Mainland Portugal were selected (Figure 4.3).

Figure 4.4 represents the average measured and modelled PM10 daily concentrations in terms of different classification of background stations, such as rural, suburban and urban. In order to understand the contribution of different aerosol compounds (OC, BC, SO_4 and Dust) to the total PM10 concentrations, the modelled values were subdivided per each aerosol compound.

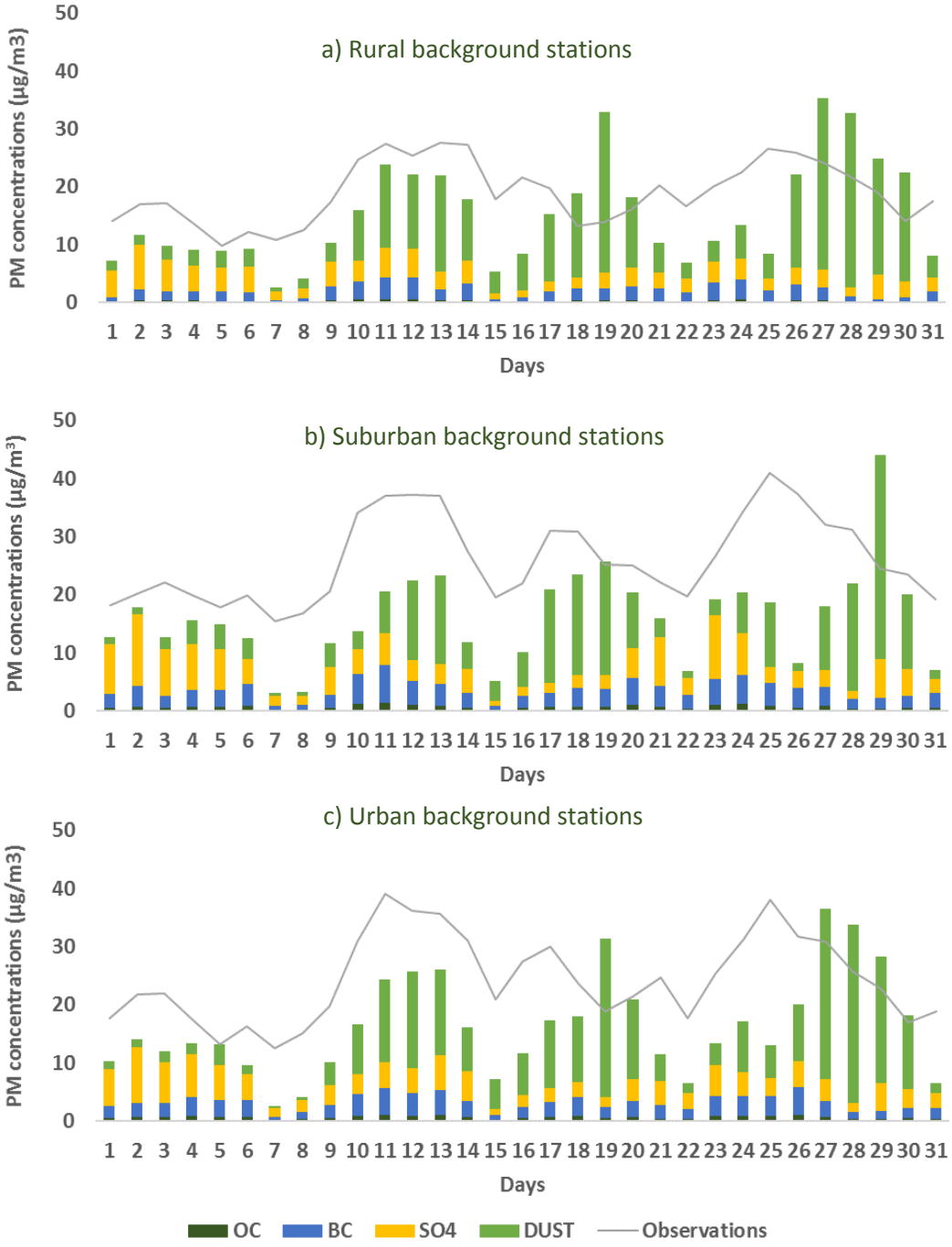

Figure 4.4. Average of measured and modelled PM10 daily concentrations for all a) Rural b) Suburban and c) Urban background stations. The modelled PM10 data were represented in terms of aerosol compound (OC, BC, SO_4 and Dust) contribution.

Analysing Figure 4.4 one clearly realises that the Urban and Suburban background stations display a better performance in obtaining the temporal profile of PM10 concentrations in

comparison with rural background stations. In general, the modelling approach underestimated PM10 concentrations. As PM10 concentrations increase, a dominance of mineral dust and/or sulphates becomes more evident in the modelling results. The aerosol compound with the biggest contribution during the study period is clearly the mineral dust, with major relevance in two periods: 9th-21st and 24th-30th May 2011. During the period of 1st-6th May 2011 a bigger contribution of sulphate was observed. The concentrations of aerosol compounds are different for each day due to the influence of meteorological conditions.

Three statistical parameters, described previously and presented on Table 4.1, were chosen to evaluate the performance of the model approach. Table 4.2 shows the results of the statistical indicators for all the background air quality stations in terms of PM10.

Table 4.2. Statistical parameters computed for PM10 daily concentrations.

Station	Classification	Observed mean (µg·m^{-3})	Predicted mean (µg·m^{-3})	Correlation coefficient	Root mean square error (µg·m^{-3})	BIAS (µg·m^{-3})
CHA	Rural	18.90	14.09	0.32	10.0	4.8
ERV	Rural	24.96	20.14	0.35	14.1	4.8
FPO	Rural	23.77	16.48	0.38	15.7	7.3
FRN	Rural	19.12	14.40	0.29	11.2	4.7
FUN	Rural	11.33	10.24	0.13	9.9	1.1
LOU	Rural	21.42	11.48	0.31	12.6	9.9
MOV	Rural	28.96	20.24	0.48	13.3	8.7
MVE	Rural	24.06	17.47	0.49	14.2	6.6
TER	Rural	21.37	12.09	0.33	13.9	9.3
	Mean	21.54	15.18	0.34	12.79	6.36
ESP	Suburban	25.06	16.69	0.40	13.1	8.4
CUS	Suburban	32.43	14.42	0.20	21.8	18.0
HRT	Suburban	20.56	15.75	0.37	9.7	4.8
ILH	Suburban	28.86	22.70	0.78	10.5	6.2
VCO	Suburban	25.26	13.64	0.26	15.4	11.6
VNT	Suburban	48.19	14.41	0.28	36.6	33.8
	Mean	30.06	16.27	0.38	17.84	13.79
ALV	Urban	24.32	19.23	0.68	10.1	5.1
ARC	Urban	29.24	18.73	0.43	15.9	10.5
AVT	Urban	24.34	15.83	0.34	13.7	8.5
ERM	Urban	31.50	13.86	0.33	20.8	17.6
COI	Urban	24.82	16.15	0.29	13.7	8.7
LAR	Urban	29.02	17.17	0.42	15.9	11.8
LOU	Urban	26.82	15.00	0.49	15.1	11.8
MEM	Urban	24.11	14.23	0.46	13.6	9.9
OLI	Urban	34.47	17.46	0.44	20.6	17.0
REB	Urban	22.70	16.07	0.55	11.0	6.6
RES	Urban	28.08	15.89	0.47	15.8	12.2
SOB	Urban	29.58	18.26	0.51	15.1	11.3
	Mean	27.42	16.49	0.45	15.11	10.93

Table 4.2 shows the magnitude of the mean values of PM10 daily concentrations obtained from the modelling approach, which, on average, are lower than the measured values. From the analysis of the correlation coefficients, one concludes that the urban background stations perform better, in terms of similarity between observed and simulated concentration values.

In all background stations considered in this analysis, PM10 concentrations tend to be underestimated by the modelling approach, especially in suburban background stations. The BIAS for the daily PM10 concentrations varies from 4.8 to 33.8 μg/m^3 and the RMSE varies from 9.7 and 36.6 μg/m^3 for this kind of background stations.

4.3.2 Aerosols vertical distribution analysis

To better understand the influence of the atmospheric processes, an analysis of the vertical distribution for each aerosol compound was performed. The main objective is to assess the influence of the each aerosol compound in the aerosol loading and to identify possible long-range transport of mineral dust in the atmosphere. For this purpose, the vertical profile of the different aerosol compounds was analysed for four locations: Cabo da Roca, Évora, Caceres and Huelva (Figure 3.2 (Chapter 3)). At all studied sites, a similar pattern of the vertical distribution was obtained. An example for Huelva on May 14, 2011 is presented in Figure 4.5.

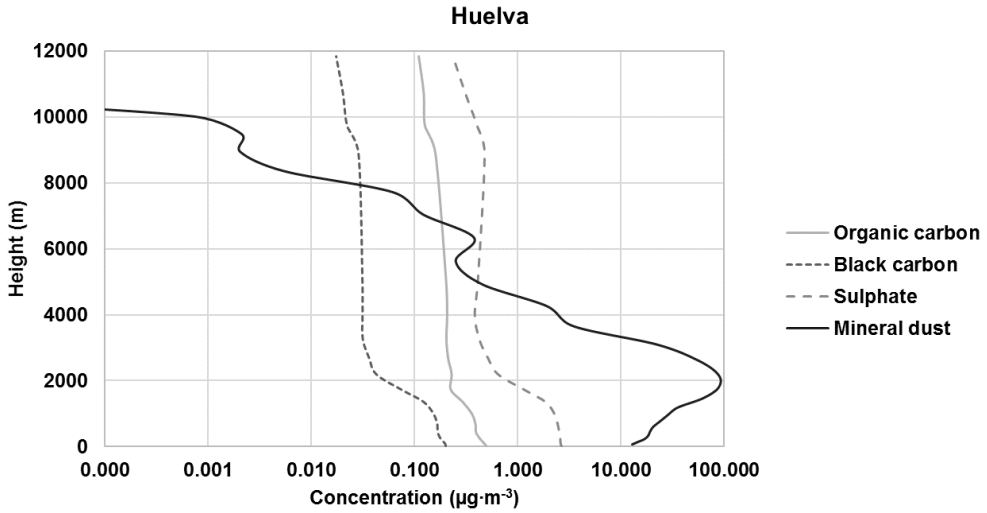

Figure 4.5. Vertical distribution of aerosol compounds concentrations in Huelva on May 14, 2011.

For the study period, the highest aerosol concentration was obtained at 2000 m and mineral dust is the compound with the largest contribution. The second compound with the most relevant contribution is sulphate, below 1200 m. This holds true for all selected locations. For mineral dust, the highest values are obtained in the Southern part of the study domain (Huelva).

4.3.3 Spatial distribution of the AOD modelling results

The WRF-CAMx results without mineral dust were analysed to assess the contribution of different aerosol compounds for the total AOD. Figure 4.6 shows the spatial distribution of the monthly mean AOD for different aerosol compounds for the studied period. Sulphate is identified as one of the highest contributors for total AOD for the study area (Figure 4.6). It exhibits higher values over the coast line, reaching a maximum of 0.14. The reason is the location of the point sources (Figure 4.1) and emission data from area sources considered for the modelling system.

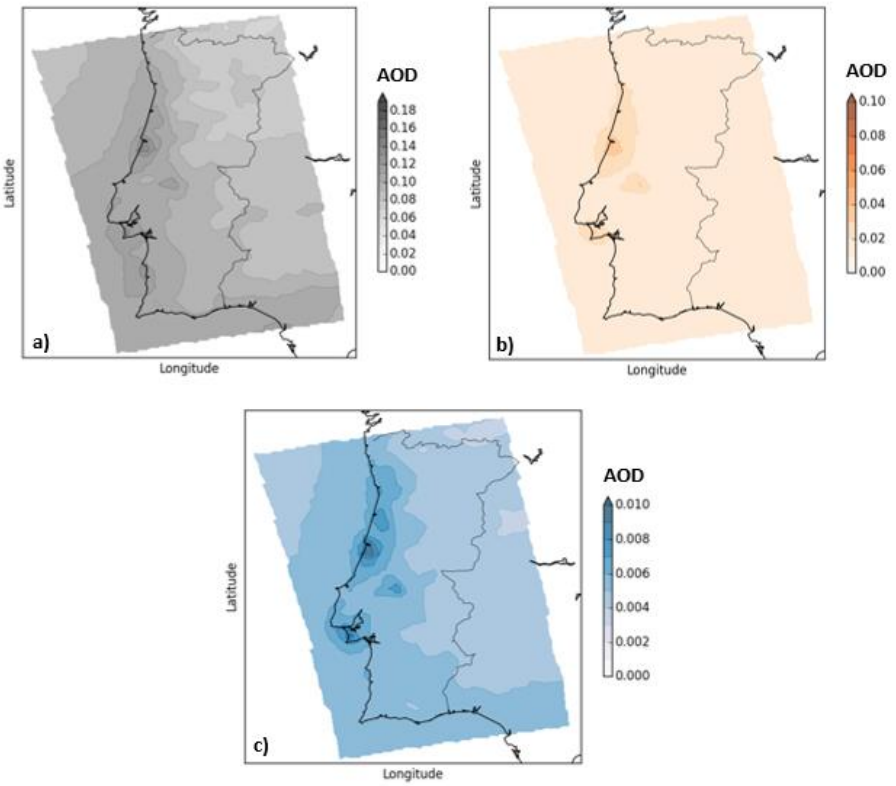

Figure 4.6. Monthly mean of AOD for May 2011 for: a) SO_4, b) OC and c) BC. (Notice the colour scales' ranges are different)

Figure 4.7b shows the monthly mean of mineral dust data distribution obtained from the NMMB/BSC-Dust model for Portugal. As can be seen in this Figure, the AOD values are higher in the Southern part of the studied region, due to the influence of mineral dust. Despite the long-range transport of mineral dust, the overall contribution of organic carbon (OC), black carbon (BC) and sulphate (SO_4) compounds is very important reaching 76% for the monthly average AOD values (see Figure 4.7a).

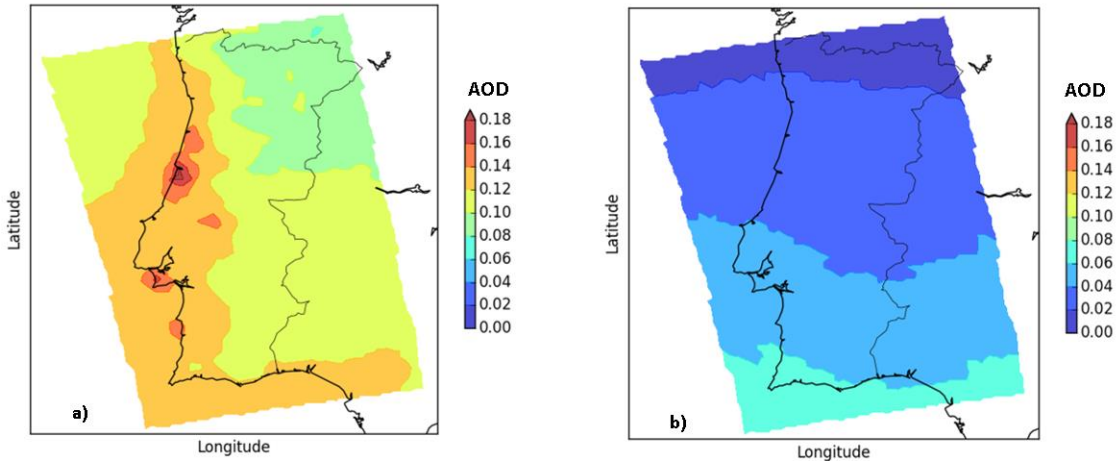

Figure 4.7. Spatial distribution of monthly mean AOD for May 2011 from: a) OC+BC+SO_4 and b) mineral dust obtained from modelling.

The spatial pattern of the modelled mineral dust AOD (Figure 4.7) shows highest AOD values over the Southern end of Portugal. According to the results in Tchepel et al. (2013), the spatial pattern is influenced by the transport of air masses and complex circulation at higher altitude, and by the transport of dust aerosols from Africa affecting AOD data at the Southern boundary of the study domain. The spring events were already noticed in previous works, over Iberian Peninsula and Western-southern Europe (Monteiro et al., 2015; Tchepel et al., 2013; Salvador et al., 2013; Pey et al., 2013; Basart et al., 2012a).

The spatial pattern is analysed in terms of the monthly averaged AOD (Figure 4.8). These results are computed based on the average of the daily AOD values obtained by the contribution of the OC, BC, SO_4 and mineral dust particulate matter compounds.

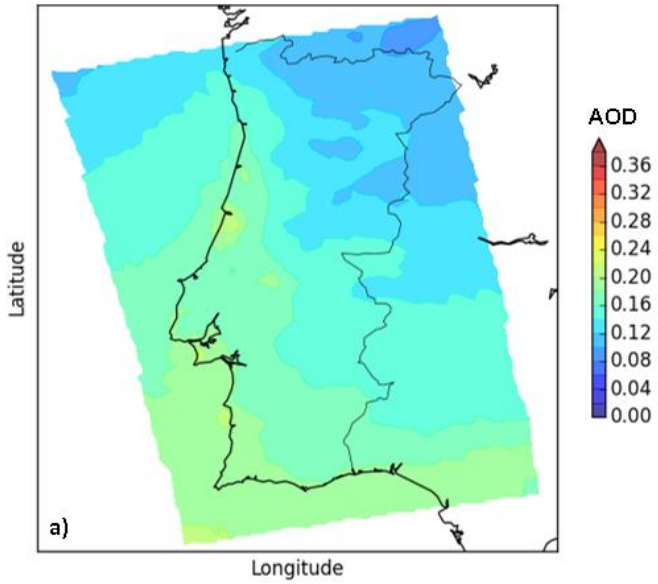

Figure 4.8. Spatial pattern of the monthly mean AOD for May 2011 obtained with modelling approach.

Figure 4.8 exhibits higher AOD values in the Southern part of the study domain, following the spatial pattern of mineral dust as discussed above (see Figure 4.7). The contribution of the sum of OC, BC and SO_4 compounds (Figure 4.7a) for the total monthly average AOD values (Figure 4.8) is very high, around 76%. This contribution was clearly influenced by the point sources emissions considered in the WRF-CAMx modelling system represented in Figure 4.1.

4.3.4 Evaluation of AOD modelling results

The AOD results from the modelling approach were assessed with Aerosol Robotic Network (AERONET) level 2.0 (cloud screened and quality-assured) AOD measurements [URL3] from 4 stations (Figure 3.2) located within the study domain. In order to use the same methodology applied to validate satellite AOD data with AERONET observations described on last chapter, the daily modelling AOD data was calculated for the same days. Figure 4.9 shows the scatterplot of the daily mean AOD values for May 2011 at all stations located within the modelling domain.

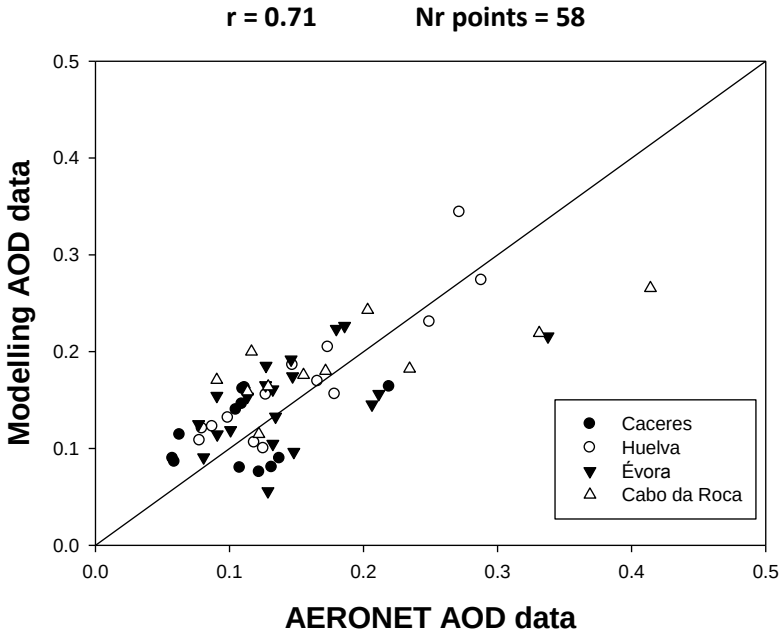

Figure 4.9. Scatterplot of daily mean AOD values from AERONET versus modelling results.

From the comparison of the AOD data provided by modelling approach with AERONET observations, a good agreement was obtained with a correlation coefficient of 0.71 (Figure 4.9). Thus, this result indicates that our modelling approach is an adequate tool to obtain the AOD data with good performance.

4.4 Summary and conclusions

This work intended to study the vertical, temporal and spatial aerosols distribution over Portugal using the results of an air quality modelling approach. In order to evaluate the performance of the air quality modelling system, the PM10 concentrations were compared with those measured by background air quality stations over mainland Portugal.

In general, the air quality modelling approach underestimated PM10 concentrations. From the analysis of the correlation coefficients, one concludes that the urban and suburban background stations yield a better agreement between observed and simulated concentration values in comparison with rural background stations. As PM10 concentrations increase, a dominance of mineral dust and/or sulphates becomes more evident in the modelling results. The aerosol compound with the highest contribution is clearly mineral

dust, especially in two periods, 9th-21st and 24th-30th May 2011. During the period of 1st-6th May 2011, a bigger contribution of sulphate was observed.

To better understand the processes in the atmosphere and to identify the potential aerosols transport, the outputs were assessed by vertical layers. For the study period, the highest aerosol concentration was obtained at 2000 m and the mineral dust is the compound with the largest contribution. The second most relevant compound is sulphate, below 1200 m. This occurred for all selected locations. For mineral dust, the highest values are obtained in the Southern part of the study domain (Huelva).

Results were assessed by means of an analysis of aerosol optical depth (AOD) at 550 nm, and compared with the measured AOD data provided by four AERONET stations located within the study domain. The results show that the highest concentrations and AOD are obtained in the South of Portugal, as a result of long-range transport of mineral dust. Furthermore, the overall contribution of OC, BC and SO_4 compounds is very important, reaching 76% for the monthly average AOD values. The comparison between AOD measured and modelled data presented a correlation coefficient of 0.71.

This work allowed understanding the behaviour and limitations of the air quality modelling approach to quantify the aerosol concentrations. In general, the air quality modelling approach demonstrates a good performance when applied over Portugal, and it is a fundamental and helpful tool to be used in air quality studies.

Chapter 5

Comparison of SEVIRI observations and Air Quality Modelling results

---

Chapter Index:

5.1 Introduction……87

5.2 Methodology……..89

5.3 Results and discussions……94

5.3.1 - Comparison of satellite observations and modelling results……..94

5.3.2 - Validation with AERONET data……..96

5.4 Summary and conclusions……100

5 Comparison of satellite observations and air quality modelling results

The contents of this chapter are partially considered for publication in:
Fernandes, A.P., *Riffler, M., Ferreira, J., Wunderle, S., Borrego, C., and Tchepel, O., (Submitted). Spatial Analysis of Aerosol Optical Depth Obtained by Air Quality Modelling and SEVIRI Satellite Observations over Portugal. Atmospheric Pollution Research.*

The aim of this chapter is to analyse the benefits of combining the AOD data provided by satellite observations with high temporal resolution and air quality modelling. Satellite data obtained by Spinning Enhanced Visible and Infra-Red Imager (SEVIRI) instrument and air quality modelling results from the Comprehensive Air Quality Model (CAMx) over Portugal previously analysed on Chapter 3 and 4 respectively were explored.

This chapter is divided in four sections. Section 5.1 gives an introduction. A description about the methodology applied to combine both sources of data is given in section 5.2. Section 5.3 presents the results and discussion. A summary and some conclusions are present in the last section (Section 5.4).

5.1 Introduction

Satellite remote sensing may provide data with high spatial and temporal coverage and allows the characterisation of atmospheric compounds for vertical columns. Moreover, the use of air quality modelling in combination with satellite observations creates new

opportunities of research to assess the contribution of different transport processes and pollution sources. The combination of satellite remote sensing data with air quality modelling would improve both the characterisation of the spatial and temporal variations and the identification of the air pollution sources and their potential effects.

Recently, the interest in using satellite data in air quality modelling has been increasing in the research community (Park et al., 2014; Li et al., 2011; Emili et al., 2011; Strunk et al., 2011; Elbern et al., 2010; Claeyman et al., 2010; Sofiev et al., 2009, Vijayaraghavan et al., 2008). In comparison with surface measurements, such as AOD data from AERONET stations, satellite data improve two main aspects: a more complete spatial coverage and a better characterisation of the aerosols compounds in the vertical column. (Fernandes et al., 2015; Duncan et al., 2014; Tchepel et al., 2013; Vijayaraghavan et al., 2008). Satellite remote sensing data may be used to improve the application of air quality models (Duncan et al., 2014; Vijayaraghavan et al., 2008). However, the usage of these data has some limitations related to accessing, processing, and correctly interpreting them (Duncan et al., 2014). Currently, almost all instruments that provide information relevant to the atmospheric composition, such as, NO_2, SO_2, formaldehyde levels and AOD (Fishman et al., 2008), are on-board of polar-orbiting satellites, which overpass a given region approximately once a day during daylight hours. Therefore, for air quality applications, data from geostationary satellites are preferred as they allow for continuous observations of the same region. Thus, the Spinning Enhanced Visible and Infra-Red Imager (SEVIRI) instrument on the Meteosat Second Generation (MSG) provides data at 15-min intervals throughout the day that gives an overview on the temporal variations and long-range transport of pollution. The relevant limitations of the satellite data described by Duncan et al. (2014) are: 1) the lack of information on the vertical distribution and chemical composition of the aerosols, 2) the gaps in spatial coverage due to clouds, 3) the complex relationship between AOD, relative humidity and PM concentrations. Therefore, high AOD values do not necessarily indicate high PM concentrations at surface level. On the other hand, satellites also have important advantages, since they can provide data everywhere in the world, covering a wide area in a very short time frame, particularly aloft, over the oceans and in areas where data may not be available, and can be used to account for the contributions of pollutants transported over long distances needed for the boundary and initial conditions of regional air quality models.

The chemical transport models are powerful tools, able to provide information with high spatial and temporal distribution, vertical profiles and aerosol composition at all points in a predefined grid that may be used to improve the performance of satellite aerosol retrievals

(Dore et al., 2015; Li et al., 2015; Hu et al., 2009; Randall, 2008). Chemical transport models have particularly advantages due to their fast run times and the ability to perform multiple simulations with good performance when compared with ground-based measurements (Dore et al., 2015).

A combination of the satellite observations with air quality modelling may provide promising results to analyse the vertical distribution and to characterise the long-range transport of atmospheric pollution, including mineral dust from natural sources. This long distance transport of mineral particles is initiated by massive resuspension processes in arid zones of North Africa. Saharan dust may contribute more than 60% to the total PM10 concentration in Mediterranean countries during a strong dust pollution event that can cause a strong impact on air quality (Fernandes et al., 2015; Monteiro et al., 2015; Basart et al., 2012a; Pay et al., 2012). This may lead to exceedances of the European limit value of 50 $\mu g \cdot m^{-3}$ for daily average PM10 concentration. Although these events are detected with a much higher frequency in the Mediterranean domain, Central and Northern Europe are also sporadically influenced. Natural episodes of high PM levels are more frequent in Spring/Summer. Therefore, an important aspect is the development of a consistent methodology to contribute to a better knowledge of the natural aerosol burden.

In this chapter an analysis of SEVIRI observations and air quality modelling results is presented as a means to assess the AOD distribution over Portugal. The AOD data from SEVIRI were described in Chapter 3 and the modelling AOD data were described in Chapter 4. The modelling results and aerosol satellite retrievals obtained by SEVIRI were evaluated against AERONET observations. The AERONET data were also described in Chapter 3.

5.2 Methodology

In this chapter, the comparison of aerosol load provided by modelling with SEVIRI satellite observations is made in terms of AOD. Data from SEVIRI and AERONET observations were used in this study. To investigate the spatial distributions of AOD over mainland Portugal, daily AOD data of May 2011 were computed. The daily average AOD values were calculated considering the period between 6-17 UTC due to the availability of satellite data for diurnal time only. The domain used to perform the comparison of AOD from modelling outputs and SEVIRI observations over mainland Portugal (Figure 5.1) comprises cells with a size of 9 x 9 km^2.

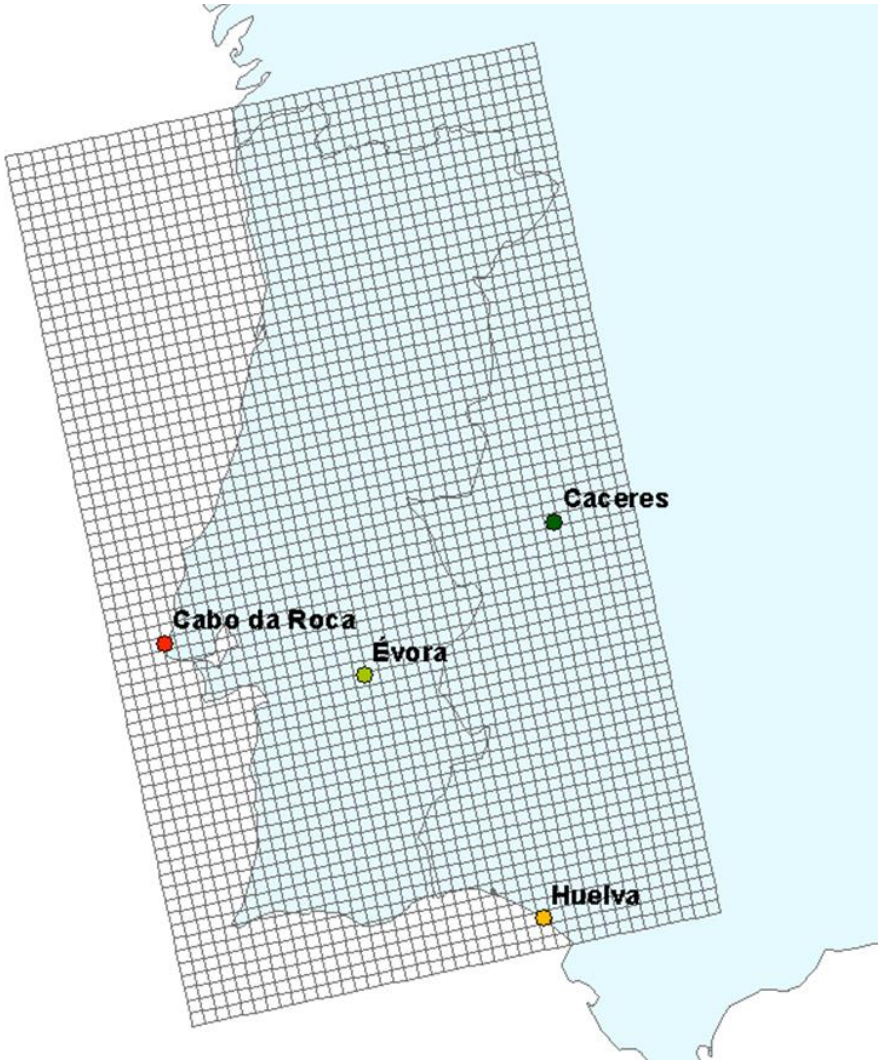

Figure 5.1. Study domain (9 x 9 km^2) and location of AERONET stations.

The SEVIRI AOD data were assessed by calculating the daily average over mainland Portugal. This instrument provides images with a repeat cycle of 15 minutes. Thus, for each hour were obtained four images. Firstly, to obtain the hourly data the maximum value for each cell was selected for each hour (Figure 5.2).

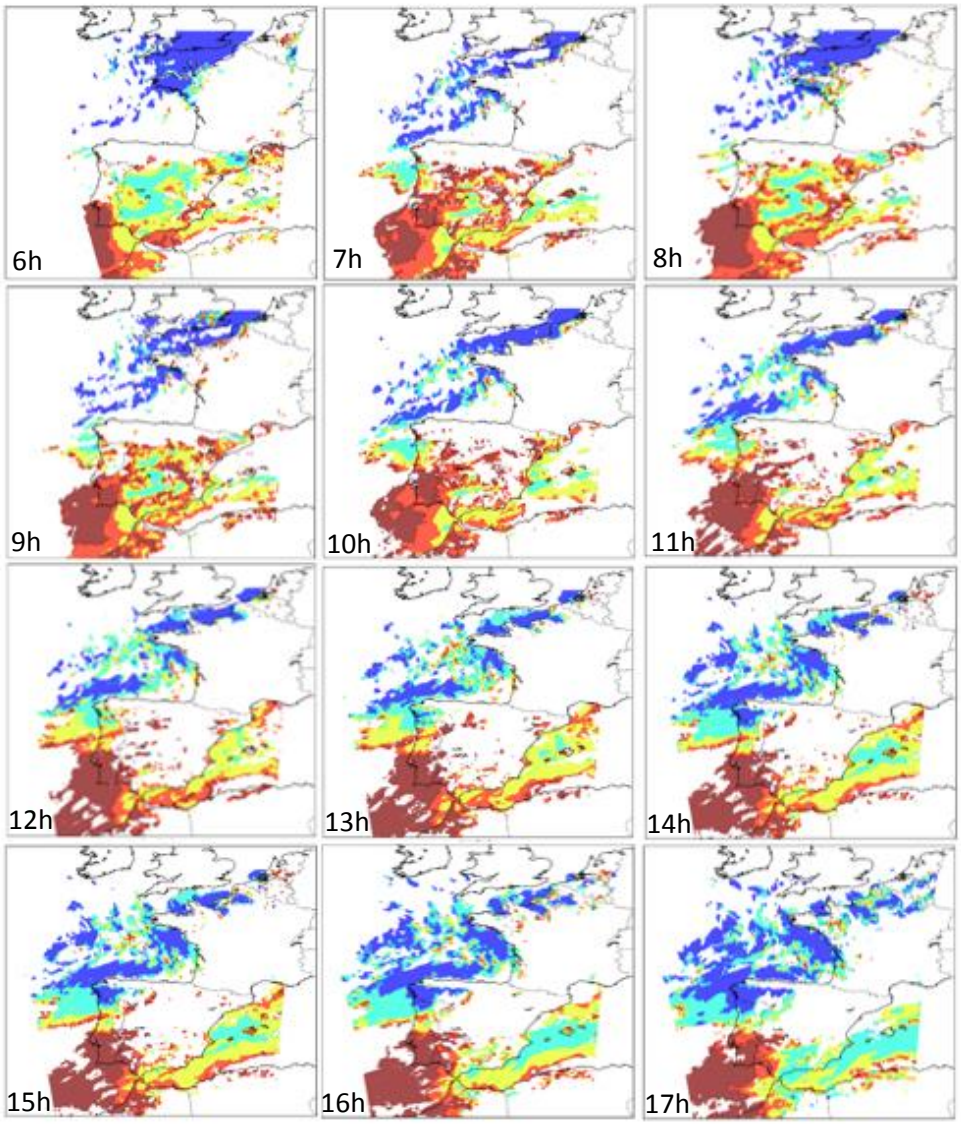

Figure 5.2. Hourly SEVIRI AOD data for 14 May 2011 (between 6h-17h) with original pixel size (3x3 km^2).

Imagens from SEVIRI during the sunlight hours were used to study the AOD distribution. Thus, the daily mean values were calculated for each point with at least six hours of data from the total of twelve hours (Figure 5.2). An example of the daily mean AOD values for 14th May is presented in Figure 5.3.

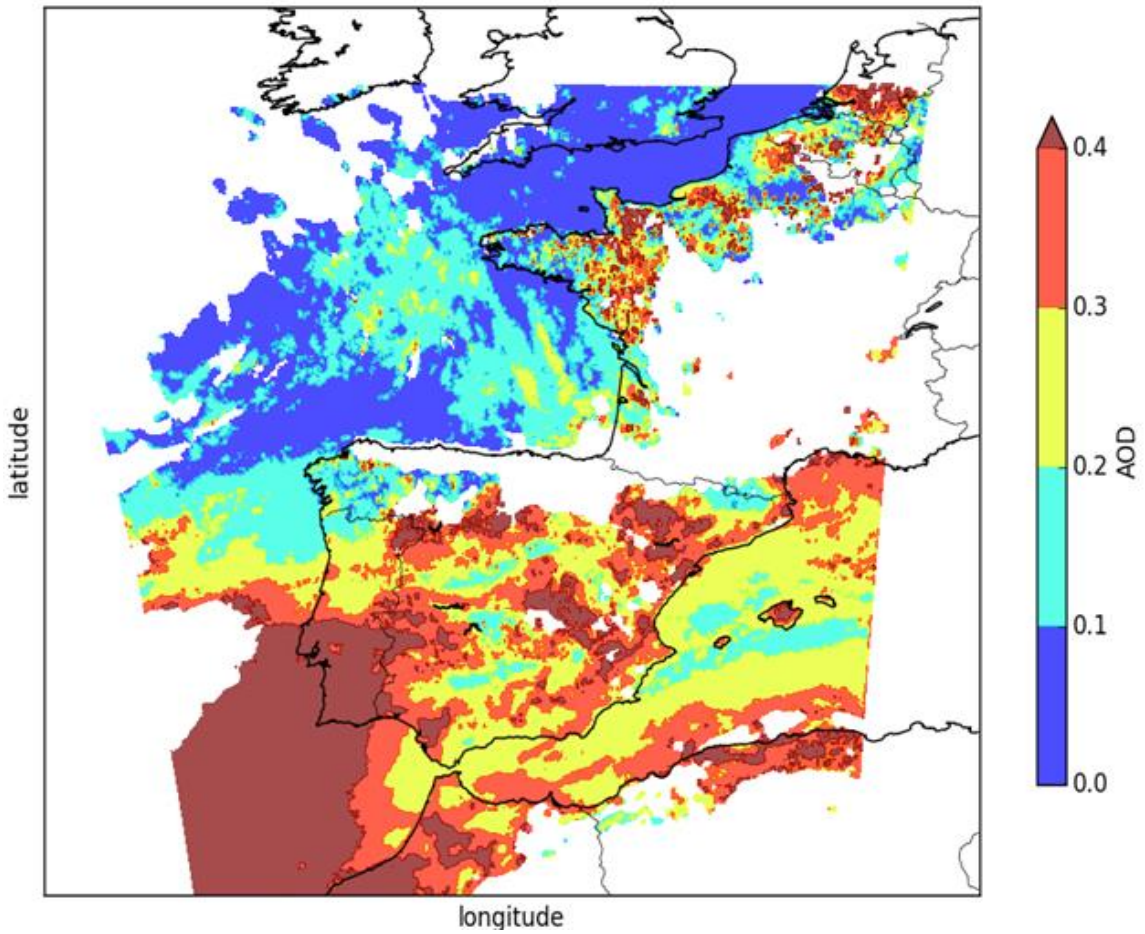

Figure 5.3. Daily mean AOD SEVIRI data (14 May 2011) with original cell size (3x3 km^2).

To adjust the SEVIRI grid data (Figure 5.3) to the grid of the modelling data (Figure 5.1), spatial analysis tools implemented within Geographic Information System (GIS) were applied. The result of this method is a grid with a daily mean AOD SEVIRI data adapted to be compared with modelling results (Figure 5.4).

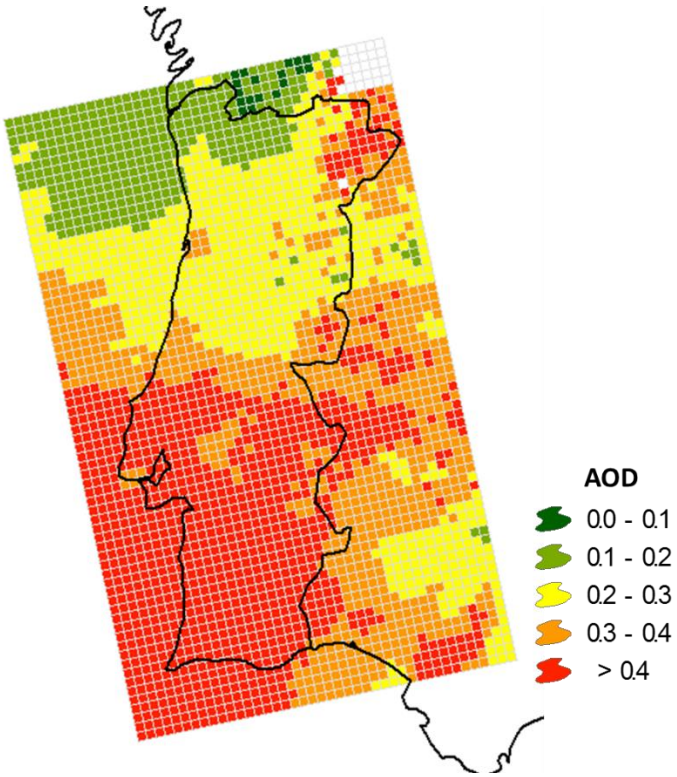

Figure 5.4. Daily mean SEVIRI data (14 May 2011) with the grid cell size and projection compatible with the modelling grid (9x9 km^2).

The comparison of the spatial AOD data obtained from modelling simulations and SEVIRI observations is quantified through the computation of the relative differences, defined as:

$$\text{Relative differences } (\%) = \frac{(\text{AOD}_{\text{Modelling}} - \text{AOD}_{\text{SEVIRI}})}{\text{AOD}_{\text{SEVIRI}}} \times 100 \qquad \text{Equation 5.1}$$

In addition, the Pearson correlation coefficient was calculated using AOD daily averages obtained by SEVIRI observations and modelling results for each pixel of the study domain.

In order to evaluate the evolution of AOD data from modelling and SEVIRI, daily AOD data and Ångström coefficients from AERONET stations (Figure 5.1) described on Chapter 3 were used. To complete the analysis, the Normalised Root Mean Square Error (NRMSE) was applied (Equation 2).

$$NRMSE = \frac{\sqrt{\frac{\sum_{i=1}^{n}(X_{obs,i} - X_{model,i})^2}{n}}}{X_{obs,max} - X_{obs,min}} \qquad \text{Equation 5.2}$$

where X_{obs} are observed values and X_{model} are modelled values at time i.

5.3 Results and discussions

In this section, results from the comparison and analysis of AOD data provided by the air quality modelling, SEVIRI satellite observations and AERONET ground-based measurements are presented and discussed.

5.3.1 Comparison of satellite observations and modelling results

To analyse the spatial pattern of the AOD data provided by modelling approach and satellite observations, the monthly mean AOD data (May 2011) was estimated, as depicted in Figure 5.5. The modelling approach results are presented in Figure 5.5a and the SEVIRI observations on Figure 5.5b.

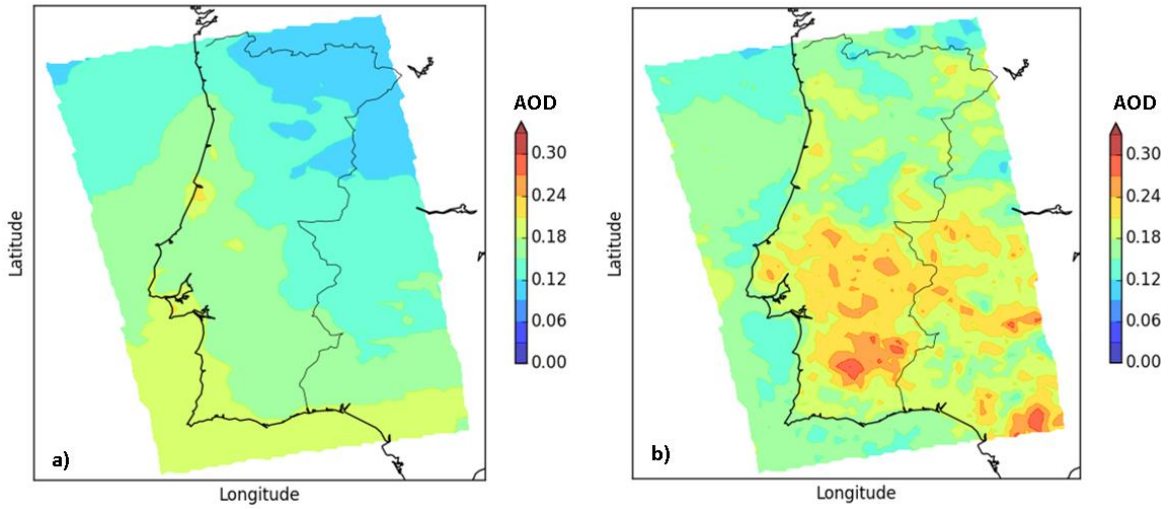

Figure 5.5. Spatial distribution of monthly mean AOD for May 2011 obtained with: a) Modelling approach and b) SEVIRI observations.

From the analysis of the spatial distribution of AOD (Figure 5.5) we observe higher AOD values (AOD>0.24) from satellite observations then from model simulations. This is particular's the case for inland regions in the southern part of the domain.

Figure 5.6 shows the spatial distribution (Figure 5.6a) and the frequency histogram (Figure 5.6b) of the relative differences between the monthly mean AOD data from modelling and SEVIRI.

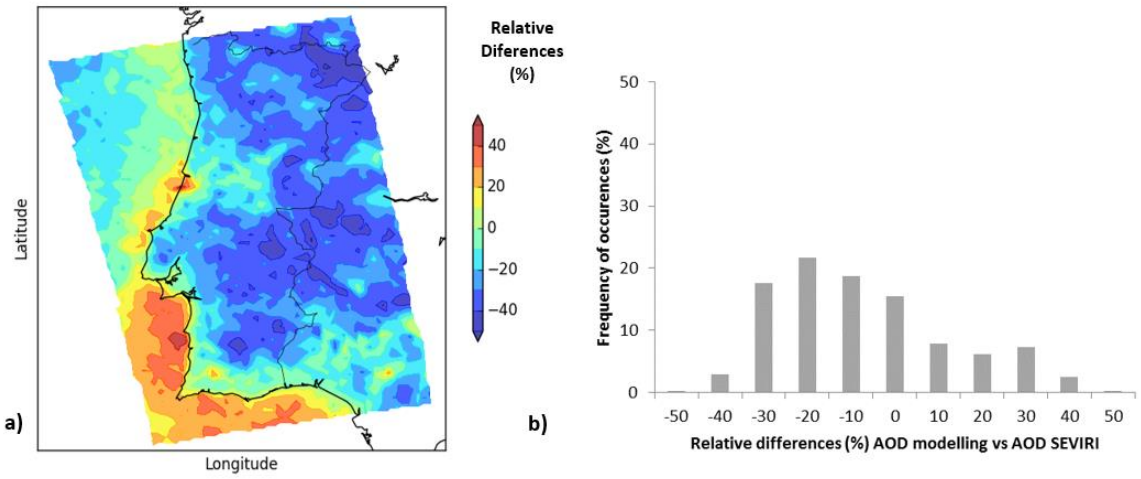

Figure 5.6. Relative differences between the monthly mean AOD obtained from the modelling system and SEVIRI: a) Spatial distribution and b) Frequency histogram.

The relative differences between the two datasets obtained for daily average AOD are mostly within ± 40% and show a bimodal distribution (Figure 5.6). As illustrated in Figure 5.6a, the spatial pattern is characterised by higher positive values (model AOD >satellite AOD) over ocean and negative values (model AOD < satellite AOD) over land. The Pearson correlation coefficient (r) was also calculated between the satellite observations and modelling results for each cell of the study domain. For this purpose, daily averages AOD obtained from SEVIRI observations and modelling results are used. As shown in Figure 5.7a, the higher values of correlation coefficient were obtained mainly in the Southern part of the domain influenced by long-range transport of mineral dust. A frequency histogram is presented in Figure 5.7b.

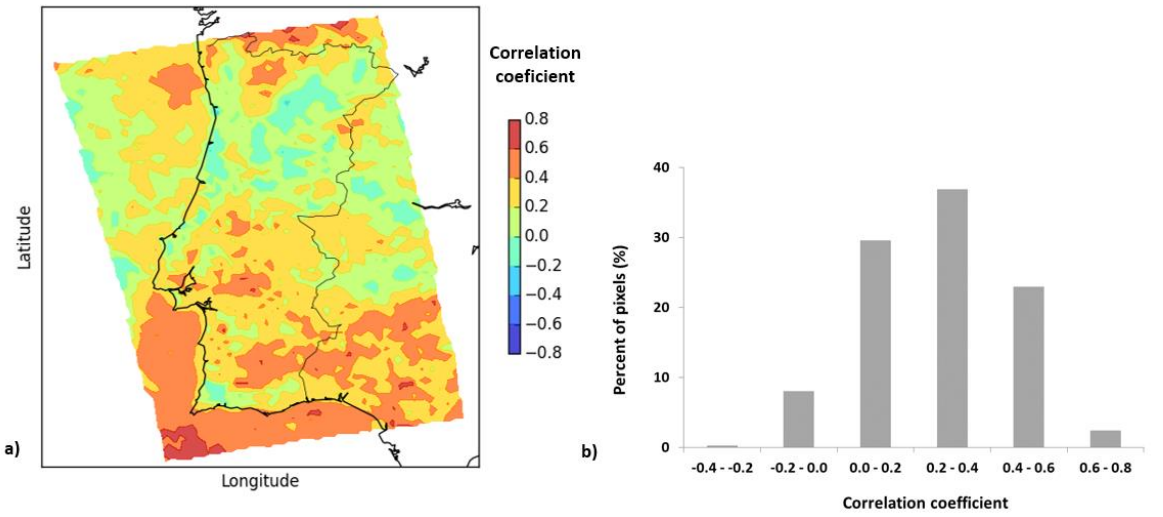

Figure 5.7. Correlation between modelling results and SEVIRI observations during May 2011 a) Spatial distribution, b) Frequency histogram (in percentage, %).

A combined analysis of Figures 5.6 and 5.7 demonstrates that cells with better correlation located in the South part of the domain are overlapped with the cells where values of AOD have the highest discrepancy between the two datasets (Figure 5.7). As demonstrated previously, this part of the study domain is strongly influenced by the long-range transport of mineral dust. Therefore, it may be concluded that the satellite data and modelling results are in good agreement in terms of the AOD temporal variations, including mineral dust events, but their estimations are differing in terms of the absolute values.

5.3.2 Validation with AERONET data

SEVIRI AOD retrievals and modelling results were compared with AERONET observations. The AERONET data available for May 2011 with level 2.0 AOD measurements from 4 stations located within the modelling domain were used in this study (Figure 5.1). For all datasets, modelling data, SEVIRI and AERONET observations, the daily mean AOD data was calculated. Only days with a minimum of 6 hours of observations were selected for the analysis. Figure 5.8 shows the evolution of the daily mean AOD values provided by SEVIRI, modelling and AERONET and the daily mean Ångström coefficient (AC) values provided by AERONET stations computed using wavelengths of 440 nm and 870nm. The AC is inversely related to the average size of the particles in the aerosol: the smaller the particles, the larger the exponent.

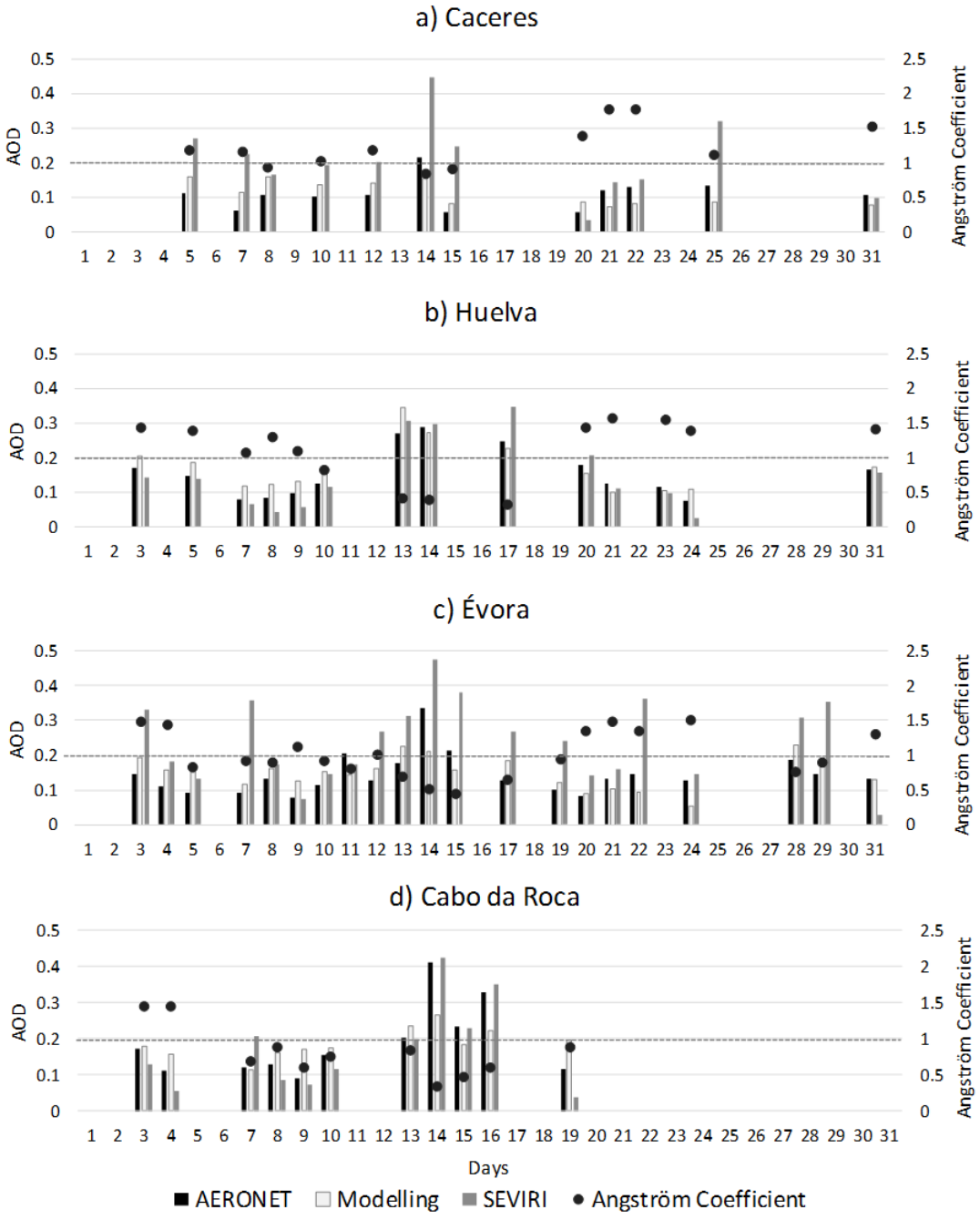

Figure 5.8. Time series of daily mean AOD and AC values from AERONET stations and daily mean AOD values from modelling and SEVIRI data. a) Caceres, b) Huelva, c) Évora and d) Cabo da Roca.

SEVIRI and modelling data present a better agreement with AERONET observations for the Cabo da Roca and Huelva stations, located in the coastline (Figure 5.1). For all the

stations, higher AOD values and low AC values are observed for the period 10th-18th May 2011 (Figure 5.8). This period was identified in previous works (Monteiro et al., 2015) as the biggest dust outbreak of 2011 over Portugal, lasting for several days (~9 days) with 65.5 $\mu g \cdot m^{-3}$ maximum daily mean concentration of mineral dust, observed on a rural background station. Another period identified by Monteiro et al., (2015) was 28th - 29th May but only Évora AERONET station data confirm that occurrence.

Also Kubilay et al. (2003), different clusters of aerosols were identified based on the AC versus AOD plot as displayed in Figure 5.9. Cluster 1 includes AOD values varying between 0.2 and 0.4, representing the desert dust events. These events are dominated by coarse particles of dust with AC<1. The background aerosols with AOD<0.2 and dominated mainly by fine particles (AC>1) are represented by Cluster 2, and the ones dominated mainly by coarse particles (AC<1) are represented with cluster 3.

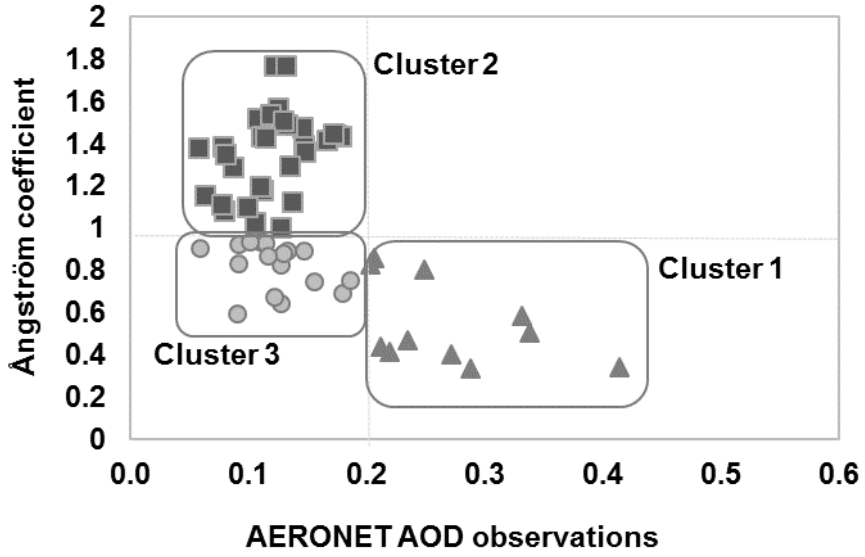

Figure 5.9. Scatter diagram of AC versus AOD provided by AERONET stations.

Daily mean AOD provided by SEVIRI and Modelling against AERONET data for the stations located within the studied domain are represented in Figure 5.10. In this Figure, all points are also classified as a function of the AC values obtained from AERONET, as represented in Figure 5.9.

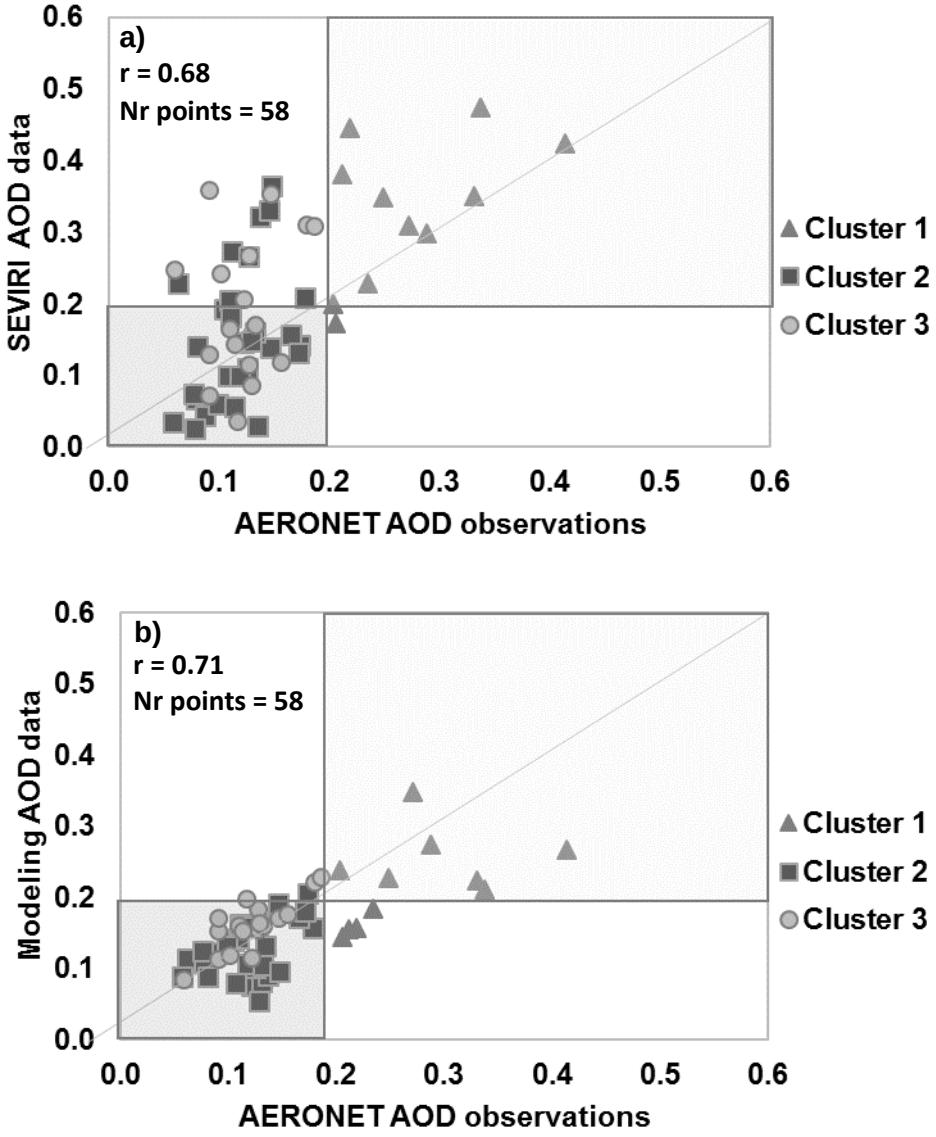

Figure 5.10. Scatterplot of daily mean AOD values from: a) AERONET versus SEVIRI, b) AERONET versus modelling approach. The daily AOD values are also represented in function of the AC values as defined from AERONET measurements: Cluster 1 (AOD>0.2 and AC<1.0, triangles), Cluster 2 (AOD <0.2 and AC>1.0, squares) and Cluster 3 (AOD<0.2 and AC<1.0, circles).

Both SEVIRI AOD and modelling AOD results present a good agreement with AERONET data with a correlation coefficient of 0.68 and 0.71, respectively. However, for the same time series, the correlation between the modelling results and the satellite observations is only 0.47 (data not shown).

The cluster-based analysis provides additional information and allows better understanding of the discrepancies displayed by the datasets. Based on this analysis, SEVIRI has a better performance for Cluster 1 with Normalised Root Mean Square Error (NRMSE) of 0.48. The highest errors are identified for background aerosols presented by Cluster 2 and Cluster 3 with NRMSE reaching 0.95. Overall, SEVIRI overestimated the AOD for all the clusters in comparison with AERONET data. On the other hand, the model is underestimating AOD related with mineral dust presented by Cluster 1. The NRMSE of the modelling is about 0.35 for all the clusters. Therefore, an estimate of long-range transport of mineral dust based on a combination of satellite observations with air pollution modelling may improve the air quality assessment.

5.4 Summary and conclusions

In this chapter, the air quality modelling approach in combination with SEVIRI observations were applied to analyse temporal variations and the spatial distribution of AOD over Portugal. Additionally, these data were compared with AERONET observations taking into account different aerosol modes.

The best correlation between the time series from SEVIRI and modelling results is obtained for the Southern part of the domain, affected by transport of mineral dust. However, the highest correlation values are found for the cells where the biggest discrepancy is identified in terms of AOD absolute values. Therefore, the model is well correlated with the satellite data in terms of the temporal occurrence of mineral dust events but disagrees in terms of the AOD magnitude. Moreover, a different pattern is identified for cells over the ocean, where the model is predicting higher values than satellite AOD values oppositely to in-land cells.

The validation of the results with AERONET observations suggest that the implemented methodology allows to obtain a good agreement between both the satellite data and modelling outputs with r=0.68 and r=0.71, respectively. However, the cluster analysis suggests that satellite data are, in general, overestimating AOD in comparison with the ground-based measurements for all analysed modes, while the modelling results are underestimating AOD for the events dominated by coarse aerosols. Nevertheless, the conclusions at each individual location may be different, particularly for background

aerosols with low AOD values underestimated by satellite at AERONET stations located in coastal zones.

It is important to stress that point validation of AOD using in-situ ground-based measurements from AERONET provide important information on the reliability of satellite data and modelling outputs to predict temporal variations of AOD in different locations, but this analysis may not highlight difficulties to characterise spatial variations. With respect to this aspect, spatial analysis and a comparison of the satellite product with air quality dispersion modelling provided deeper insight on the advantages and limitations of the considered methods to describe AOD spatial patterns and to improve the air quality assessment.

The study presented in this chapter contributes with relevant background knowledge to improve air pollution assessment, taking advantage of the joint analysis and interpretation of air quality modelling outputs and SEVIRI satellite observations.

Chapter 6

Integration of Air Quality Modelling and Satellite observations

Chapter Index:

6.1 Introduction……106
6.2 Data fusion……..109
6.2.1 - Data fusion of AOD from modelling and satellite observations……..110
6.2.2 - Comparison between modelling results before and after data fusion...113
6.2.3 - AOD data validation with AERONET observations……..115
6.3 Quantification of PM concentrations using data fusion…….118
6.3.1 - Methodology to obtain new PM concentrations after data fusion……..118
6.3.2 - Validation of PM concentrations before and after data fusion……...119
6.4 Summary and conclusions……121

6 Integration of Air Quality Modelling and Satellite observation

The contents of this chapter will be considered for publication in:

Fernandes, A.P., *Wunderle, S., Borrego, C., and Tchepel, O., (In preparation). New PM concentrations after integration of AOD satellite data with air quality modelling outputs. Atmospheric Research.*

The first aim of this chapter is to present, discuss and validate the methodology developed for integration of the Aerosol Optical Depth (AOD) data provided by satellite observations with air quality modelling outputs. In order to achieve this objective, satellite data obtained by Spinning Enhanced Visible and Infra-Red Imager (SEVIRI) instrument with high temporal resolution (15 min) were used in combination with air quality modelling results from the Comprehensive Air Quality Model (CAMx) over Portugal, previously analysed in Chapter 3 and 4, respectively, and compared in Chapter 5. The final goal of this chapter is to improve the quantification of PM concentrations at surface level based on AOD data after data fusion.

This chapter is divided into four sections. Section 6.1 gives a general introduction of data integration approaches and of methodologies to establish a relationship between AOD and particulate matter (PM). A description about the applied data fusion methodology and its validation is given in section 6.2. Section 6.3 presents the methodology applied to quantify PM concentrations near the surface after data fusion and validation. In the last section (Section 6.4) summary and conclusions are presented.

6.1 Introduction

Ground-based observations from air quality stations can provide important information on temporal variation of PM mass concentrations. However, due to the high variability of concentrations in space and time and high operational cost, *in situ* observations are insufficient to capture high-resolution, temporal and spatial variation of PM concentrations, especially at regional scale (You et al., 2016). The development of a methodology that contributes to improve the quantification of the atmospheric aerosol loading is an important part of an air pollution assessment. In this sense, the integration of satellite remote sensing data with air quality modelling is a promising approach.

Some methods, such as data fusion and data assimilation are used to integrate the multiple data and knowledge representing the same real-world object into a consistent, accurate, and useful representation (Haghighat et al., 2016; Denby et al., 2009). These methods are often used taking into account the case study application. Many of the techniques used in data fusion and data assimilation are actually developed for the same objectives, namely to improve the final results.

Data assimilation refers to a modelling technique that incorporates monitoring data directly into air quality model calculations during the modelling process itself. It is the measured data that assist the model towards an optimal solution, and one that is consistent with the physical description provided by the air quality model. The most common type of data assimilation applied in the field of air pollution is the variational methods (3DVar and 4DVar) (Elbern et al., 2010; Elbern et al., 1999), which are also extensively used in meteorological forecast, but other methods, such as Ensemble Kalman filters (van Loon et al., 2000) are also applied. These different methods are based on Equation 6.1 (Kalnay, 2003):

$$x_a = x_b + W[y_o - H(x_b)] \qquad \text{Equation 6.1}$$

where x_a is the analysis, x_b is the background, y_o is the observations, H is the observation operator that performs the necessary interpolation and transformation from model variables to observation space and W is the weights that are determined based on the estimated statistical error covariances of the forecast and the observations. The several methods of data assimilation use different approaches to combine the background and the observations to produce the analysis. Data assimilation is applied for air quality assessment purposes (Denby et al, 2008) and now is used operationally in air quality forecasting (e.g. Sahu et al.,

2009). Moreover, data assimilation is most often applied on the regional scale and is rarely applied on the urban scale, due to the complexities of the urban environment.

Data fusion can be seen as a post-processing of modelling results (Denby et al., 2009) and it is considered by Lahoz and Schneider (2014) as a subset of data assimilation. Data fusion is generally defined when combining data from multiple sources to create a new data set that is potentially more accurate than if they were achieved by means of a single source (Haghighat et al., 2016; Zhang et al., 2012a,b). For example, it is possible to fuse interpolated monitoring data, satellite data and air quality modeling data into a single integrated map (e.g. Sarigiannis et al., 2004). The fusing will most likely take the form of a weighted linear combination of the different data sources, with the weighting being dependent on the estimated uncertainty of each of the data sources. Data fusion methods are generally not concerned with any physical or chemical constraints, but are mainly subject to statistical constraints. The data fusion is frequently referred in the literature as passive data assimilation, decision fusion, data combination, data aggregation, multisensor data fusion, and sensor fusion.

Nowadays, one of the data fusion approaches mostly used is fusing AOD data from multiple sensors that can potentially reduce data missingness and increase accuracy. However, directly merging AOD data products from different sensors is problematic due to different error structures (Puttaswamy et al., 2013). The same problems are expected when fusing AOD data from different sources such as modelling outputs and satellite observations.

A literature review reveals several methods implemented to combine AOD data sets from different sources. The examples of methods used in these studies are the optimum interpolation (Xue et al., 2012, 2014; Yu et al., 2003), the least squares estimation (Guo et al., 2013), and the maximum likelihood estimate (Nirala, 2008; Zubko et al., 2010; Xu et al., 2015). All these methods were applied to do a temporal statistical analysis. Kinne (2009) developed a scoring concept to create a satellite composite data-set using annual averages of the AOD data from numerous sensors combined with monthly statistics of AERONET AOD for increased accuracy. Fuentes and Raftery (2005) combined observations and numerical model output at different resolutions using Bayesian melding. Recently, a spatiotemporal statistical data fusion framework based on a Bayesian maximum entropy (BME) method was applied by Tang et al. (2016) for merging satellite AOD products. They produce merged AOD data with higher accuracy.

The other type of the AOD combining method are geostatistical methods. These methods were applied to do spatial statistical analysis. This kind of methods include the universal kriging method (Chatterjee et al., 2010; Li et al., 2014), the geostatistical inverse modelling (Wang et al., 2013), and the spatial statistical data fusion (SSDF) method (Nguyen et al., 2012). SSDF is considered by Tang et al. (2016) a variant of kriging method specifically designed to optimally combine information from two or more data sets and has been used for AOD fusion. The geostatistical methods include the spatial correlation into the fusion to obtain the errors and estimate the AOD values with high accuracy. However, these geostatistical fusion methods did not consider the temporal correlation. In addition to the spatial correlation among the AODs, the temporal correlation is important to provide information for the AOD estimation (Cressie et al., 2010; Kang et al., 2010).

One of the major issues is to derive a relationship between PM and AOD (PM-AOD) (Stafoggia et al., 2017; Sorek-Hamer et al., 2017; Benas et al., 2013) because the AOD values represent the columnar aerosol loading from the surface to the top of the atmosphere (Engel-Cox et al., 2004b), whereas the ground based measurements represent mass concentration of PM near the surface. The drawbacks of ground-level monitoring have led to an ongoing exploration for PM estimation from AOD data (Benas et al., 2013), which has the following advantages. Firstly, the image derived from the integration approach of modelling outputs and satellite data could provide complete and general information on air quality anywhere in the world (Hadjimitsis, 2009). Secondly, the AOD data from the integration approach also provides the opportunity to acquire global air quality, making possible to discover the source of urban air pollutants and even global transport of air pollutants (Wang et al., 2013). Furthermore, this method costs less than air quality monitoring. Previous studies have shown agreement between AOD data and PM mass concentrations for some regions and in specific situations with stable meteorological conditions and fixed pollution sources (Wang and Christopher, 2003; Gupta et al., 2006; Chu et al., 2003). Most of these studies have concluded that AOD do not explain surface PM concentrations well, since the PM-AOD relationship is affected by various factors, including relative humidity, aerosol vertical distribution, aerosol type, aerosol size and its chemical composition, as well as its spatial and temporal variability, which are governed by spatio-temporal distribution of emissions and meteorological conditions (Chu et al., 2003).

Currently, the PM-AOD estimation models can be classified into two types: observation and simulation methods (Lin et al., 2015). Simulation methods are mainly based on chemical transport models (Drury et al., 2010; Liu et al., 2004; van Donkelaar et al., 2010), while

observation methods mainly rely on statistical analysis (Lin et al., 2015). The statistical methods used for PM estimation include the simple linear regression model, the multiple linear regression (MLR) model, the geographically weighted regression (GWR) model and artificial neural network (ANN) algorithms. Van Donkelaar et al (2010) generated a map of global satellite-derived PM2.5 using the averaged AOD from MISR and MODIS during 2001 and 2006. Recently, You et al. (2016) used the Geographically Weighted Regression (GWR) model with the 3 km resolution AOD product to estimate PM2.5 concentrations at a national-scale. Their model explained 81% of the daily PM2.5 variations. In observation models, linear regression is most often used and spatial regression can consider the spatial autocorrelation. In more complex models, other factors, such as meteorological conditions are also taken into consideration to improve the AOD-PM estimates. Finally, the PM distribution estimated from the integrated approach of modelling results and satellite data can contribute for the quantification of the atmospheric aerosol loading.

The main objective of the work presented in this chapter is to improve the quantification of PM concentrations at surface level based on data fusing of AOD data. For this purpose, an integrated approach of the air quality modelling outputs with satellite observations was developed. The data used were described previously in Chapter 3 and Chapter 4. The integration of these diferent data sources was performed based on statistical estimation. The weighting factors of the air quality modelling and the satellite observations were obtained using different geoprocessing approaches.

6.2 Data fusion

In this study, the main target is improving the AOD data. To achieve that, the data fusion methodology was applied using new parametrizations. For this purpose, satellite data obtained by Spinning Enhanced Visible and Infra-Red Imager (SEVIRI) instrument with high temporal resolution (15 min) were used in combination with air quality modelling results from the Comprehensive Air Quality Model (CAMx) over Portugal, presented in Chapter 3 and 4, respectively.

6.2.1 Data fusion of AOD from modelling and satellite observations

In this sub-section, the methodology developed for the AOD data fusion application is presented. This methodology is based on statistical estimation by geoprocessing approaches to combine two datasets from different sources.

In general, the best estimate of the state of the atmosphere (x_a) presented on Equation 6.1 may be obtained from combining the prior information about the atmosphere (background or first guess) (x_b) with the observations (y_o) (Kalnay, 2003). To perform an optimally combination, statistical information to estimate the weighting factors is also needed.

In this work, the studied variable is the AOD, where "analysis" is the best estimate of the AOD values ($x_a = AOD_a$), the AOD outputs from the modelling system are assumed as the background field ($x_b = AOD_{mod}$), and the satellite data are considered as observations ($y_o = AOD_{sat}$).

The AOD_a is a linear combination of the two datasets with different weighting factors considered, one for the model outputs (a_{mod}) and other for satellite observations (a_{sat}):

$$AOD_a = a_{mod} \times AOD_{mod} + a_{sat} \times AOD_{sat}, \quad \text{Equation 6.2}$$

Where

$$a_{mod} + a_{sat} = 1 \quad \text{Equation 6.3}$$

The main difficulty in implementing the data fusion is related to the calculation of the data weighting factors. In this study, the weights are obtained based on a spatial standard deviation of AOD, widely used in aerosol algorithms for AOD filtering, as discussed by Emili et al. (2011), Riffler et al. (2010) and Popp et al. (2007). In the currently study, the weights are given by:

$$a_{sat} = \sigma_{mod}/(\sigma_{mod} + \sigma_{sat}) \quad a_{mod} = \sigma_{sat}/(\sigma_{mod} + \sigma_{sat}) \quad \text{Equations 6.4}$$

The σ_{sat} and σ_{mod} is a spatial standard deviation of AOD for satellite data and for modelling outputs, respectively. They were computed following the geoprocessing approaches described below. Figure 6.1 shows the scheme of the described methodology.

In order to integrate two datasets from different sources, two geoprocessing approaches were used (Figure 6.1). For that purpose, several post-processors programs in python language were developed and the ModelBuilder tool (Allen, 2011) provided by Geographical Information Systems (ArcGIS) was used.

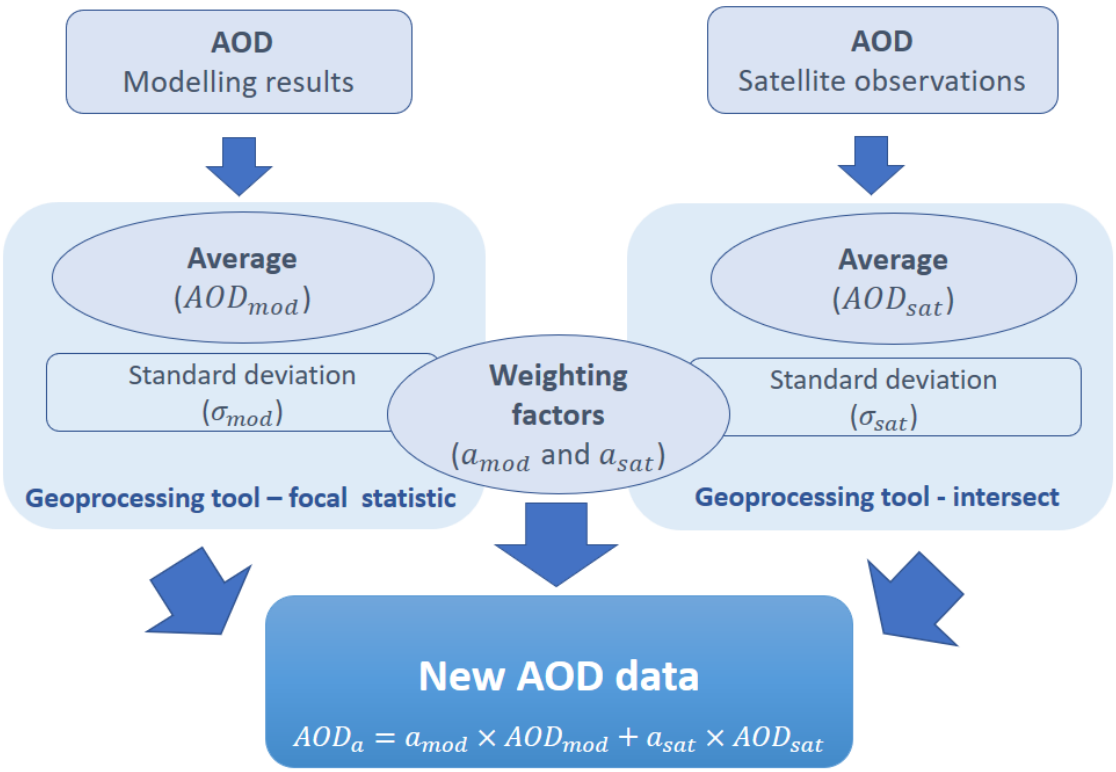

Figure 6.1. Scheme of the data fusion methodology applied to AOD data.

To perform the geoprocessing of the modelling outputs, the spatial analyst tool (focal statistics) from ArcGIS was applied. The focal statistics tool performs a neighbourhood operation that computes an output grid where the value for each output cell is a function of the values of all the input cells in the neighbours of that location (see Figure 6.2). This tool computes the average and standard deviation for each central cell using a moving grid window with the dimension previously defined. In this work, a grid window with the dimension of 3 x 3 cells was selected. This spatial analyst tool was applied for all cells of the modelling domain described in Chapter 4. From that application two output grids data were obtained, one grid with AOD average and other grid with AOD standard deviation.

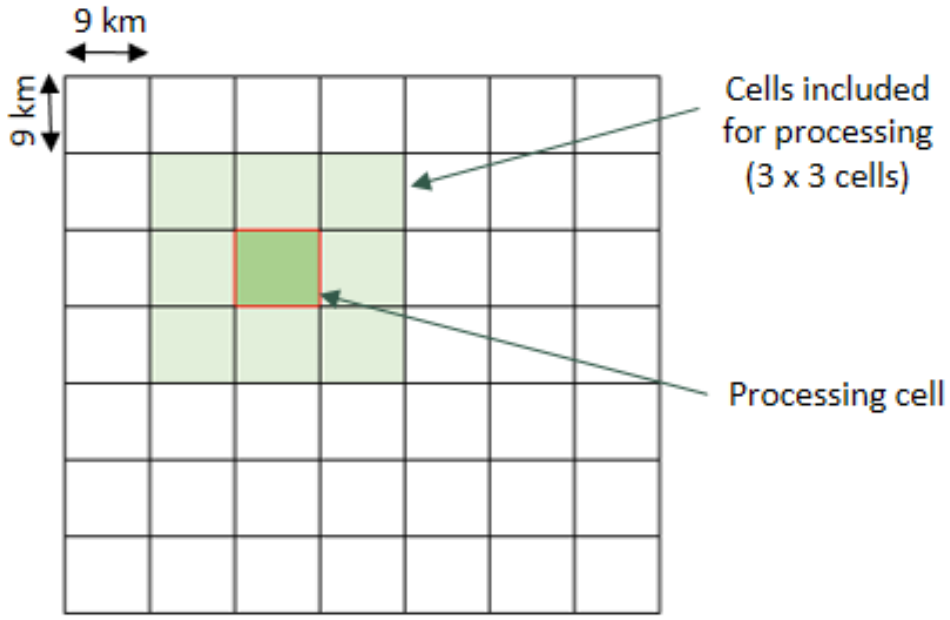

Figure 6.2. Illustrations of the focal statistics tool used for a neighborhood operation.

To perform the geoprocessing of the satellite observations, the intersect geoprocessing approach was developed and implemented in python language. The satellite data and modelling outputs have different spatial resolution and projection. Thus, the combination of the satellite data with the modelling grid leads to variations related with this spatial approximation. To estimate these spatial variations of AOD values, the satellite observations were intersected with the modelling grid using an intersect approach. Thus, as could be seen on Figure 6.3, for the center point of each modelling cell, satellite data with maximum distance of 4500 meters were selected. This distance is corresponding a half of the modelling cell (9 km). After removing NoData cells, the average and standard deviation were calculated for each central cell using more than two available AOD values. Two grids data were obtained from this geoprocessing: one grid with AOD average and other grid with AOD standard deviation.

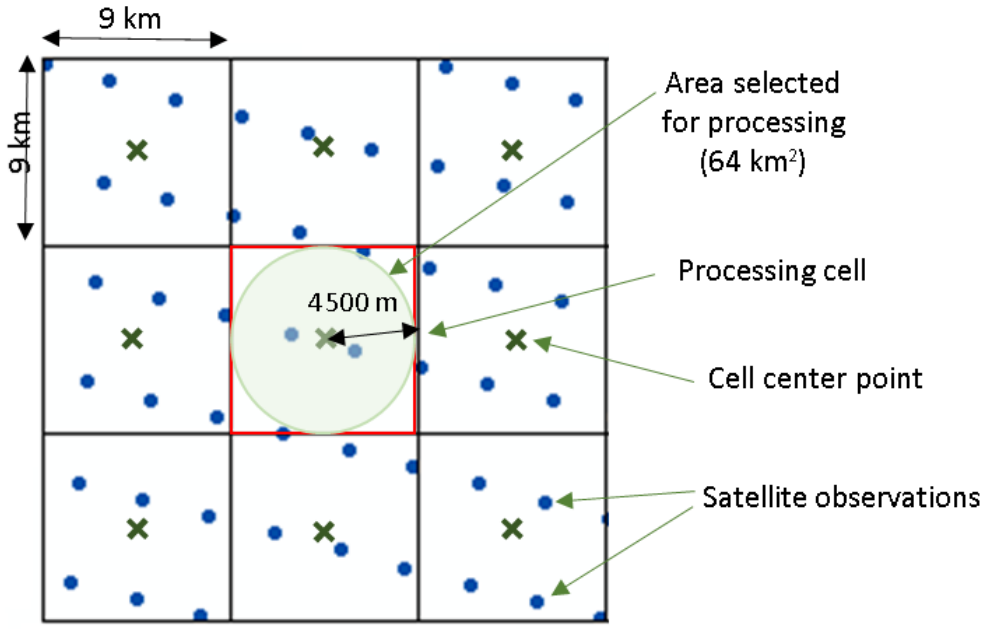

Figure 6.3. Scheme of the satellite data processing.

From the methodology explained above, four AOD grids data were obtained for each day. Two for modelling outputs and two for satellite observations with the same spatial resolution (9x9 km^2). For each data source, one grid with AOD average and other with AOD standard deviation were obtained. After that, the weighting factors were calculated using the AOD standard deviation obtained from modelling and satellite data (Equations 6.4). Finally, Equation 6.2 was applied in order to calculate the new AOD values. To perform these tasks several scripts in python language were developed.

6.2.2 Comparison between the modelling results before and after data fusion

The influence of the data fusion application in terms of the spatial pattern distribution of AOD over Portugal region was evaluated. This spatial analysis of the monthly AOD results obtained from modelling results before and after data fusion application are presented in Figure 6.4 a) and b) respectively.

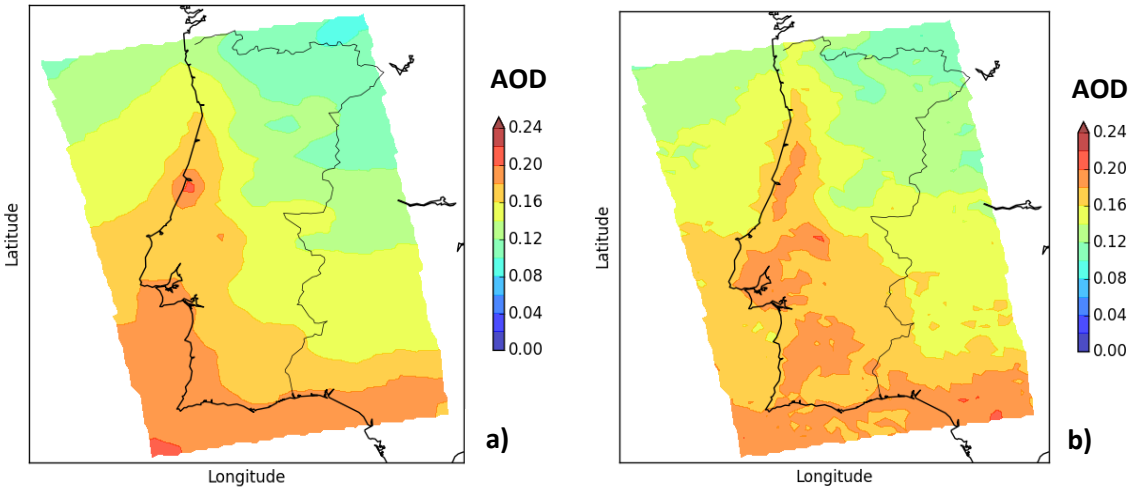

Figure 6.4. Spatial pattern of monthly average AOD for May 2011: a) Modelling results before data fusion and b) Modelling results after data fusion.

The analysis of the Figure 6.4 shows higher AOD values for both cases on South part of the study domain. This is more evident in Figure 6.4b after the data fusion methodology was applied. Also, in Figure 6.4 higher AOD values over the Portugal coast line are shown.

In order to understand the differences between the modelling results before and after data fusion, the differences are calculated for the monthly mean AOD as following:

$$\text{AOD differences} = AOD_{before\ data\ fusion} - AOD_{after\ data\ fusion} \qquad \text{Equation 6.5}$$

Figure 6.5 shows the spatial distribution of the differences between the monthly mean AOD data.

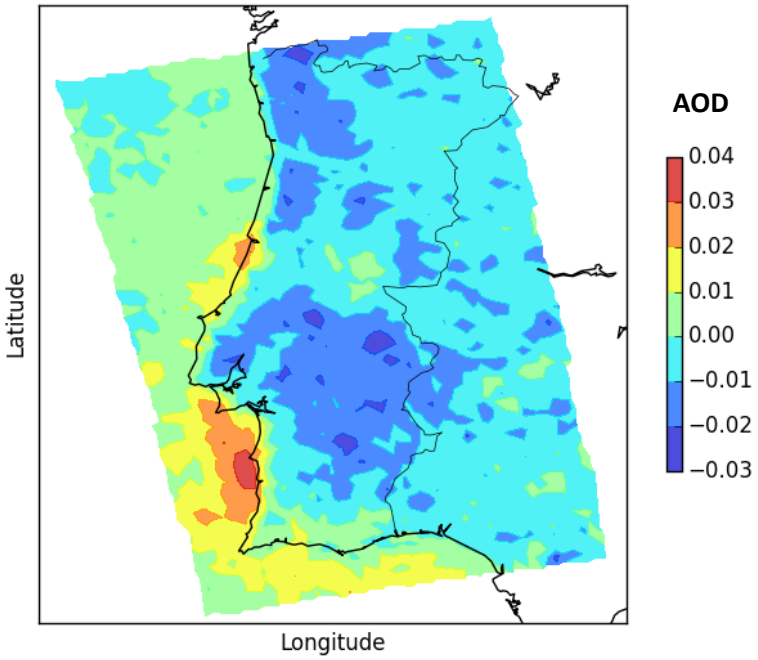

Figure 6.5. Differences between the monthly AOD values before data fusion minus AOD values after data fusion.

The differences between the two datasets (before and after data fusion) obtained for monthly average AOD are within -0.03 and 0.04 as illustrated in Figure 6.5. Negative values (AOD after satellite data fusion > AOD before satellite data fusion) over land and positive values (AOD after satellite data fusion < AOD before satellite data fusion) over the coast line and ocean were found. As expected, these results are influenced by the spatial pattern of the AOD provided by satellite observations previously presented in Chapter 3.

6.2.3 AOD data validation with AERONET observations

In this subsection a validation of AOD modelling data before (Figure 6.6a) and after (Figure 6.6b) data fusion is provided. For this purpose, AOD data from Aerosol Robotic Network (AERONET) station presented and analysed in Chapter 3 were used. This validation exercise was performed to evaluate the performance of the data fusion methodology. For

this purpose, daily average AOD data are compared with observations provided by the four AERONET stations located within the study domain (Figure 3.5 in Chapter 3).

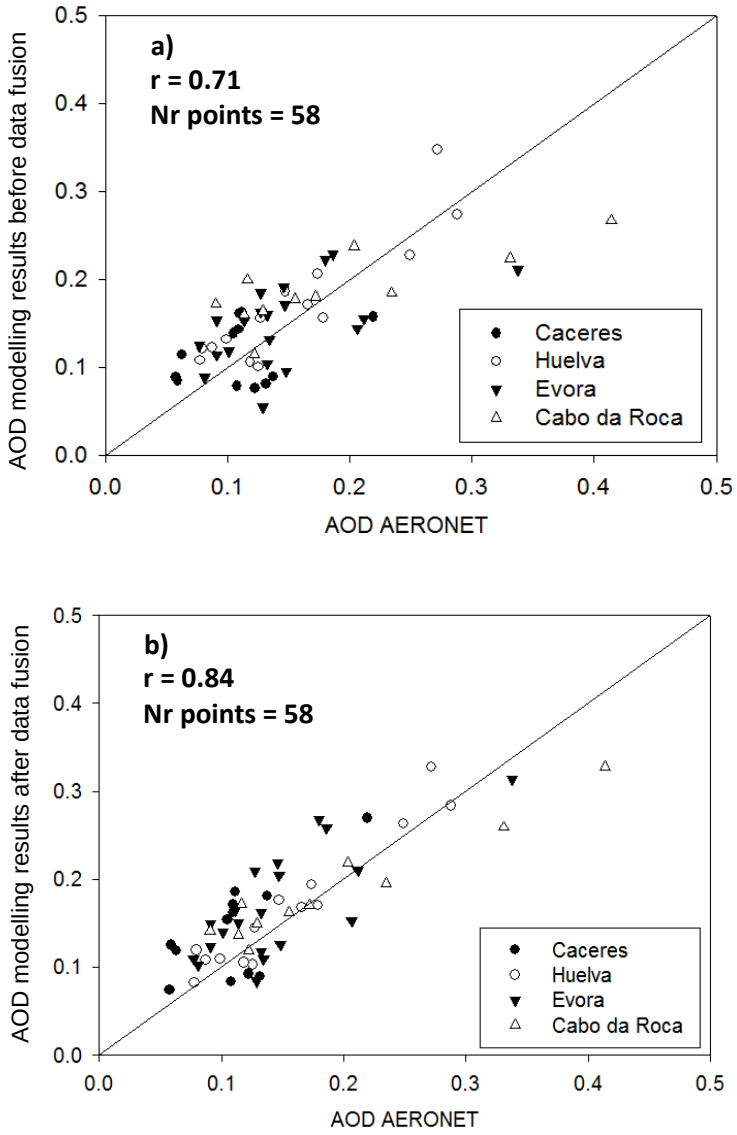

Figure 6.6. Scatter plot of daily average AOD values from modelling results versus AERONET observations. a) Before data fusion and b) After data fusion.

The modelling results before satellite data fusion present a good agreement with AERONET observations with a correlation coefficient of 0.71 as illustrate in Figure 6.6a and previously analysed in Chapter 4. After the satellite data fusion, modelling results present better agreement with the AERONET observations with a correlation coefficient of 0.84 as shown in Figure 6.6b.

To evaluate how the methodology of data fusion contributes to improve the AOD data a Taylor diagram was applied with results before and after data fusion as shown in Figure 6.7. To perform this Taylor diagram one python program was developed. Taylor diagram is a mathematical diagram designed to graphically indicate which of several approximate representations of a system is most realistic. It is used to quantify the degree of correspondence between the modelled and observed behaviour in terms of three statistics parameters: correlation (R), root-mean-square error (RMSE) and standard deviation (SD).

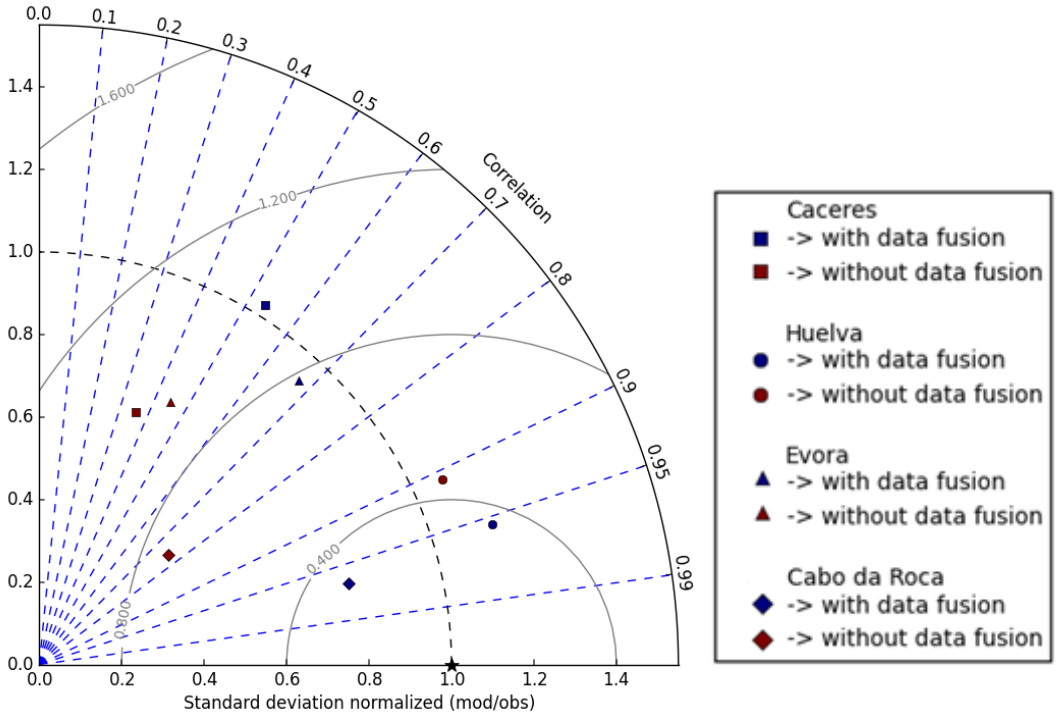

Figure 6.7. Taylor diagram with AOD values from: modelling data before data fusion, modelling data after data fusion. All values are normalized with AERONET observations.

From the analysis of Figure 6.7 it is possible to observe a better agreement for modelling results after data fusion in all locations considered. It is more evident in Caceres, Cabo da Roca and Évora locations. Thus, the data fusion methodology presented in this work shown a good option to improve the AOD modelling results using satellite observations.

6.3 Quantification of PM concentrations using data fusion

After the improvement of the aerosol optical depth (AOD) values using a data fusion methodology to integrate the air quality modelling outputs and satellite observations, a methodology to obtain the particulate matter (PM) concentration near the surface was developed. To perform that, the PM vertical profile from air quality modelling system was adjusted and applied. For this purpose, daily AOD values after the data fusion were used

6.3.1 Methodology to obtain new PM concentrations after data fusion

The AOD values represents the columnar aerosol loading from the surface to the top of the atmosphere, whereas the ground based measurements represent dry mass concentration of particulate matter (PM) near the surface. The relationship between AOD and PM concentrations depends on various factors, including relative humidity, aerosol vertical distribution, aerosol size, aerosol type and its chemical composition. Thus, it is important to develop the methodology to estimate PM concentrations at surface level based on AOD from data fusion methodology to improve air pollution assessment. This is more important in locations without monitoring networks. Therefore, to perform the PM concentrations estimation a new post-processor was developed using python language.

The new PM concentrations near the surface were estimated using improved results of AOD after the data fusion application previously described. For this purpose, firstly was estimated the relative contribution of PM mass concentrations in all vertical levels using the 3D modelling results. Finally, the relative PM mass contribution at near-surface level was multiplied by AOD data after data fusion to obtain the new PM mass concentrations in this level. On Figure 6.8 could be seen the scheme of this procedure.

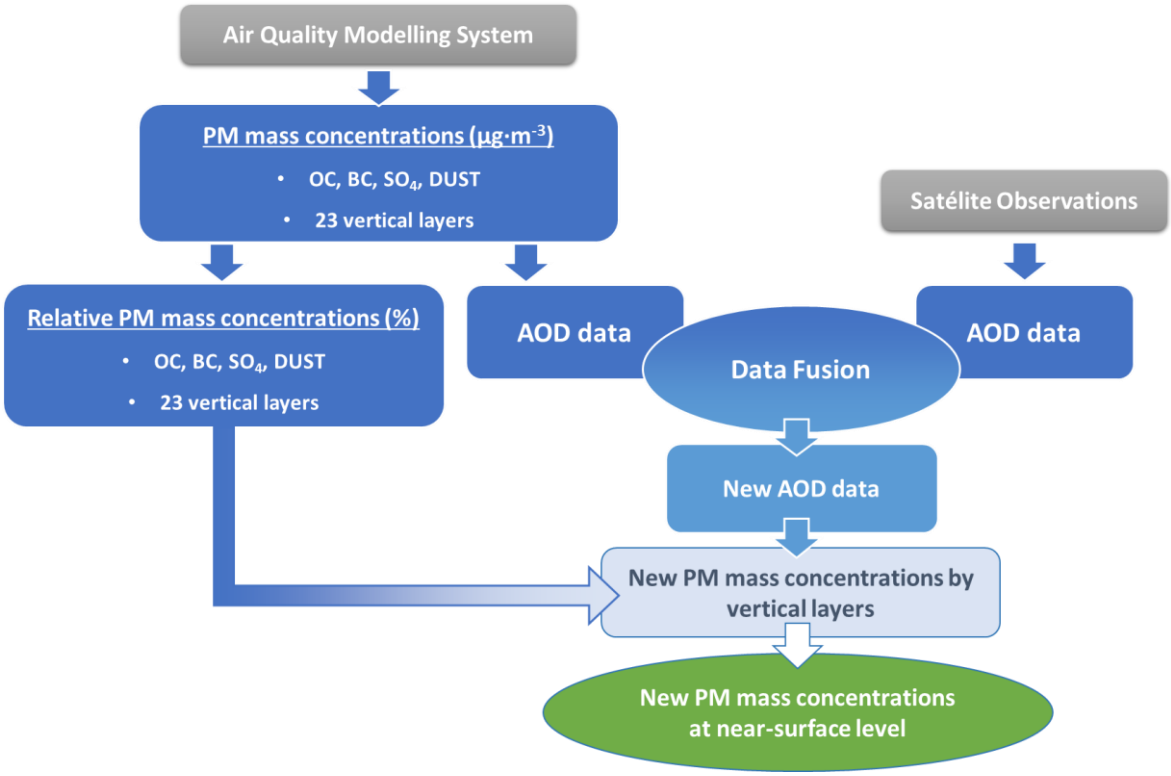

Figure 6.8. Schematic representation of methodology used to obtain new PM mass concentrations at near-surface level.

6.3.2 Validation of PM concentrations before and after data fusion

In order to validate the performance of the PM results from air quality modelling system at surface level before and after satellite data fusion, the DELTA tool (Version 5.4) was applied. The Delta tool (Thunis et al., 2012) is an IDL-based evaluation software tested in a set of studies which addresses model applications for the air quality Framework Directive (FD) (Directive 2008/50/EC).

The DELTA tool processes information needed for the accurate validation of the modelling system based on the target plot and Taylor diagram. It is a specific software which provides summary statistics. The target plot represents the discrepancy between the measured and modelled data, combining several statistical parameters, such as systematic error (BIAS), correlation (R) or standard deviation (SD). The performance criterion for the target indicator is set to unity (circle limit, T=1) regardless of spatial scale and pollutant and it is expected to be fulfilled by at least 90% of the available air quality stations considered. The Model Quality Indicator (MQI) is used as main indicator, it is defined as the ratio between the

model-measured bias and a quantity proportional to the measurement uncertainty. The MQI ideal value is lower than 1. The Taylor diagram is used to quantify the degree of correspondence between the modelled and observed data in terms of three statistics parameters (R, root-mean-square error (RMSE) and SD) as previously explained. The performance of the daily average PM10 concentrations are exhibited in Figure 6.9 for modelling results before and after satellite data fusion for all air quality stations previously represented on Figure 4.3 in Chapter 4. Note that Figure 6.9 is intended to show the global behaviour of air quality stations considered and not an individual assessment.

Validation of modelling results before satellite data fusion

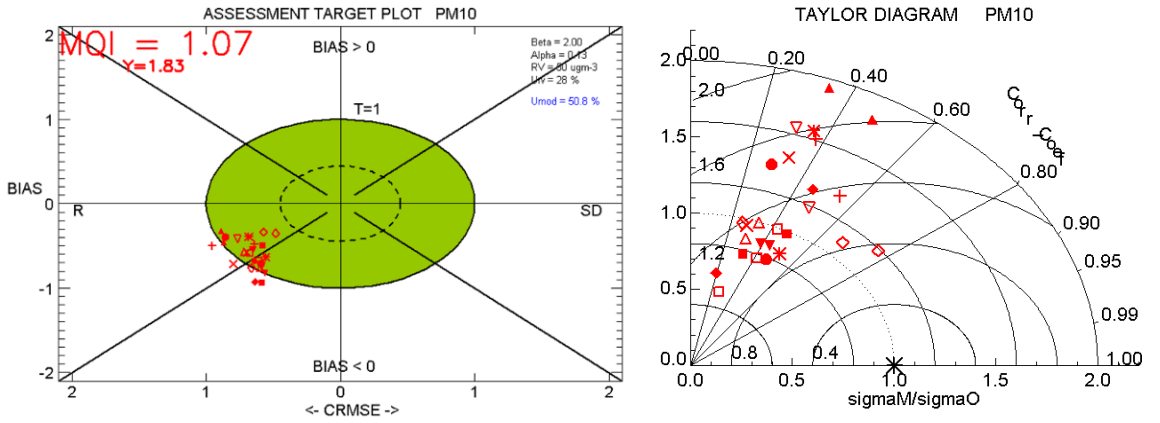

Validation of modelling results after satellite data fusion

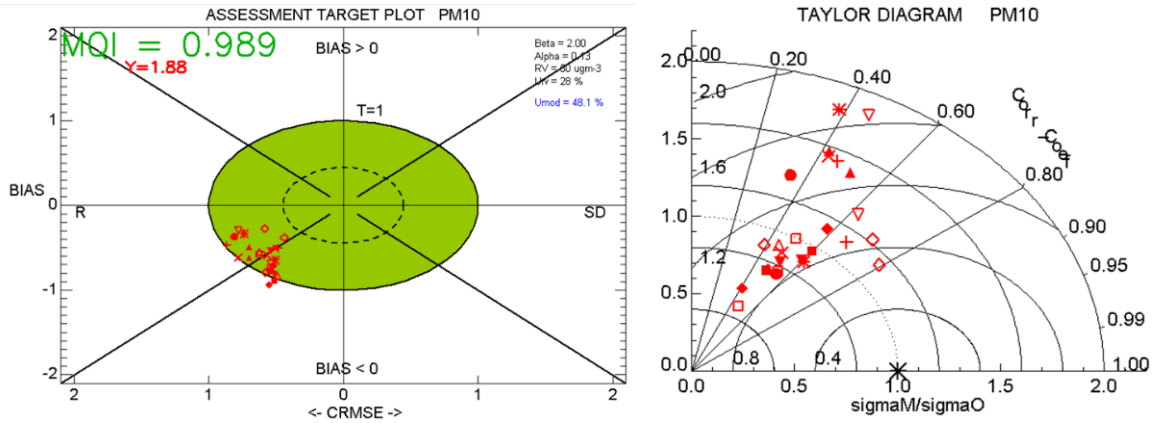

Figure 6.9. Delta tool plots for modelling system for PM10 data before (above) and after (below) satellite data fusion (target plot (left) and Taylor diagram (right)). The red marks represent the air quality stations available and considered in this study (see Figure 4.3).

In this study the air quality modelling system shows a good agreement for PM10 atmospheric pollutant when compared with observation from air quality stations. As Figure 6.9 shows, an improvement of the PM10 concentrations provided by the data fusion is notorious in all the graphs.

Considering the information from the target plots (Figure 6.9), the results before data fusion show a lowest number of air quality stations that fulfil the criteria and the MQI is higher than 1. For the other hand the results after data fusion show highest number of air quality stations that fulfil the criteria and the MQI is lower than 1. These results proven that the data fusion methodology improve the number of air quality stations fulfil the criteria. The BIAS are negative, which indicates that the model underestimates the PM10 concentrations.

From the analysis of the Taylor diagrams (Figura 6.9) could be concluded that the satellite data fusion improves the performance of the air quality modelling for the near surface PM concentrations. Taylor diagrams presented in Figure 6.9 shows data improvement when validation of the modelling results after data fusion is performed. Before data fusion the correlation coeficients were centred between 0.2-0.6 and after the satellite data fusion the coefficients are located between 0.4-0.8.

6.4 Summary and conclusions

The methodology implemented in this study demonstrates that data fusion contributes to improve the quality of air pollution assessment. In this sense, the integration of satellite remote sensing data with air quality modelling is a promising approach. The Aerosol Optical Depth (AOD) data previously analysed in Chapter 3 and 4 were used in this analysis.

The spatial analysis of modelling results shown higher AOD values on South part of the study domain for both results, before and after satellite data fusion. However, for modelling results with satellite data fusion this conclusion is more evident. The differences between the two datasets obtained for monthly average AOD are within -0.03 and 0.04. From the spatial pattern of differences negative values over land and positive values over the coast line and ocean were obtained. As expected, these results are influenced by the spatial pattern of the AOD provided by satellite observations (Chapter 3).

The validation of AOD values against the observations provided by four AERONET stations located within the studied domain were performed. From this analysis, we can conclude that the modelling results before data fusion present a good agreement with AERONET observations with a correlation coefficient of 0.71 and after data fusion, modelling results present better agreement with a correlation coefficient of 0.84. Also, the Taylor diagram analysis shows a better agreement for modelling results after data fusion in all AERONET locations considered. The improvement is evident for all stations, except Huelva.

New particulate matter (PM) mass concentrations at surface layer were computed after data fusion. For this purpose, the AOD data after data fusion application and the information about the relative PM mass from modelling at vertical levels were used. In order to validate the PM mass concentrations at surface level before and after data fusion, the DELTA tool framework was applied. The DELTA tool produces the necessary information needed for the validation of the modelling system, namely the target plot and Taylor diagram. The target plots and Taylor diagrams show an improvement of the PM10 concentrations provided by application the data fusion of the satellite observations.

The study presented in this chapter highlights that data fusion methodology provides an improvement of the modelling results in terms of the AOD data and the PM concentrations near the surface. Therefore, the use of this methodology can improve air pollution assessment in terms of PM concentrations.

Chapter 7

Conclusions

Chapter Index:

7.1 Research question 1……125

7.2 Research question 2……126

7.3 Research question 3……128

7.4 Future developments……...129

7 Conclusions

The main purpose of the research presented in this thesis was to develop a consistent approach based on air quality modelling system and satellite observations for assessing the contribution of natural sources to the atmospheric pollution and to improve the quantification of particulate matter (PM) in Portugal. This research intends to contribute to implementation of the Directive 2008/50/EC on ambient air quality. The main achievements are presented and organized in seven chapters starting with the introduction, mineral dust assessment, analysis of remote sensing data and air quality modelling results, comparison and integration of satellite observations with modelling outputs. Throughout this structure, the three main questions formulated in Chapter 1 were answered to accomplish the thesis goals.

7.1 Research question 1

How is air quality in Portugal is affected by mineral dust?

In order to answer the first question, the mineral dust transported to Portugal was investigated in terms of long-term and also high episode peaks (Chapter 2). The application of the BSC-DREAM8b v1.0 model for the entire year of 2011, allows the characterisation of the magnitude and spatial distribution of mineral dust over Portugal. The annual mean of the simulated dust has a magnitude of 2-6 $\mu g \cdot m^{-3}$, where the monthly average highlights the largest mineral dust values in April and May. Thus, it was concluded that the influence of the transport of mineral dust to Portugal follows a seasonal pattern. At the Southern part of

the study domain the trajectories of air masses coming from the North African coast are predominant during the episode days with frequency above 70%. The prevalence of the flow regimes coming from Northern Africa during the episode days decreases for the upper latitude sites. This finding was important to select the study period (May 2011) applied in the following tasks of this Thesis.

7.2 Research question 2

What are the advantages and the limitations of Air Quality Modelling and Satellite Observations to perform the aerosols characterization?

The development of methodologies that contribute to improve the quantification of the atmospheric aerosol loading is an important point to perform air pollution assessment. In this sense, the use of remote sensing data is one of the promising approaches. Data from two different remote sensing techniques, AERONET and SEVIRI, were studied and discussed in Chapter 3. The data were treated as daily averages. The analysis performed in Chapter 3 was important to evaluate the spatial and temporal distribution of AOD from SEVIRI observations. Furthermore, the results from the air quality modelling approach applied and presented in Chapter 4 were intended to study the vertical, temporal and spatial distribution of aerosols. Finally, in Chapter 5, the air quality modelling results were compared with SEVIRI observations to analyse the agreement between the two datasets in terms of AOD distribution over Portugal.

The temporal evolution of the daily mean Aerosol Optical Depth (AOD) and Ångström coefficient (AC) values from four AERONET stations was analysed. The evolution of the daily average of AOD for all stations shows higher values during the period 10^{th}-18^{th} of May 2011. In the same period, the Ångström coefficient presents values lower than 1.0. This fact could be due to the presence of mineral dust aerosols.

The SEVIRI observations studied show a good agreement in comparison with AERONET observations. For the AERONET stations, and during the analysed period (May 2011), a correlation coefficient of 0.68 was found. Caceres and Évora are the only sites for which the AOD values given by SEVIRI are higher than the ones measured by the AERONET stations. The stations that show the best agreement between SEVIRI and AERONET were Cabo da Roca and Huelva. In terms of the spatial analyses of the AOD observations show, in the

Southern part of the domain, higher AOD values compared with the other regions of the study domain, influenced mainly by mineral dust.

The air quality modelling system was evaluated in terms of 3D PM concentrations and AOD. The PM concentrations at surface layer were compared with those measured by background air quality stations over mainland Portugal (Chapter 4). In general, the air quality modelling approach underestimated PM concentrations at surface layer. From the statistical analysis based on the correlation coefficients, one concludes that the urban and suburban background stations yield a better agreement between observed and simulated concentration values in comparison with rural background stations. As PM concentrations increase, a dominance of mineral dust and/or sulphates becomes more evident in the modelling results. The aerosol compound with the highest contribution is clearly mineral dust, especially in two periods, 9th-21st and 24th-30th May 2011. During the period of 1st-6th May 2011, a bigger contribution of sulphate was observed.

To better understand the processes in the atmosphere and to identify the potential aerosols transport, the PM concentrations were assessed by vertical layers. For the study period, the highest aerosol concentration was obtained at 2000 m and the mineral dust is the compound with the largest contribution. The second most relevant compound is sulphate, below 1200 m. This occurred for all selected locations. For mineral dust, the highest values are obtained in the Southern part of the study domain (Huelva). Spatial analyses of the modelling results show that the highest concentrations and AOD are obtained in the South of Portugal, as a result of long-range transport of mineral dust (Chapter 4). Furthermore, the overall contribution of OC, BC and SO_4 compounds is very important, reaching 76% for the monthly average AOD values. The comparison between AOD measured and modelled data presented a correlation coefficient of 0.71.

From the comparison of SEVIRI observations with modelling results, the best correlation was obtained for the Southern part of the domain, affected by long range transport of mineral dust (Chapter 5). However, the highest correlation values are found for the cells where the biggest discrepancy is identified in terms of AOD values. Therefore, the model is well correlated with the satellite data in terms of the temporal occurrence of mineral dust events but disagrees in terms of the AOD magnitude. Moreover, a different spatial pattern is identified for cells over the ocean, where the model is predicting higher values than satellite AOD values oppositely to in-land cells.

In general, the air quality modelling approach and SEVIRI observations demonstrate a good performance when applied over Portugal. The spatial analysis and a comparison of the satellite product with air quality dispersion modelling provide deeper insight on the advantages and limitations of the considered methods to describe AOD spatial patterns and to improve the air quality assessment.

7.3 Research question 3

What is the best strategy to combine modelling and observation data in order to improve aerosols quantification?

The integration of satellite remote sensing data with air quality modelling is a promising approach. In this sense, the development and application of a data fusion methodology that contributes to improve the quantification of the atmospheric aerosol loading is an important aspect in an air pollution assessment (Chapter 6). For this purpose, AOD data previously analysed on Chapter 3, 4 and 5 were used.

The spatial analysis of results obtained from the modelling system show higher AOD values in South part of the study domain, before and after satellite data fusion (Chapter 6). However, data fusion improves the results and this conclusion becomes more evident. The differences between the two dataset obtained for monthly average AOD are within -0.03 and 0.04. From the spatial pattern of AOD differences negative values were obtained over land and positive values over the coast line and ocean. As expected, these results are influenced by the spatial pattern of the AOD provided by satellite observations (Chapter 3).

The validation of AOD data was performed with observations provided by four AERONET stations. From these analyses could be concluded that the modelling results after data fusion present better agreement with a correlation coefficient of 0.84 than before data fusion application (r=0.71). Also, Taylor diagram analysis showed a better agreement for modelling results after data fusion in all AERONET locations considered. Furthermore, to validate the particulate matter (PM) mass concentrations at surface level before and after data fusion, the DELTA tool framework was applied. The DELTA tool produces the necessary information needed for the accurate validation of the modelling system namely the target plot and Taylor diagram. These plots also show an improvement of the PM10 concentrations provided by application the data fusion of the satellite observations.

The data fusion methodology developed and applied in this Thesis provide an improvement of the aerosol modelling results in terms of the AOD data and the PM concentrations near the surface, for this reason it is a fundamental and helpful tool to be used in air quality studies.

7.4 Future developments

An improvement of the methodology for aerosols quantification using different data sources is a continuous task. Therefore, it will be important to apply the developed methodology for a large time period to verify if the improvements performed would remain. Also, it will be important to study the particulate matter with an equivalent aerodynamic diameter less than 2.5 μm (PM2.5), due to its relation to human health effects. Moreover, gaseous pollutants should also be analysed, such as, ozone (O_3) and nitrogen dioxide (NO_2). These pollutants are considered critical pollutants in Portugal due to the high number of exceedances observed in several air quality stations, which generate detrimental effects on the human health. To accomplish this purpose, satellite data products for those pollutants will be required.

Due to the continuous development of the scientific and technological knowledge, it will be important to do a continuous follow-up of the new AOD satellite products. Also, for future applications more AERONET stations should be taken into account to obtain AOD data spatially representative to be compared with modelling outputs and satellite data. For this, a broader domain study will be required.

Data fusion is a complex task. More developments and applications will be required. Thus, it will be important to assess other data fusion methodologies. Other important research point is related with the methodology used to obtain the particulate matter mass concentrations at near-surface level using AOD data after data fusion. A sensitivity analysis of this methodology will be important to find the best method to characterize the particulate matter mass concentrations at near-surface.

References

References

Alexandrov, M.D., Lacis A.A., Carlson B.E., and Cairns B., 2002. Remote sensing of atmospheric aerosols and trace gases by means of multifilter rotating shadowband radiometer. Part II: Climatological applications. J. Atmos. Sci., 59, 544-566, doi:10.1175/1520-0469(2002)059<0544:RSOAAA>2.0.CO;2.

Alizadeh Choobari O., Zawar-Reza P., and Sturman A., 2014. The global distribution of mineral dust and its impacts on the climate system: A review. Atmospheric Research. 138, 152–165. doi:10.1016/j.atmosres.2013.11.007

Allen D., 2011. Getting to Know ArcGIS ModelBuilder. ESRI PR. 362 pp.

Allen R. J., and Sherwood S. C., 2010. The impact of natural versus anthropogenic aerosols on atmospheric circulation in the Community Atmosphere Model. Climate Dynamics, 36, 1959-1978.

Alonso-Perez, S., Cuevas, E., Perez, C., Querol, X., Baldasano, J.M., Draxler, R., and Bustos, J.J., 2011. Trend changes of African airmass intrusions in the marine boundary layer over the subtropical Eastern North Atlantic region in winter. Tellus B 63, 255–265. doi:10.1111/j.1600-0889.2010.00524.x

Amiridis, V., Kafatos, M., Perez, C., Kazadzis, S., Gerasopoulos, E., Mamouri, R.E., Papayannis, A., Kokkalis, P., Giannakaki, E., Basart, S., Daglis, I., and Zerefos, C., 2009. The potential of the synergistic use of passive and active remote sensing measurements for the validation of a regional dust model. Annales Geophysicae 27, 3155–3164. doi:10.5194/angeo-27-3155-2009

Andreae, M.O., 2007. Aerosols before pollution. Sciencie. 315(50-51), 5808.

Angström, A., 1929. On the atmospheric transmission of sun radiation and on dust in the air. Geograf. Ann. Deut., 11, 156–166.

Balzarini, A., Pirovano, G., Honzak, L., Žabkar, R., Curci, G., Forkel, R., Hirtl, M., San José, R., Tuccella, P., and Grell, G. A., 2015. WRF-Chem model sensitivity to chemical mechanisms choice in reconstructing aerosol optical properties. Atmospheric Environment, 115, 604–619, doi:10.1016/j.atmosenv.2014.12.033.

Basart, S., Pay, M.T., Jorba, O., Pérez, C., Jiménez-Guerrero, P., Schulz, M., and Baldasano, J.M., 2012a. Aerosols in the CALIOPE air quality modelling system: evaluation and analysis of PM levels, optical depths and chemical composition over Europe. Atmospheric Chemistry and Physics 12, 3363–3392. doi:10.5194/acp-12-3363-2012

Basart, S., Pérez, C., Nickovic, S., Cuevas, E., and Baldasano, J.M., 2012b. Development and evaluation of the BSC-DREAM8b dust regional model over Northern Africa, the Mediterranean and the Middle East. Tellus B 64. doi:10.3402/tellusb.v64i0.18539

Benas N., Beloconi A., and Chrysoulakis N., 2013. Estimation of urban PM10 concentration, based on MODIS and MERIS/AATSR synergistic observations. Atmospheric Environment, 79, 448-454. Doi: 10.1016/j.atmosenv.2013.07.012

Black, T., 1994. The New NMC Mesoscale Eta Model: Description and Forecast Examples. Weather and Forecasting 9, 265–278. doi:10.1175/1520-0434(1994)009<0265:TNNMEM>2.0.CO;2

Bonyoung, K., Naresh, K., Eladio, K., Uarporn, N., Tanarit, S., Mehmet, T.O., Armistead, G. R., and Greg, Y., 2015. Chemical transport model consistency in simulating regulatory outcomes and the relationship to model performance. Atmospheric Environment. Volume 116, Pages 159–171. doi:10.1016/j.atmosenv.2015.06.036

Borge, R., Alexandrov, V., del Vas, J. J., Lumbreras, J., and Rodríguez, E., 2008. A comprehensive sensitivity analysis of the WRF model for air quality applications over the Iberian Peninsula. Atmospheric Environment, 42, 8560–8574. doi:10.1016/j.atmosenv.2008.08.032.

Borge, R., Lumbreras, J., Vardoulakis, S., Kassomenos, P., and Rodriguez, E., 2007. Analysis of long-range transport influences on urban PM10 using two-stage atmospheric trajectory clusters. Atmospheric Environment 41, 4434–4450. doi:10.1016/j.atmosenv.2007.01.053.

Borrego, C., Monteiro, A., Ferreira, J., Miranda, A.I., Costa, A.M., Carvalho, A.C., and Lopes, M., 2008. Procedures for estimation of modelling uncertainty in air quality assessment. Environment International 34, 613–620. doi: 10.1016/j.envint.2007.12.005.

Borrego, C., Monteiro, A., Sá, E., Carvalho, A., Coelho, D., Dias, D., and Miranda, A.I., 2012b. Reducing NO_2 Pollution over Urban Areas: Air Quality Modelling as a Fundamental Management Tool. Water Air and Soil Pollution. doi: 10.1007/s11270-012-1281-7

Borrego, C., Sá, E., Carvalho, A., Sousa, J., and Miranda, A.I., 2012a. Plans and Programmes to improve air quality over Portugal: a numerical modelling approach, International Journal Environment Pollution, Vol.48, Nos. 1/2/3/4.

Boucher, O., Randall D., Artaxo P., Bretherton C., Feingold G., Forster P., Kerminen V.-M., Kondo Y., Liao H., Lohmann U., Rasch P., Satheesh S.K., Sherwood, Stevens S. B. and Zhang X.Y., 2013. Clouds and Aerosols. In: Climate Change 2013: The Physical Science Basis. Contribution of Working Group I to the Fifth Assessment Report of the Intergovernmental Panel on Climate Change [Stocker, T.F., D. Qin, G.-K. Plattner, M. Tignor, S.K. Allen, J. Boschung, 5 A. Nauels, Y. Xia, V. Bex and P.M. Midgley (eds.)]. Cambridge University Press, Cambridge, United Kingdom and New York, NY, USA.

Cahynová, M., and Huth, R., 2009. Enhanced lifetime of atmospheric circulation types over Europe: fact or fiction? Tellus A 61, 407–416. doi:10.1111/j.1600-0870.2009.00393.x

Catalano, F., and Moeng, C.H., 2010. Large-Eddy Simulation of the Daytime Boundary Layer in an Idealized Valley Using the Weather Research and Forecasting Numerical Model. Boundary-Layer Meteorology, 137(1), 49-75.

Catalano, F., and Moeng, C.H., 2010. Large-Eddy Simulation of the Daytime Boundary Layer in an Idealized Valley Using the Weather Research and Forecasting Numerical Model. Boundary-Layer Meteorology, 137(1), 49-75.

Cesnulyte, V., Lindfors, A. V., Pitkänen, M. R. A., Lehtinen, K. E. J., Morcrette, J.-J., and Arola, A. 2014. Comparing ECMWF AOD with AERONET observations at visible and UV wavelengths, Atmos. Chem. Phys., 14, 593-608, doi:10.5194/acp-14-593-2014

Chatterjee A, Michalak AM, Kahn RA, Paradise SR, Braverman AJ, and Miller CE. 2010. A geostatistical data fusion technique for merging remote sensing and ground-based observations of aerosol optical thickness. J Geophys Res. 115:12.

Chin, M., Ginoux, P., Kinne, S., Torres, O., Holden, B.N., Duncan, B.N., Martin, R.V., Logan, J.A., and Higurashi, A., and Nakajima, T., 2002. Tropospheric aerosol optical thickness from the GOCART model and comparisons with satellite and Sun photometer measurements. J. Atmos. Sci., 59(3), 461–483.

Christopher, S.A., Zhang, J., Holben, B.N., and Yang, S.-K., 2002. GOES-8 and NOAA-14 AVHRR retrieval of smoke aerosol optical thickness during SCAR-B. Int. J. Remote Sens. 23, 4931–4944.

Chu D.A., Kaufman Y.J., Zibordi G., Chern J.D., Mao J., Li C., and Holben B.N., 2003. Global monitoring of air pollution over land from the Earth Observing System-Terra Moderate Resolution Imaging Spectrora-diometer (MODIS), J. Geophys. Res., 108(D21), 4661, doi:10.1029/2002JD003179

Chu, D.A., Kaufman, Y.J., Ichoku, C., Remer, L.A., Tanré, D., and Holben, B.N., 2002. Validation of MODIS aerosol optical depth retrieval overland. Geophys. Res. Lett. 29. doi:10.1029/2001GL013205.

Claeyman, M., J.-L. Attié, L. El Amraoui, D. Cariolle, V.-H. Peuch, H. Teyssèdre, B. Josse, P. Ricaud, S. Massart, A. Piacentini, J.-P. Cammas, N.J. Livesey, H.C. Pumphrey, and D.P. Edwards, 2010: A linear CO chemistry parameterization in a chemistry-transport model: evaluation and application to data assimilation. Atmos. Chem. Phys., 10, 6097-6115

Creamean, J.M., Suski, K.J., Rosenfeld, D., Cazorla, A., DeMott, P.J., Sullivan, R.C., White, A.B., Ralph, F.M., Minnis, P., Comstock, J.M., Tomlinson, J.M., and Prather, K.A., 2013. Dust and biological aerosols from the Sahara and Asia influence precipitation in the western US. Science 339, 1572–1578.

Cressie, N., Shi T., and Kang E. L., 2010. Fixed rank filtering for spatio-temporal data, J. Comput. Graphical Stat., 19(3), 724–745, doi:10.1198/jcgs.2010.09051.

D'Almeida, G.A., 1987. On the variability of desert aerosol radiative characteristics. Journal of Geophysical Research-Atmospheres 92, art. no. D3, 3017–3026. doi:10.1029/JD092iD03p03017.

Denby B, Garcia V, Holland DM, and Hogrege C., 2009. Integration of air quality modeling and monitoring data for enhanced health exposure assessment. Environmental Management. Springer-Verlag, New York, NY, pp 46–49

Denby B., Schaap M., Segers A., Builtjes P. and Horálek J., 2008. Comparison of two data assimilation methods for assessing PM10 exceedances on the European scale. Atmos. Environ. 42, 7122-7134.

Diner D.J., Beckert J.C., Reilly T.H., Bruegge C.J., Conel J.E., Kahn R.A., Martonchik J.V., Ackerman T.P., Davies R., Gerstl S.A.W., Gordon H.R., Muller J.-P., Myneni R., Sellers R. J., Pinty B., and Verstraete M., 1998. Multi-angle Imaging Spectro Radiometer (MISR) instrument description and experi-ment overview, IEEE Trans. Geosci. Rem. Sens., 36, 1072–1087.

Dore, A.J., Carslaw, D.C., Braban, C., Cain, M., Chemel, C., Conolly, C., Derwent, R.G., Griffiths, S.J., Hall, J., Hayman, G., Lawrence, S., Metcalfe, S.E., Redington, A., Simpson, D., Sutton, M.A., Sutton, P., Tang, Y.S., Vieno, M., Werner, M., and Whyatt, J.D., 2015. Evaluation of the performance of different atmospheric chemical transport models and inter-comparison of nitrogen and sulphur deposition estimates for the UK. Atmospheric Environment. 119, 131-143. doi:10.1016/j.atmosenv.2015.08.008.

Dorling, S.R., Cavies, T.D., and Pierce, C.E., 1992. Cluster analysis : a technique for estimating the synoptic meteorological controls on air and precipitation chemistry - Method and applications. Atmospheric Environment 26A, 2575-2581. doi: 10.1016/0960-1686(92)90110-7.

Draxler, R.R., and Hess, G.D., 1997. Description of the HYSPLIT 4 Modeling System. NOAA Technical Memorandum ERL ARL-224, 24.

Draxler, R.R., and Hess, G.D., 1998. An Overview of the HYSPLIT 4 Modelling System for Trajectories, Dispersion, and Deposition. Australian Meteorological Magazine 47, 295–308.

Drury, E., Jacob, D. J., Spurr, R. J., Wang, J., Shinozuka, Y., Anderson, B. E, Clarke A. D., Dibb J., McNaughton C., and Weber R., 2010. Synthesis of satellite (MODIS), aircraft (ICARTT), and surface (IMPROVE, EPA-AQS, AERONET) aerosol observations over eastern North America to improve MODIS aerosol retrievals and constrain surface aerosol concentrations and sources. Journal of Geophysical Research, Atmospheres, 115(D14), doi:10.1029/2009JD012629.

Dubovik O., and King M.D., 2000. A flexible inversion algorithm for retrieval of aerosol optical properties from sun and sky radiance measurements. Journal of Geophysical Research, 105(D16):20676.

Duncan, B.N., Prados A. I., Lamsal L. N., Liu Y., Streets D. G., Gupta P., Hilsenrath E., Kahn R. A., Nielsen J. E., Beyersdorf A. J., Burton S. P., Fiore A. M., Fishman J., Henze D. K., Hostetler C. A., Krotkov N. A., Lee P., Lin M., Pawson S., Pfister G., Pickering K. E., Pierce R. B., Yoshida Y., and Ziemba L. D., 2014. Satellite data of atmospheric pollution for U.S. air quality applications: Examples of applications, summary of data end-user resources, answers to FAQs, and common mistakes to avoid. Atmos. Environ., 94, 647-662.

EC (European Comission), 2007. Green paper - Towards a new culture for urban mobility. Brussels: Publication COM (2007) 551 final. European Commission. Commission of the European Communities.

EC (European Commission), 2011. Commission Staff Working Paper establishing guidelines for demonstration and subtraction of exceedances attributable to natural sources under the Directive 2008/50/EC on ambient air quality and cleaner air for Europe, 38 pages. Available at: http://ec.europa.eu/environment/air/quality/legislation/pdf/sec_2011_0208.pdf

Elbern, H. and Schmidt H., 1999. A four-dimensional variational chemistry data assimilation scheme for eulerian chemistry transport modeling. JGR, 104, 18583-18598.

Elbern, H., Schwinger J., and Botchorishvili R., 2010. Chemical state estimation for the middle atmosphere by four-dimensional variational data assimilation: System configuration, J. Geophys. Res., 115, D06302, doi:10.1029/2009JD011953

Elbern, H., Strunk, A., Schmidt, H., and Talagrand, O., 2007. Emission rate and chemical state estimation by 4-dimensional variational inversion. Atmos. Chem. Phys. 7, 3749–3769. doi: 10.5194/acp-7-3749-2007

Emili, E., Popp, C., Wunderle, S., Zebisch, M., and Petitta, M., 2011. Mapping particulate matter in alpine regions with satellite and ground-based measurements: An exploratory study for data assimilation. Atmospheric environment, 45(26), pp. 4344-4353. Oxford: Pergamon 10.1016/j.atmosenv.2011.05.051

Emmons, L. K., Apel, E. C., Lamarque, J.-F., Hess, P. G., Avery, M., Blake, D., Brune, W., Campos, T., Crawford, J., DeCarlo, P. F., Hall, S., Heikes, B., Holloway, J., Jimenez, J. L., Knapp, D. J., Kok, G., Mena-Carrasco, M., Olson, J., O'Sullivan, D., Sachse, G., Walega, J., Weibring, P., Weinheimer, A., and Wiedinmyer, C., 2010a. Impact of Mexico City emissions on regional air quality from MOZART-4 simulations, Atmospheric Chemistry and Physics, 10, 6195-6212, doi:10.5194/acp-10-6195-2010.

Emmons, L. K., Walters, S., Hess, P. G., Lamarque, J.-F., Pfister, G. G., Fillmore, D., Granier, C., Guenther, A., Kinnison, D., Laepple, T., Orlando, J., Tie, X., Tyndall, G., Wiedinmyer, C., Baughcum, S. L., and Kloster, S., 2010b. Description and evaluation of the Model for Ozone and Related chemical Tracers. Version 4 (MOZART-4), Geoscientific Model Development, 3, 43–67.

Engel-Cox J.A., Holloman C.H., Coutant B.W., and Hoff R.M., 2004b. Qualitative and quantitative evaluation of MODIS satellite sensor data for regional and urban scale air quality. Atmos. Environ., 38, 2495–2509.

Engel-Cox, J.A., Hoff, R.A., and Haymet, A.D.J., 2004a. Recommendations on the use of satellite remote-sensing data for urban air quality. Journal of the Air & Waste Management Association, 54, 1360–1371.

ENVIRON, 2013. User's guide to the Comprehensive Air Quality model with extensions (CAMx) version 6.00 (May, 2013), http://www.camx.com.

EPA, 2011a. Policy Assessment for the Review of the Secondary National Ambient Air Quality Standards for Oxides of Nitrogen and Oxides of Sulfur. Office of Air Quality Planning and Standards, Research Triangle Park, NC. http://www.epa.gov/ttn/naaqs/standards/no2so2sec/data/20110114pamain.pdf.

EPA, 2011b. Air Quality Modelling Final Rule Technical Support Document. Office of Air Quality Planning and Standards, Research Triangle Park, NC. http://www.epa.gov/crossstaterule/pdfs/AQModelling.pdf

Escudero, M., Querol, X., Ávila, A., and Cuevas, E., 2007a. Origin of the exceedances of the European daily PM limit value in regional background areas of Spain. Atmospheric Environment 41, 730–744. doi:10.1016/j.atmosenv.2006.09.014

Escudero, M., Querol, X., Pey, J., Alastuey, A., Pérez, N., Ferreira, F., Alonso, S., Rodríguez, S., and Cuevas, E., 2007b. A methodology for the quantification of the net African dust load in air quality monitoring networks. Atmospheric Environment 41, 5516–5524. doi:10.1016/j.atmosenv.2007.04.047

European Environment Agency (EEA), 2012, Particulate matter from natural sources and related reporting under the EU Air Quality Directive in 2008 and 2009, EEA Technical Report No 10/2012, ISSN 1725-2237, doi:10.2800/55574.

European Environment Agency (EEA), 2013. Air quality in Europe — 2013 report. EEA Report No 9/2013, ISSN 1725-9177, doi:10.2800/92843.

Fernandes, A.P., Riffler, M., Ferreira, J., Wunderle, S., Borrego, C., and Tchepel, O., 2015. Comparisons of aerosol optical depth provided by seviri satellite observations and CAMx air quality modelling, Int. Arch. Photogramm. Remote Sens. Spatial Inf. Sci., XL-7/W3, 187-193, doi:10.5194/isprsarchives-XL-7-W3-187-2015.

Ferreira, J., Rodriguez, A., Monteiro, A., Miranda, A.I., Dios, M., Souto, J.A., Yarwood, G., Nopmongcol, U., and Borrego, C., 2012. Air quality simulations for North America - MM5-CAMx modelling performance for main gaseous pollutants. Atmospheric Environment. 53, 212-224. doi: 10.1016/j.atmosenv.2011.10.020.

Fialho, P., Freitas, M.C., Barata, F., Vieira, B., Hansen, A.D.A., and Honrath, R.E., 2006. The Aethalometer calibration and determination of iron concentration in dust aerosols. Journal of Aerosol Science 37, 1497–1506. doi:10.1016/j.jaerosci.2006.03.002

Fishman, J., Bowman, K.W., Burrow, J.P., Richter, A., Chance, K.V., Edwards, D.P., Martin, R.V., Morris, G.A., Pierce, R.B., Ziemke, J.R., Al-Saadi, J.A., Creilson, J.K., Schaack, T.K., and Thompson, A.M., 2008. Remote sensing of tropospheric pollution from space. Bull. Am. Meteorol. Soc., 805e821. doi:10.1175/ 2008BAMS2526.1.

Fraser, R.S., Kaufman, Y.J., and Mahoney, R.L., 1984. Satellite measurements of aerosol mass and transport. Atmos. Environ. 18, 2577–2584.

Freitas, M.C., Dionísio, I., Fialho, P., and Barata, F., 2007. Aerosol chemical elemental mass concentration at lower free troposphere. Nuclear Instruments and Methods in Physics Research Section A: Accelerators, Spectrometers, Detectors and Associated Equipment 579, 507–509. doi:10.1016/j.nima.2007.04.148

Fuentes M., and Raftery AE., 2005. Model evaluation and spatial interpolation by Bayesian combination of observations with outputs from numerical models. Biometrics. 61:36–45.

Gallisai, R., Peters, F., Volpe, G., Basart, S. and Baldasano, J. M., 2014. Saharan dust eposition may affect phytoplankton growth in the Mediterranean Sea at ecological time scales. PLoS One. 9(10), e110762. DOI: 10.1371/journal.pone.0110762.

Gama C., Tchepel O., Baldasano J.M., Basart S., Ferreira J., Pio C., Cardoso J., and Borrego C., 2015. Seasonal patterns of Saharan dust over Cape Verde - a combined approach using observations and modelling. Tellus Series B-chemical And Physical Meteorology. 67, 24410, doi:10.3402/tellusb.v67.24410.

García-Díez, M., Fernandez, J., Fita, L., and Yague, C., 2011. WRF sensitivity to PBL parametrizations in Europe over an annual cycle. Quarterly Journal of the Royal Meteorological Society, 00, 2–15.

Gkikas, A., Houssos, E.E., Hatzianastassiou, N., Papadimas, C.D., and Bartzokas, A., 2012. Synoptic conditions favouring the occurrence of aerosol episodes over the broader Mediterranean basin. Quarterly Journal of the Royal Meteorological Society 138, 932–949. doi:10.1002/qj.978

Gordon H.R. and Wang M.,1994. Retrieval of water-leaving radi-ance and aerosol optical thickness over the oceans with Sea-WiFS: A preliminary algorithm. Appl. Opt.33: 443–452.

Govaerts, Y.M., Arriaga, A., and Schmetz, J., 2001. Operational vicarious calibration of the MSG/SEVIRI solar channels, Advances in Space Research, 28, pp 21-30.

Guo, J., Gu X., Yu T., Cheng T., Chen H., and Xie D., 2013. Trend analysis of the aerosol optical depth over China using fusion of MODIS and MISR aerosol products via adaptive weighted estimate algorithm, paper presented at Proc. SPIE 8866, Earth Observing Systems XVIII, 88661X, Sept. 23, doi:10.1117/12.2024687.

Gupta, P., Christopher, S. A., Wang, J., Gehrig, R., Lee, Y., and Kumar, N., 2006. Satellite remote sensing of particulate matter and air quality assessment over global cities. Atmospheric Environment, 40, 5880–5892.

Hadjimitsis, D.G., 2009. Aerosol optical thickness (AOT) retrieval over land using satellite image-based algorithm. Air Quality, Atmosphere & Health, 2(2), pp. 89-97.

Haghighat M., Abdel-Mottaleb M., and Alhalabi W., 2016. Discriminant Correlation Analysis: Real-Time Feature Level Fusion for Multimodal Biometric Recognition. IEEE Transactions on Information Forensics and Security, 11(9), 1984-1996.

Hanson, C., and Muller J., 2005. MSG Level 1.5 Image Product - Quality Indicators, Doc.No.: EUM/OPSMSG/TEN/05/0421, Issue: v1, EUMETSAT, Darmstadt, Germany,19 p.

Haustein, K., Pérez, C., Baldasano, J. M., Jorba, O., Basart, S., Miller, R. L., Janjic, Z., Black, T., Nickovic, S., Todd, M. C., Washington, R., Müller, D., Tesche, M., Weinzierl, B., Esselborn, M., and Schladitz, A., 2012. Atmospheric dust modelling from meso to global scales with the online NMMB/BSC-Dust model – Part 2: Experimental campaigns in Northern Africa. Atmospheric Chemistry and Physics, 12, 2933-2958, doi:10.5194/acp-12-2933-2012.

Haustein, K., Pérez, C., Baldasano, J.M., Müller, D., Tesche, M., Schladitz, A., Esselborn, M., Weinzierl, B., Kandler, K., and von Hoyningen-Huene, W., 2009. Regional dust model performance during SAMUM 2006. Geophysical Research Letters 36, art. no. L03812. doi:10.1029/2008GL036463

Holben, B. N., Eck, T. F., Slutsker, I., Tanr´e, D., Buis, J. P., Setzer, A., Vermote, E., Reagan, J. A., Kaufman, Y. J., Nakajima, T., Lavenu, F., Jankowiak, I., and Smirnov, A.1998. AERONET – A federated instrument network and data archive for aerosol characterization, Remote Sens. Environ., 66, 1–16.

Hsu, N. C., Herman J. R., Torres O., Holben B. N., Tanré D., Eck T. F., Smirnov A., Chatenet B., and Lavenu F., 1999. Comparisons of the TOMS aerosol index with Sun-photometer aerosol optical thickness: Results and applications. J. Geophys. Res., 104(D6), 6269-6279, doi:10.1029/1998JD200086.

Hu, R.M., Sokhi, R.S., and Fisher, B.E.A., 2009. New algorithms and their application for satellite remote sensing of surface PM2.5 and aerosol absorption. Journal of Aerosol Science 40 (5), 394-402.

Hu, Y.T., Chang, M.E., Russell, A.G., and Odman, M.T., 2010. Using synoptic classification to evaluate an operational air quality forecasting system in Atlanta. Atmospheric Pollution Research. 1 (4), 280e287.

Hurley, P., Physick, W., and Luhar, A., 2005. TAPM: a practical approach to prognostic meteorological and air pollution modelling. Environmental Modelling & Software, 20(6), 737-752. doi:10.1016/j.envsoft.2004.04.006

Ichoku, C., Chu, D.A., Mattoo, S., Kaufman, Y.J., Remer, L.A., Tanré, D., Slutsker, I., and Holben, B.N., 2002. A spatio-temporal approach for global validation and analysis of MODIS aerosol products. Geophys. Res. Lett. 29. doi:10.1029/2001GL013206.

IES-JRC (Institute for Environment and Sustainability - Joint Research Centre), 2007. Contribution of natural sources to air pollution levels in the EU–a technical basis for the development of guidance for the Member States, 102 pages.

IPCC (Intergovernmental Panel on Climate Change), 2001. Climate Change 2001: The Scientific Basis. Contribution of Working Group I to the Third Assessment Report of the Intergovernmental Panel on Climate Change. [Houghton, J.T.,Y. Ding, D.J. Griggs, M. Noguer, P.J. van der Linden, X. Dai, K. Maskell, and C.A. Johnson (eds.)]. Cambridge University Press, Cambridge, United Kingdom and New York, NY, USA, 881 pages.

IPCC (Intergovernmental Panel on Climate Change), 2007. Climate Change 2007: The Physical Science Basis. Contribution of Working Group I to the Fourth Assessment Report of the Intergovernmental Panel on Climate Change. [Solomon, S., D. Qin, M. Manning, Z. Chen, M. Marquis, K.B. Averyt, M. Tignor and H.L. Miller (eds.)]. Cambridge University Press, Cambridge, United Kingdom and New York, NY, USA, 996 pages.

IPCC (Intergovernmental Panel on Climate Change), 2013. Climate Change 2013: The Physical Science Basis. Contribution of Working Group I to the Fifth Assessment Report of the Intergovernmental Panel on Climate Change. In: IPCC, S., Stocker, T.F., Qin, D., Plattner, G.-K., Tignor, M., Allen, S.K., Boschung, J., Nauels, A., Xia, Y., Bex, V., Midgley, P.M. (Eds.), Cambridge University Press, Cambridge, United Kingdom and New York, NY, USA 1535 pp.

Jääskeläinen, E., Manninen, T., Tamminen, J., and Laine, M., 2016. An Aerosol Optical Depth time series 1982–2014 for atmospheric correction based on OMI and TOMS Aerosol Index, Atmos. Meas. Tech. Discuss., doi:10.5194/amt-2016-180.

Jickells, T., An, Z., Andersen, K., Baker, A., Bergametti, G., Brooks, N., Cao, J., Boyd, P., Duce, R., Hunter, K., Kawahata, H., Kubilay, N., laRoche, J., Liss, P., Mahowald, N., Prospero, J., Ridgwell, A., Tegen, I., and Torres, R., 2005. Global iron connections between dust, ocean biogeochemistry and climate. Science 308, 67–71.

Jiménez-Guerrero, P., Pérez, C., Jorba, O., and Baldasano, J.M., 2008. Contribution of Saharan dust in an integrated air quality system and its on-line assessment. Geophysical Research Letters 35, art. no. L03814. doi:10.1029/2007GL031580

Jorba, O., Pérez, C., Rocadenbosch, F., Baldasano, J.M., 2004. Cluster Analysis of 4-Day Back Trajectories Arriving in the Barcelona Area, Spain, from 1997 to 2002. American Meteorological Society 43, 887–901. doi:10.1175/1520-0450(2004)043<0887:CAODBT>2.0.CO;2

Junge, C., 1979. 'The Importance of Mineral Dust as an Atmospheric Constituent', in Saharan Dust: Mobilization, Transport, Deposition, Morales, Ed., SCOPE Report 14, J. Wiley and Sons, Chichester.

Kalnay, E., 2003. Atmospheric modeling, data assimilation, and predictability. Cambridge University Press, Cambridge, 341 pp.

Kanamitsu, M., 1989. Description of the NMC Global Data Assimilation and Forecast System. Weather and Forecasting 4, 335–342. doi:10.1175/1520-0434(1989)004<0335:DOTNGD>2.0.CO;2

Kang, E. L., Cressie N., and Shi T., 2010. Using temporal variability to improve spatial mapping with application to satellite data, Can. J. Stat., 38(2), 271–289, doi:10.1002/cjs.10063.

Kaufman Y.J., Tanré D., Remer L.A., Vermote E., Chu A., and Holben B.N., 1997. Operational remote sensing of tropospheric aerosol over land from EOS moderate resolution imaging spectroradiometer, J. Geophys. Res., 102, 17,051 – 17, 067.

Kinne S., 2009. Remote sensing data combinations: superior global maps for aerosol optical depth. In: Kokhanovsky A, Leeuw G, editors. Satellite aerosol remote sensing over land. Berlin Heidelberg: Springer.

Kishcha P., Nickovic S., Starobinets B., di Sarra A., Udisti R., Becagli S., Sferlazzo D., Bommarito C., and Alpert P., 2011. Sea-salt aerosol forecasts compared with daily measurements at the island of Lampedusa (Central Mediterranean). Atmospheric Research, 100, 28-35.

Klein, H., Nickovic, S., Haunold, W., Bundke, U., Nillius, B., Ebert, M., Weinbruch, S., Schuetz, L., Levin, Z., Barrie, L.A., and Bingemer, H., 2010. Saharan dust and ice nuclei over Central Europe. Atmospheric Chemistry and Physics 10, 10211–10221. doi:10.5194/acp-10-10211-2010

Knapp, K. P., Frouin, R., Kondragunta, S., and Prados, A., 2005 Toward aerosol optical depth retrieval over land from GOES visible radiances: determining surface reflectance, Int. J. Remote Sens., 26, 4097–4116.

Knapp, K.R., 2002. Quantification of aerosol signal in GOES 8 visible imagery over the United States. J. Geophys. Res. 107 (D20), 4426, doi:10.1029/2001JD002001.

Knapp, K.R., Vonder Haar, T.H., and Kaufman, Y.J., 2002. Aerosol optical depth retrieval from GOES-8: Uncertainty study and retrieval validation over South America. J. Geophys. Res. 107 (D7), doi:10.1029/2001JD000505.

Kokhanovsky A.A. and de Leeuw G., 2009. Satellite aerosol remote sensing over land, Springer-Praxis (Berlin), ISBN 978-3-540-69396-3, 388 pp.

Kokhanovsky, A. A., 2013. Remote sensing of atmospheric aerosol using spaceborne optical observations. Earth Sci. Rev. 116, 95–108. doi:10.1016/j.earscirev.2012.10.008

Kokhanovsky, A.A., Breon, F.M., Cacciari, A., Carboni, E., Diner, D., Di Nicolantonio, W., Grainger, R.G., Grey, W.M.F., Holler, R., Lee, K.H., Li, Z., North, P.R.J., Sayer, A.M., Thomas, G.E., and von Hoyningen- Huene, W., 2007. Aerosol remote sensing over land: a comparison of satellite retrievals using different algorithms and instruments. Atmospheric Research, 85(3–4):372–394.

Kokkalis, P., Mamouri, R. E., Todua, M., Didebulidze, G. G., Papayannis, A. and co-authors. 2012. Ground-, satellite- and simulation-based analysis of a strong dust event over Abastumani, Georgia, during May 2009. Int. J. Remote Sens. 33, 4886 4901. doi:10.1080/01431161.2011.644593.

Kokkalis, P., Mamouri, R.E., Todua, M., Didebulidze, G.G., Papayannis, A., Amiridis, V., Basart, S., Pérez, C., and Baldasano, J.M., 2012. Ground-, satellite- and simulation-based analysis of a strong dust event over Abastumani, Georgia, during May 2009. International Journal of Remote Sensing 33, 4886–4901. doi:10.1080/01431161.2011.644593

Koren, I., Oreopoulos, L., Feingold, G., Remer, L.A., and Altaratz, O., 2008. How small is a small cloud? Atmospheric Chemistry and Physics 8, 3855–3864.

Koren, I., Remer, L.A., Kaufman, Y.J., Rudich, Y., and Vanderlei Martins, J., 2007. On the twilight zone between clouds and aerosols. Geophysical Research Letters 34, L08805. doi:10.1029/2007GL029253.

Kubilay, N., Cokacar T., and Oguz T., 2003. Optical properties of mineral dust outbreaks over the northeastern Mediterranean, J. Geophys. Res., 108(D21), 4666, doi:10.1029/2003JD003798.

Lahoz, W. A., and Schneider P., 2014. Data assimilation: making sense of Earth Observation, Front. Environ. Sci., 2(16), 1–28, doi:10.3389/fenvs.2014.00016.

Laszlo, I, Ciren, P, Liu, HQ, Kondragunta, S, Tarpley, JD, and Goldberg, MD., 2008. Remote sensing of aerosol and radiation from geostationary satellites. ADVANCES IN SPACE RESEARCH, 41(11), 1882-1893.

Laurent, B., Marticorena, B., Bergametti, G., Léon, J.F., and Mahowald, N.M., 2008. Modeling mineral dust emissions from the Sahara desert using new surface properties and soil database. Journal of Geophysical Research-Atmospheres 113, art. no. D14218. doi:10.1029/2007JD009484

Lee, K. H., and Kim, Y. J., 2010. Satellite remote sensing of Asian aerosols: a case study of clean, polluted, and Asian dust storm days, Atmos. Meas. Tech., 3, 1771–1784, doi:10.5194/amt-3-1771-2010.

Lee, K.H., Li, Z., Kim, Y.J., and Kokhanovsky, A.A., 2009. Atmospheric aerosol monitoring from satellite observations: a history of three decades. In: Kim, Y.J., Platt, U., Gu, M.B., Iwahashi, H. (Eds.), Atmospheric and Biological Environmental Monitoring, pp. 13–38.

Lelieveld, J., Barlas, C., Giannadaki, D., and Pozzer, A., 2013. Model calculated global, regional and megacity premature mortality due to air pollution. Atmospheric Chemistry and Physics, 13, 7023–7037, doi:10.5194/acp-13-7023-2013.

Levy, R. C., 2009: The dark-land MODIS collection 5 aerosol retrieval: Algorithm development and product evaluation. Satellite Aerosol Remote Sensing over Land, A. A. Kokhanovsky, G. de Leeuw, Eds., Springer Praxis, 19–68, doi:10.1007/978-3-540-69397-0_2.

Li S., Garay M. J., Chen L., Ree E., and Liu Y., 2013. Comparison of GEOS-Chem aerosol optical depth with AERONET and MISR data over the contiguous United States, Journal of Geophysical Research: Atmospheres, 118, 11,228–11,241, doi:10.1002/jgrd.50867.

Li, C., Hsu, N.C., and Tsay, S.-C., 2011. A study on the potential applications of satellite data in air quality monitoring and forecasting. Atmos. Environ. 45, 3663-3675.

Li, F., Vogelman, A., and Ramanathan, V., 2004. Saharan dust aerosol radiative forcing measured from space. J. Clim. 17, 2558–2571.

Li, L., Shi R., Zhang L., Zhang J., and Gao W., 2014. The data fusion of aerosol optical thickness using universal kriging and stepwise regression in East China, paper presented at Remote Sensing and Modeling of Ecosystems for Sustainability XI, San Diego, Calif., 17 Aug.

Li, S., Kahn R., Chin M., Garay M., and Liu Y., 2015. Improving satellite-retrieved aerosol microphysical properties using GOCART data, Atmos. Meas. Tech., 8, 1157-1171, doi:10.5194/amt-8-1157-2015.

Lin, C., Li, Y., Yuan, Z., Lau, A.K., Li, C. and Fung, J.C., 2015. Using satellite remote sensing data to estimate the high-resolution distribution of ground-level PM 2.5. Remote Sensing of Environment, 156, pp.117-128.

Liu, Y., Park, R.J., Jacob, D.J., Li, Q., Kilaru, V. and Sarnat, J.A., 2004. Mapping annual mean ground level PM2. 5 concentrations using Multiangle Imaging Spectroradiometer aerosol optical thickness over the contiguous United States. Journal of Geophysical Research: Atmospheres, 109(D22).

Mahowald, N., Albani S., Kok J. F., Engelstaedter S., Scanza R., Ward D. S., and Flanner M.G., 2014. The size distribution of desert dust aerosols and its impact on the Earth system. Aeolian Res., 15, 53–71, doi:10.1016/j.aeolia.2013.09.002

Mallone S, Stafoggia M, Faustini A, Gobbi GP, Marconi A, and Forastiere F., 2011. Saharan dust and associations between particulate matter and daily mortality in Rome, Italy. Environ Health Perspect. 2011;119:1409–1414

Marell L., 2007. Contribution of natural sources to air pollution levels in the Eu – a technical basis for the development of guidance for the Member States. European Commission, Joint Research Center (JRC), Institute for Environment and Sustainability (IES). EUR 22779 EN, ISSN 1018-559, p. 102.

Mélin, F., Zibordi G., and Djavidnia S., 2007. Development and validation of a technique for merging satellite derived aerosol optical depth from SeaWiFS and MODIS, Remote Sens. Environ., 108(4), 436–450, doi:10.1016/j.rse.2006.11.026.

Menut, L., and Bessagnet, B., 2010. Atmospheric composition forecasting in Europe. Annales Geophysicae. 28 (1), 61e74.

Mercader, J., Codina, B., Sairouni, A., and Cunillera, J., 2010. Results of the meteorological model WRF-ARW over Catalonia, using different parameterizations of convection and cloud microphysics. Journal of Mediterranean Meteorology & Climatology Tethys 2010, 7, 75–86.

Mie, G., 1908: A contribution to the optics of turbid media: special colloidal metal solutions (in German: Beitrage zur Optik tru¨ber Medien speziell kolloidaler Metallösungen). Ann. Phys. 25: 377–445.

Monteiro A., Sá E., Fernandes A., Gama C., Sorte S., Borrego C., Lopes M. and Russo M.A. (2017) How healthy will be the air quality in 2050?. Air Quality, Atmosphere And Health. doi:10.1007%2Fs11869-017-0466-z

Monteiro, A., Fernandes, A.P., Gama, C., Borrego, C., and Tchepel, O., 2015. Assessing the mineral dust from North Africa over Portugal region using BSC-DREAM8b model. Atmospheric Pollution Research, 6, 1, 70-81. doi: 10.5094/APR.2015.009.

Morales, C., 1986. The airborne transport of Sahara dust: A review. Climatic Change 9:219-42.

Nguyen, H., Cressie N., and Braverman A., 2012. Spatial statistical data fusion for remote sensing applications, J. Am. Stat. Assoc., 107(499), 1004–1018, doi:10.1080/01621459.2012.694717.

Niemi J.V., Saarikoski S., Aurela M., Tervahattu H., Hillamo R., Luoto T., Aarnio P., Koskentalo T., Makkonen U., Martikainen J., Vehkamäki H., Hussein T., and Kulmala M., 2006. Long-range transport episodes of fine aerosol particles in southern Finland during 1999 - August 2006, Report Series in Aerosol Science No. 83. Finnish Association for Aerosol Research (FAAR), pp. 268-272.

Niemi, J.V., Saarikoski, S., Aurela, M., Tervahattu, H., Hillamo, R., Westphal, D.L., Aarnio, P., Koskentalo, T., Makkonen, U., Vehkamäki, H., and Kulmala, M., 2009. Long-range transport episodes of fine particles in southern Finland during 1999–2007. Atmospheric Environment 43, 1255–1264. doi:10.1016/j.atmosenv.2008.11.022

Nirala, M., 2008. Technical note: Multi-sensor data fusion of aerosol optical thickness, Int. J. Remote Sens., 29(7), 2127–2136, doi:10.1080/01431160701395336.

O'Neill, N.T., Dubovik, O., and Eck, T.F., 2001. Modified angstrom exponent for the characterization of submicrometer aerosols, Appl. Optics, 40(15), 2368–2375.

Odman, M.T., Hu, Y., Russell, A.G., Hanedar, A., Boylan, J.W., and Brewer, P.F., 2009. Quantifying the sources of ozone, fine particulate matter, and regional haze in the Southeastern United States. Journal of Environmental Management. 90 (10), 3155e3168.

Okin, G.S., Mladenov, N., Wang, L., Cassel, D., Caylor, K.K., Ringros, S., and Macko, S.A., 2008. Spatial pattern of soil nutrients in two southern African savannas. J. Geophys. Res. 111. doi: 10.1029/2007JG000584.

Ossés de Eicker M, Zah R, Triviño R, and Hurni H., 2008. Spatial accuracy of a simplified disaggregation method for traffic emissions applied in seven mid-sized Chilean cities. Atmospheric Environment, 42, 1491-1502.

Painter, T., Barrett, A., Landry, C.C., Neff, J.C., Cassidy, M.P., Lawrence, C.R., McBride, K.E., and Farmer, G.L., 2007. Impact of disturbed desert soils on duration of mountain snow cover. Geophys. Res. Lett. 34. doi: 10.1029/2007GL030284.

Palacios, M., Martín, F., and Cabral, H., 2001. Methodologies for estimating disaggregated anthropogenic emissions—application to a coastal Mediterranean region of Spain. Journal of the Air & Waste Management Association, 51, 642-657.

Park, M.E., Song, C.H., Park, R.S., Lee, J., Kim, J., Lee, S., Woo, J.-H., Carmichael, G.R., Eck, T.F., Holben, B.N., Lee, S.-S., Song, C.K., and Hong, Y.D., 2014. New approach to monitor transboundary particulate pollution over Northeast Asia. Atmos. Chem. Phys. 14, 659e674. doi:10.5194/acp-14-659-2014.

Pay, M.T., Jiménez-Guerrero, P., Jorba, O., Basart, S., Querol, X., Pandolfi, M., and Baldasano, J.M., 2012. Spatio-temporal variability of concentrations and speciation of particulate matter across Spain in the CALIOPE modeling system. Atmospheric Environment 46, 376–396. doi:10.1016/j.atmosenv.2011.09.049

Pay, M.T., Piot, M., Jorba, O., Gassó, S., Gonçalves, M., Basart, S., Dabdub, D., Jiménez-Guerrero, P., and Baldasano, J.M., 2010. A full year evaluation of the CALIOPE-EU air quality modeling system over Europe for 2004. Atmospheric Environment 44, 3322–3342. doi:10.1016/j.atmosenv.2010.05.040

PEA, 2011. Emissões de Poluentes Atmosféricos por Concelho 2009: Gases acidificantes e eutrofizantes, precursores de ozono, partículas, metais pesados e gases com efeito de estufa (in Portuguese). Portuguese Environmental Agency/Ministry for the Environment and Land Use Planning, Amadora.

Pérez García-Pando C, Stanton MC, Diggle PJ, Trzaska S, Miller RL, Perlwitz JP, Baldasano JM, Cuevas E, Ceccato P, Yaka P, and Thomson MC., 2014. Soil dust aerosols and wind as predictors of seasonal meningitis incidence in Niger. Environ Health Perspect 122:679–686; doi:10.1289/ehp.1306640

Pérez L, Tobias A, Querol X, Künzli N, Pey J, Alastuey A, Viana M, Valero N, González-Cabré M, and Sunyer J., 2008. Coarse particles from Saharan dust and daily mortality. Epidemiology. 2008;19:800–807.

Perez, C., Haustein, K., Janjic, Z., Jorba, O., Huneeus, N., Baldasano, J. M., Black, T., Basart, S., Nickovic, S., Miller, R. L., Perlwitz, J. P., Schulz, M., and Thomson, M., 2011. Atmospheric dust modelling from meso to global scales with the online NMMB/BSC-Dust model – Part 1: Model description, annual simulations and evaluation. Atmospheric Chemistry and Physics, 11, 13001–13027, doi:10.5194/acp-11-13001-2011.

Pérez, C., Nickovic, S., Baldasano, J.M., Sicard, M., Rocadenbosch, F., and Cachorro, V.E., 2006b. A long Saharan dust event over the western Mediterranean: Lidar, Sun photometer observations, and regional dust modeling. Journal of Geophysical Research-Atmospheres 111, art. no. D15214. doi:10.1029/2005JD006579

Pérez, C., Nickovic, S., Pejanovic, G., Baldasano, J.M., and Özsoy, E., 2006a. Interactive dust-radiation modeling: A step to improve weather forecasts. Journal of Geophysical Research-Atmospheres 111, art. no. D16206. doi:10.1029/2005JD006717

Pey, J., Querol, X., Alastuey, A., Forastiere, F., and Stafoggia, M., 2013. African dust outbreaks over the Mediterranean Basin during 2001–2011: PM10 concentrations, phenomenology and trends, and its relation with synoptic and mesoscale meteorology. Atmospheric Chemistry and Physics 13, 1395–1410. doi:10.5194/acp-13-1395-2013

Pinty, B., Roveda, F., Verstraete, M.M., Gobron, N., Govaerts, Y., Martonchik, J.V., Diner, D.J., and Kahn, R.A, 2000a. Surface albedo retrieval from Meteosat, 1. Theory. J. Geophys. Res. 105 (D14), 18,099–18,112.

Pinty, B., Roveda, F., Verstraete, M.M., Gobron, N., Govaerts, Y., Martonchik, J.V., Diner, D.J., and Kahn, R.A., 2000b. Surface albedo retrieval from Meteosat, 2. Applications. J. Geophys. Res. 105 (D14), 18,113–18,134.

Pokhrel, R. P., Wagner, N. L., Langridge, J. M., Lack, D. A., Jayarathne, T., Stone, E. A., Stockwell, C. E., Yokelson, R. J., and Murphy, S. M., 2016. Parameterization of single-scattering albedo (SSA) and absorption Ångström exponent (AAE) with EC / OC for aerosol emissions from biomass burning, Atmos. Chem. Phys., 16, 9549-9561, doi:10.5194/acp-16-9549-2016

Pope, C.A., and Dockery, D.W., 2006. Health Effects of Fine Particulate Air Pollution: Lines that Connect. Journal of the Air and Waste Management Association 56, 709–742. doi:10.1080/10473289.2006.10464485

Popp, C., Hauser, A., Foppa, N., and Wunderle, S., 2007. Remote sensing of aerosol optical depth over central Europe from MSG-SEVIRI data and accuracy assessment with ground-based AERONET measurements. Journal of Geophysical Research, 112, D24S11.

Pozzer, A., de Meij, A., Yoon, J., Tost, H., Georgoulias, A. K., and Astitha, M., 2015. AOD trends during 2001–2010 from observations and model simulations. Atmospheric Chemistry and Physics, 15, 5521-5535, doi:10.5194/acp-15-5521-2015.

Preißler, J., Wagner F., Pereira S.N., and Guerrero-Rascado J.L., 2011. Multi-instrumental observation of anexceptionally strong Saharan dust outbreak over Portugal, J. Geophys. Res., 116, D24204, doi:10.1029/2011JD016527.

Puttaswamy S. J., Nguyen H. M., Braverman A., Hu X., and Liu Y., 2013. Statistical data fusion of multi-sensor AOD over the Continental United States, Geocarto International, 29:1, 48-64, doi:10.1080/10106049.2013.827750

Rahman, H., and Dedieu, G, 1994. SMAC: a simplified method for the atmospheric correction of satellite measurements in the solar spectrum, Int. J. Remote Sens., 15(1), 123–143.

Randall, V.M., 2008. Satellite remote sensing of surface air quality. Atmos. Environ. 42, 7823e8784. doi:10.1016/j.atmosenv.2008.07.01.

Rao C.R.N., Stowe L.L., and McClain E.P., 1989. Remote sensing of aerosols over the oceans using AVHRR data: Theory, practice, and applications, Int. J. Remote Sens., 10, 743 – 749.

Reis, M.A., Oliveira, O.R., Alves, L.C., Rita, E.M.C., Rodrigues, F., Fialho, P., Pio, C.A., Freitas, M.C., and Soares, J.C., 2002. Comparison of continental Portugal and Azores Islands aerosol during a Sahara dust storm. Nuclear Instruments and Methods in Physics Research Section B: Beam Interactions with Materials and Atoms 189, 272–278. doi:10.1016/S0168-583X(01)01056-4

Remer, L. A., Chin M., DeCola P., Feingold G., Halthore R., Kahn R. A., Quinn P. K., Rind D., Schwartz S. E., Streets D., and Yu H., 2009: Executive Summary, in Atmospheric Aerosol Properties and Climate Impacts, A Report by the U.S. Climate Change Science Program and the Subcommittee on Global Change Research. [Mian Chin, Ralph A. Kahn, and Stephen E. Schwartz (eds.)]. National Aeronautics and Space Administration, Washington, D.C., USA.

Riffler, M., Popp, C., Hauser, A., Fontana, F. and Wunderle, S., 2010. Validation of a modified AVHRR aerosol optical depth retrieval algorithm over Central Europe. Atmospheric Measurement Techniques (AMT), 3(5), pp. 1255-1270. Göttingen: Copernicus Publications 10.5194/amt-3-1255-2010

Rodríguez, S., Querol, X., Alastuey, A., Kallos, G., and Kakaliagou, O., 2001. Saharan dust contributions to PM10 and TSP levels in Southern and Eastern Spain. Atmospheric Environment 35, 2433–2447. doi:10.1016/S1352-2310(00)00496-9

Rotunno, R., Chen, Y., Wang, W., Davis, C., Dudhia, J., and Holland G.J., 2009. Large-Eddy Simulation of an Idealized Tropical Cyclone. Bulletin of the American Meteorological Society, 90, 1783-1788.

Roy, B., Mathur, R., Gilliland, A.B., and Howard, S.C., 2007. A comparison of CMAQ-based aerosol properties with IMPROVE, MODIS, and AERONET data. Journal of Geophysical Research, 112. D14301.

Sá, E., Martins H., Ferreira J., Marta-Almeida M., Rocha A., Carvalho A., and Borrego C., 2016. Climate change and pollutant emissions impacts on air quality in 2050 over Portugal. Atmospheric Environment, Volume 131, April 2016, 209–224. doi:10.1016/j.atmosenv.2016.01.040.

Sahu, S., Yip, S., and Holland, D. M. 2009. Improved space-time forecasting of next day ozone concentrations in the eastern U.S.. Atmospheric Environment, 43, 494–501.

Salvador P., Artíñano B., Molero F., Viana M., Pey J., Alastuey A., and Querol X., 2013. African dust contribution to ambient aerosol levels across central Spain: Characterization of long-range transport episodes of desert dust. Atmospheric Research 127, 117–129. doi:10.1016/j.atmosres.2011.12.011

Sarigiannis D.A., Soulakellis N.A., and Sifakis N.I., 2004. Information fusion for computational assessment of air quality and health effects. Photogrammetric Eng & Remote Sensing 70(2): 235–245. doi:10.14358/PERS.70.2.235

Satheesh S.K., and Krishnamoorthy K., 2005. Radiative effects of natural aerosols: A review. In: Atmospheric Environment, 39, 2089-2110.

Schaap, M., Timmermans, R.M.A., Roemer, M, Boersen, G.A.C., Builtjes, P.J.H., Sauter, F.J., Velders G.J.M., and Beck, J.P., 2008. The LOTOS-EUROS model: description, validation and latest developments. International Journal Environment and Pollution, 32(2), 270-90.

Schmetz, J., Pili, P., Tjemkes, S., Just, D., Kerkmann, J., Rota, S., and Ratier, A., 2002. An introduction to Meteosat Second Generation. Bulletin of the American Meteorological Society. 83:977-992.

Seaman, N.L., 2000. Meteorological modelling for air quality assessments. Atmospheric Environment, 34, 2231-2259.

Seinfeld, J. H., and Pandis, S. N., 2006. Atmospheric chemistry and physics: from air pollution to climate change. Second Edition, Wiley, Hoboken, N.J., USA, Wiley, 1203 pp. ISBN: 978-0-471-72018-8

Skamarock, W.C., Klemp, J.B., Dudhia, J., Gill, D.O., Barker, D.M., Huang, X.Y., Wang, W., and Powers, J.G., 2008. A Description of the Advanced Research WRF Version 3. NCAR Technical Note NCAR/TN-475+STR, pp. 113, doi:10.5065/D68S4MVH.

Smoydzin L., Teller A., Tost H., Fnais M., and Lelieveld J., 2012. Impact of mineral dust on cloud formation in a Saharan outflow region. Atmos. Chem. Phys., 12, 11383–11393. doi:10.5194/acp-12-11383-2012

Sofiev, M., Vankevich R., Lotjonen M., Prank M., Petukhov V., Ermakova T., and Kukkonen J., 2009: An operational system for the assimilation of satellite information on wild-land fires for the needs of air quality modelling and forecasting. Atmos. Chem. Phys. Discuss., 9, 6483-6513, http://www.atmos-chem-phys-discuss.net/9/6483/2009/acpd-9-6483-2009.pdf

Sorek-Hamer M., Broday D.M., Chatfield R., Esswein R., Stafoggia M., Lepeule J., Lyapustin A. and Kloog I. (2017). Monthly analysis of PM ratio characteristics and its relation to AOD. Journal of the Air & Waste Management Association. 67(1):27-38. doi: 10.1080/10962247.2016.1208121.

Stafoggia M., Schwartz J., Badaloni C., Bellander T., Alessandrini E., Cattani G., Donato F., Gaeta A., Leone G., Lyapustin A., Sorek-Hamer M.,Hoogh K., Di Q., Forastiere F. and Kloog I. (2017). Estimation of daily PM10 concentrations in Italy (2006-2012) using finely resolved satellite data, land use variables and meteorology. Environment International.;99 234-244.

Stowe L.L., McClain E.P., Carey R., Pellegrino P., Gutman G., Davis P., Long C., and Hart S., 1991. Global distribution of cloud cover derived from NOAA/AVHRR operational satellite data, Advance Space Research, 11:51–54.

Strunk, A., Elbern H., and Ebel A., 2011: Using Satellite Observations for Air Quality Assessment with an Inverse Model System, Numerical Methods and Applications, Lecture Notes in Computer Science, Volume 6046, Dimov, I., Dimova, S., Kolkovska, N. (Eds.), ISBN: 978-3-642-18465-9, Springer, 174-181

Taghavi, M., Cautenet, S., and Arteta J., 2005. Impact of a highly detailed emission inventory on modelling accuracy. Atmospheric Research, 74, 65-88.

Talagrand, O., 1997. Assimilation of observations, an introduction. Journal of the Meteorological Society of Japan 75 (1B), 191e209.

Tang, Q., Bo Y., and Zhu Y., 2016. Spatiotemporal fusion of multiplesatellite aerosol optical depth (AOD) products using Bayesian maximum entropy method, J. Geophys. Res. Atmos., 121, 4034–4048, doi:10.1002/2015JD024571.

Tchepel O., Ferreira J., Fernandes A.P., Basart S., Baldasano J.M., and Borrego C., 2013. Analysis of long-range transport of aerosols for Portugal using 3D Chemical Transport Model and satellite measurements. Atmospheric Environment. 64, 229-241. doi:10.1016/j.atmosenv.2012.09.061.

Tegen, I., and Lacis, A., 1996. Modeling of particle size distribution and its influence on the radiative properties of mineral dust aerosol. Journal of Geophysical Research-Atmospheres 101, art. no. D14, 19237–19244. doi:10.1029/95JD03610

Tegen, I., Hollrig, P., Chin, M., Fung, I., Jacob, D., and Penner, J., 1997. Contribution of different aerosol species to the global aerosol extinction optical thickness: Estimates from model results. J. Geophys. Res. 102, 23,895–823,915, October 827 1997.

Tesche, T.W., Morris, R., Tonnesen, G., Mcnally, D., Boylan, J., and Breweer, P., 2006. CMAQ/CAMx annual 2002 performance evaluation over the Eastern US. Atmospheric Environment, 40(26), 4906-4919.

Thunis, P., Perderzoli, A., and Pernigotti, D., 2012. Performance criteria to evaluate air quality modelling applications. Atmospheric Environment, 59, 476-482.

Todd, M.C., Bou Karam, D., Cavazos, C., Bouet, C., Heinold, B., Baldasano, J.M., Cautenet, G., Koren, I., Pérez, C., Solmon, F., Tegen, I., Tulet, P., Washington, R., and Zakey, A., 2008. Quantifying uncertainty in estimates of mineral dust flux: An intercomparison of model performance over the Bodélé Depression, northern Chad. Journal of Geophysical Research-Atmospheres 113, art. no. D24107. doi:10.1029/2008JD010476

Torres, O., Bhartia,P. K., Herman, J. R., Sinyuk,A., Ginoux, P., and Holben, B. 2002: A Long-Term Record of Aerosol Optical Depth from TOMS Observations and Comparison to AERONET Measurements. J. Atmos. Sci., 59, 398-413. doi: doi:10.1175/1520-0469(2002)059<0398:ALTROA>2.0.CO;2.

Torres, O., Tanskanen, A., Veihelmann, B., Ahn, C., Braak, R., Bhartia, P. K., Veefkind, P., and Levelt, P., 2007. Aerosols and surface UV products from Ozone Monitoring Instrument observations: An overview, J. Geophys. Res.,112, D24S47,doi:10.1029/2007JD008809.

Tuia, D., Ossés de Eicker, M., Zah, R., Osses, M., Zarate, E., and Clappier, A., 2007. Evaluation of a simplified top-down model for the spatial assessment of hot traffic emissions in mid-sized cities. Atmospheric Environment, 41, 3658-3671.

URL1 - http://www.bsc.es/earth-sciences/mineral-dust-forecast-system/bsc-dream8b-forecast, accessed in 2014.

URL2 - http://www.bsc.es/earth-sciences/mineral-dust/catalogo-datos-dust, accessed in 2014.

URL3 - http//aeronet.gsfc.nasa.gov, accessed in 2014.

van Donkelaar, A., Martin, R.V., Brauer, M., Kahn, R., Levy, R., Verduzco, C., and Villeneuve, P.J., 2010. Global estimates of ambient fine particulate matter concentrations from satellite-based aerosol optical depth: development and application. Environmental Health Perspectives, 118(6), pp.847.

van Loon, M, Builtjes P.J.H., and Segers A., 2000. Data assimilation of ozone in the atmospheric transport chemistry model LOTOS. Environmental Modeling and Software 15, 603-609.

van Loon, M., 2004. Model intercomparison in the framework of the review of the unified EMEP model. Technical report TNO-MEP R2004/282, Apeldoorn, The Netherlands.

Vautard, R., Builtjes, P., Thunis, P., Cuvelier, K., Bedogni, M., Bessagnet, B., Honoré, C., Moussiopoulos, N., Pirovano G., Schaap, M., Stern, R., Tarrason, L., and Van Loon, M., 2007. Evaluation and intercomparison of ozone and PM10 simulations by several chemistry-transport models over 4 European cities within the City-Delta project. Atmospheric Environment, 41, 173-188.

Vermote, E., Tanré, D., and Morcrette, J.-J., 1997. Second simulation of the satellite signal in the solar spectrum, 6S: an overview, IEEE T. Geosci. Remote, 35(3), 675–686.

Viana M., Pey J., Querol X., Alastuey A., de Leeu F., and Lükewille A., 2014. Natural sources of atmospheric aerosols influencing air quality across Europe. Science of the Total Environment 472, 825–833. doi:10.1016/j.scitotenv.2013.11.140

Vijayaraghavan K., Snell H.E., and Seigneur C., 2008. Practical aspects of using satellite data in air quality modelling. Environmental Science and Technology, 42, 8187 – 8192.

Volz F. E., 1959: Photometer mit selen-photoelement zur spektralen messung der sonnenstrahlung und zur bestimmung der wellenlangenabra'ngigkeit der dunsttrubung. Arch. Meteorol. Geophys. Bioklim, B10, 100-131.

von Hoyningen-Huene W.,Freitag M., and Burrows J.P., 2003. Retrieval of aerosol optical thickness over land surfaces from top-of-atmospher radiance. J. Geophys. Res. 108: 4260, doi:10.1029/2001JD002018

Wagner, F., Bortoli, D., Pereira, S., Costa, M.J., Silva, A.M., Weinzierl, B., Esselborn, M., Petzold, A., Rasp, K., Heinold, B., and Tegen, I., 2009. Properties of dust aerosol particles transported to Portugal from the Sahara desert. Tellus B 61, 297–306. doi:10.1111/j.1600-0889.2008.00393.x

Wang J., and Christopher S.A., 2003. Intercomparison between satellite-derived aerosol optical thickness and PM2.5 mass: implications for air quality studies. Geophysical Research Letters, 30, 2095.

Wang, J., Brown D. G., and Hammerling D., 2013. Geostatistical inverse modeling for super-resolution mapping of continuous spatial processes, Remote Sens. Environ., 139, 205–215, doi:10.1016/j.rse.2013.08.007.

Wehrli C., 2000. Calibrations of filter radiometers for determination of atmospheric optical depth. Metrologia, 37, 419-422.

WHO (World Health Organization), 2006a. Air Quality Guidelines. Global update 2005. Particulate matter, ozone, nitrogen dioxide and sulfur dioxide, 496 pages. Available at: http://www.who.int/phe/health_topics/outdoorair/outdoorair_aqg/en/

WHO (World Health Organization), 2006b. Health risks of particulate matter from long-range transboundary air pollution, 113 pages. Available at: http://www.euro.who.int/__data/assets/pdf_file/0006/78657/E88189.pdf

WHO (World Health Organization), 2013. Health effects of particulate matter. Policy implications for countries in eastern Europe, Caucasus and central Asia. Copenhagen: WHO Regional Office for Europe.

Xu, H., Guang J., Xue Y., de Leeuw G., Che Y. H., Guo J., He X. W., and Wang T. K., 2015. A consistent aerosol optical depth (AOD) dataset over mainland China by integration of several AOD products, Atmos. Environ., 114, 48–56, doi:10.1016/j.atmosenv.2015.05.023.

Xue, Y., Xu H., Guang J., Mei L., Guo J., Li C., Mikusauskas R., and He X., 2014. Observation of an agricultural biomass burning in central and east China using merged aerosol optical depth data from multiple satellite missions, Int. J. Remote Sens., 35(16), 5971–5983, doi:10.1080/2150704X.2014.943321.

Xue, Y., Xu H., Mei L., Guang J., Guo J., Li Y., Hou T., Li C., Yang L., and He X., 2012. Merging aerosol optical depth data from multiple satellite missions to view agricultural biomass burning in central and east China, Atmos. Chem. Phys. Discuss., 12(4), 10,461–10,492, doi:10.5194/acpd-12-10461-2012.

Yap, X.Q., and Hashim, M., 2013. A robust calibration approach for PM10 prediction from MODIS aerosol optical depth. Atmospheric Chemistry and Physics, 13(6), 3517-3526.

Yarwood, G., Rao S., Yocke M., and Whitten G., 2005. Updates to the Carbon Bond Chemical Mechanism: CB05. Final Report to the US EPA, RT-0400675. Available at http://www.camx.com/publ/pdfs/CB05_Final_Report_120805.pdf.

You, W., Zang, Z., Zhang, L., Zhang, M., Pan, X., and Li, Y., 2016. A nonlinear model for estimating ground-level PM 10 concentration in Xi'an using MODIS aerosol optical depth retrieval. Atmospheric Research, 168, pp. 169-179.

Yu, H. B., Dickinson R. E., Chin M., Kaufman Y. J., Holben B.N., Geogdzhayev I.V., and Mishchenko M.I., 2003. Annual cycle of global distributions of aerosol optical depth from integration of MODIS retrievals and GOCART model simulations, J. Geophys. Res., 108(D3), 4128, doi:10.1029/2002JD002717.

Zhang, J., Christopher, S.A., and Holben, B.N., 2001. Intercomparison of smoke aerosol optical thickness derived from GOES-8 imager and ground based sun photometers. J. Geophys. Res. 106, 7387–7397.

Zhang, Y., Bocquet, M., Mallet, V., Seigneur, C., and Baklanov, A., 2012a. Real-time air quality forecasting, part I: History, techniques, and current status. Atmospheric Environment, 60, 632-655.

Zhang, Y., Bocquet, M., Mallet, V., Seigneur, C., and Baklanov, A., 2012b. Real-time air quality forecasting, part II: State of the science, current research needs, and future prospects. Atmospheric Environment, 60, 656-676.

Zhang, Y., Smith J. A., Ntelekos A. A., Baeck M. L., Krajewski W. F., and Moshary F., 2009. Structure and Evolution of Precipitation along a Cold Front in the Northeastern United States. Journal of Hydrometeorology, 10, 1243-1256.

Zhao Y., Nielsen C.P., Lei Y., McElroy M.B., and Hao J., 2011. Quantifying the uncertainties of a bottom–up emission inventory of anthropogenic atmospheric pollutants in China Atmospheric Chemistry and Physics, 11, 2295–2308. doi:10.5194/acp-11-2295-2011.

Zubko V, Leptoukh GG, and Gopalan A., 2010. Study of data-merging and interpolation methods for use in an interactive online analysis system: MODIS terra and aqua daily aerosol case. IEEE Trans Geosci Remote Sens. 48:4219–4235.